INTRODUCTION

The Nuclear Physics Laboratory of the University of Washington has for over 40 years supported a broad program of experimental physics research. The current program includes "in-house" research using the local tandem Van de Graaff and superconducting linac accelerators and non-accelerator research in solar neutrino physics at the Sudbury Neutrino Observatory in Canada and at SAGE in Russia, double beta decay and gravitation as well as user-mode research at large accelerator and reactor facilities around the world.

The Mass-8 experiment has made significant progress by nearly doubling the amount of data for both ^{8}Li and ^{8}B beta decay. Monitoring of the gas counter performance was added to insure the quality of the data. The new high energy gamma ray beamline and detector setup has been completed and first data have been taken toward obtaining a precise spectrum of photons from the 17 MeV excited states of ^{8}Be.

As an important step in interpreting GDR emission spectra, a measurement of pre-equilibrium particle loss prior to compound nuclear formation was made for 200 MeV ^{18}O + ^{100}Mo. The result is, on average, a compound nucleus that is 3 mass units lighter and 20% lower excitation energy than the compound nucleus formed in complete fusion.

In a study of sub-barrier fusion of Ca with Ti isotopes it has been shown that quasi-elastic scattering excitation functions can be used to obtain barrier distributions with similar structure to that obtained from fusion data.

We have measured the angular distribution of fission fragments in various near- and sub-barrier heavy-ion reactions with actinide targets. We find no evidence of strong peaklike structures in fission fragment anisotropies as a function of center-of-mass energy. An analysis of C+U and O+Th fission fragment anisotropies yields no evidence of an effect due to the entrance channel mass asymmetry. A study of the three reactions C + ^{235,236,238}U indicates a strong influence of the ground state spin of actinide targets on the anisotropy of fission fragments at sub-barrier energies.

A coincidence study of the fragmentation of C_{60} (buckyballs) in collisions with hydrogen has demonstrated that near-binary fragmentation competes with dimer evaporation in producing fragments in the C_{40} to C_{50} mass range. Also, a new pathway for producing doubly negative carbon clusters by fragmenting alkali carbide anions has been demonstrated.

Our development of beryllium targets for a planned $^{7}\mathrm{Be}(\mathrm{p},\gamma)$ experiment has achieved a ^{9}Be target

Our development of beryllium targets for a planned $^{7}\mathbf{Be(p,\gamma)}$ experiment has achieved a ^{9}Be target, fabricated in the same manner as will be used eventually to make a ^{7}Be target, with an impurity/Be ratio of 2/1.

The Russian-American Gallium Experiment (SAGE) has published the results from a successful ^{51}Cr neutrino source experiment. Analysis of the solar neutrino results is near completion.

Work continues at a rapid pace toward completion of the Sudbury Neutrino Observatory. Following four years of planning and development, installation of the acrylic vessel is now over 60% complete, with final completion scheduled for this fall. The UW SNODAQ group has prototyped most of the software elements necessary for the SNO data acquisition, and has made significant progress in the coding of the online data-monitoring system. The code needed for bulk testing of the production front-end electronics is mostly in place. MiniSNO has been used to test the electronics calibration algorithms, and will be used again in the near future to test some of the optical calibration sources. The Neutral-Current Detector project has also made great strides in the last year with production of prototype counters. Preamplifiers, endcaps, cable terminations and delay lines for the proportional counters are being assembled. We have received the majority of the required CVD Ni tubing. The assembly equipment is ready and the production phase will begin soon. We have taken delivery of the remotely operated submersible vehicle to be used to deploy the neutral current detectors in the acrylic vessel.

A successful run on the parity nonconserving neutron spin-rotation in ^{4}He was carried out on the NG-6 beamline at the Cold Neutron Research Facility at NIST in Gaithersburg, MD. In December, the emiT experiment, a search for time-reversal violation in neutron beta decay of free neutrons, moved onto this beamline. The emiT system, which includes four beta and four proton detectors segments as well as beam and spin transport systems, observed first data in early January and is scheduled to continue to acquire data through mid-1997.

A new algorithm for simulating the effects of multiparticle Bose-Einstein statistics and Coulomb interactions in ultrarelativistic heavy ion collisions at NA49 and STAR has been implemented in a code that is now being tested and will be used to generate a library of Bose-Einstein correlated events simulating collisions at CERN and RHIC.

New limits for short range equivalence principle violations have been obtained with the rotating source torsion balance apparatus. A new continuously rotating torsion balance apparatus to test the equivalence principle for a variety of sources that are as exotic as dark matter is under construction.

As always, we encourage outside applications for the use of our facilities. As a convenient reference for potential users, the table on the following page lists the vital statistics of our accelerators. For further information, please write or telephone Professor Derek W. Storm, Director, Nuclear Physics Laboratory

As always, we encourage outside applications for the use of our facilities. As a convenient reference for potential users, the table on the following page lists the vital statistics of our accelerators. For further information, please write or telephone Professor Derek W. Storm, Director, Nuclear Physics Laboratory, University of Washington, Seattle, WA 98195; (206) 543-4085 (e-mail; STORM@NPL.WASHINGTON.EDU).

We close this introduction with a reminder that the articles in this report describe work in progress and are not to be regarded as publications or to be quoted without permission of the authors. In each article the names of the investigators have been listed alphabetically, with the primary author to whom inquiries should be addressed underlined.

We thank Richard J. Seymour and Karin M. Hendrickson for their help in producing this report.

Kurt Snover

Editor

Barbara Fulton

Assistant Editor

TANDEM VAN DE GRAAFF ACCELERATOR

A High Voltage Engineering Corporation Model FN purchased in 1966 with NSF funds; operation funded primarily by the U.S. Department of Energy. See W.G. Weitkamp and F.H. Schmidt, "The University of Washington Three Stage Van de Graaff Accelerator," Nucl. Instrum. Meth. **122**, 65 (1974).

Some Available Energy Analyzed Beams

Ion	*Max. Current* (particle μA)	*Max. Energy* *(MeV)*	*Ion Source*
^{1}H or ^{2}H	50	18	DEIS or 860
^{3}He or ^{4}He	2	27	Double Charge-Exchange Source
^{3}He or ^{4}He	30	7.5	Tandem Terminal Source
^{6}Li or ^{7}Li	1	36	860
^{11}B	5	54	860
^{12}C or ^{13}C	10	63	860
* ^{14}N	1	63	DEIS or 860
^{16}O or ^{18}O	10	72	DEIS or 860
F	10	72	DEIS or 860
* Ca	0.5	99	860
Ni	0.2	99	860
I	0.01	108	860

* Negative ion is the hydride, dihydride, or trihydride.

Additional ion species available include the following: Mg, Al, Si, P, S, Cl, Fe, Cu, Ge, Se, Br and Ag. Less common isotopes are generated from enriched material.

BOOSTER ACCELERATOR

We give in the following table maximum beam energies and expected intensities for several representative ions. See "Status of and Operating Experience with the University of Washington Superconducting Booster Linac," D.W. Storm *et al*., Nucl. Instrum. Meth. A **287**, 247 (1990).

Available Energy Analyzed Beams

Ion	*Max. Current* (pμA)	*Max. Practical Energy* MeV
p	>1	35
d	>1	37
He	0.5	65
Li	0.3	94
C	0.6	170
N	0.03	198
O	0.1	220
Si	0.1	300
^{35}Cl	0.02	358
^{40}Ca	0.001	310
Ni	0.001	395

1.0 FUNDAMENTAL SYMMETRIES, WEAK INTERACTIONS AND NUCLEAR ASTROPHYSICS

1.1 Beta delayed alpha spectra from ^{8}Li and ^{8}B decays and the neutrino spectrum in ^{8}B decay

E.G. Adelberger, L.D. Carr, J.-M. Casandjian, H.E. Swanson and K.B. Swartz*

SNO will measure the energy spectrum of ^{8}B solar neutrinos reaching the earth. If neutrino oscillations occur, the spectrum will be distorted from its original shape and the deviation will contain information on the neutrino mixing parameters. Bahcall *et al.*[1] have pointed out that our ability to predict the undistorted shape of the ^{8}B neutrinos is limited by our knowledge of the final state continuum fed in ^{8}B decay. Two kinds of data are useful here, the beta spectrum and the beta-delayed alpha spectrum in ^{8}B decay. Bahcall *et al.* showed that existing delayed-alpha data were inconsistent and chose to use a single measurement of the beta spectrum in obtaining a "standard" ^{8}B spectrum. Because of the difficulty of making accurate beta spectrum shape measurements, we have chosen to make a careful remeasurement of the delayed alpha spectra in ^{8}Li and ^{8}B decays, paying special attention to the absolute calibration of the energy scale and to understanding the energy response of detectors.

We use the "Mass 8" rotating target and moveable catcher foil apparatus to implant ^{8}Li (produced by ^{7}Li(d, p)) and ^{8}B (produced by ^{6}Li(^{3}He, n)) into 10 microgram/cm^{2} C catcher foils. The foils are viewed on opposite sides by a pair of Si telescopes consisting of 75 micron thick E counters followed by 500 micron thick veto detectors. The telescopes have small solid angles ($\Delta\Omega / 4\pi = 2.2 \times 10^{-3}$) to minimize summing of alphas with the associated beta particle. We can, without breaking vacuum, insert thin ^{148}Gd and ^{241}Am sources in front of the detectors. In addition we can place thin Al sheets in front of the telescopes to eliminate the alphas and see only betas. Finally we can measure the thickness of the catcher foil by measuring the energy loss of ^{244}Cm alphas passing through the foils - all without breaking vacuum. The detector telescopes are cooled to 0°C, and the electronics (except for preamps) is mounted in a special temperature-controlled rack.

Analysis of ^{8}Li data is in progress. A ^{8}B data taking run is scheduled.

---

*Yale University, New Haven, CT.

[1] J.N. Bahcall *et al*., Phys. Rev. C **54**, 411 (1996).

1.2 Progress in the Mass-8 β-decay experiment

M. Beck, L.D. Carr, H. Lawler, D.W. Storm, H.E. Swanson and J.P.S. van Schagen

The Mass-8 isospin triplet presents an ideal system to test CVC and look for the existence of second class currents.[2] The weak-decay from ^{8}Li and ^{8}B nuclei is being extensively studied in our lab using the Mass-8 apparatus.[3] Several hardware improvements were implemented. Air-cooled Ta-slits were installed to stop the beam when it is swept away during the catcher foil arm rotation. Furthermore, the collimator assembly near the target was improved to further reduce the activity landing on the catcher frame. A method has been developed in which the wires of the α-counters are cleaned prior to an experiment by submerging the wire frames in trichloroethane and using ultrasound. The wires are then rinsed with acetone.

The software used to obtain an *in situ* calibration of the β -counters[4] was extended to include the possibility to use radioactive β-sources. The program used to fit the $\beta-\alpha$ angular correlation has also been extended. For each energy E_β this angular correlation is given by: $W(\theta_{\beta-\alpha}) = a_0[1 + a_1\cos(\theta_{\beta-\alpha}) + a_2\cos^2(\theta_{\beta-\alpha})]$ (1)
or an equivalent expression in terms of Legendre polynomials. The new software is able to determine the best values for the coefficients a_0, a_1 and a_2 by a χ^2-minimization procedure either by fitting the angular correlation for each β-energy bin independently or from a global fit in which either or both of a_0 and a_2 can be constrained to a linear polynomial in E_β.

We have performed a three week experiment in which the weak decay from ^{8}Li has been studied. In total $1.5\times10^{+8}$ events were collected. The preliminary results of the ^{8}Li experiment are summarized in Fig. 1.2-1 below. In this fit, the angular correlation was fitted using Eq. 1 and the coefficient a_2 was constrained to a_2 / E_β = *constant*. We find $a_{2u} / E_\beta = (3.20\pm0.15)\times10^{-3}\,\mathrm{MeV}^{-1}$ and $a_{2d} / E_\beta = (2.93\pm0.15)\times10^{-3}\,\mathrm{MeV}^{-1}$, where u,d corresponds to the upstream and downstream α-counter, respectively, with a typical χ^2/ν of 0.98. These results are in good agreement with a previous measurement[5] where a value $a_2 / E_\beta = (3.34\pm0.26)\times10^{-3}\,\mathrm{MeV}^{-1}$ was obtained. Currently, additional data is being collected for ^{8}B. Furthermore, the γ-ray decay from the isobaric analog state in ^{8}Be will be studied in the near future using the extended NaI set-up (see Sections 6.6 and 6.7).

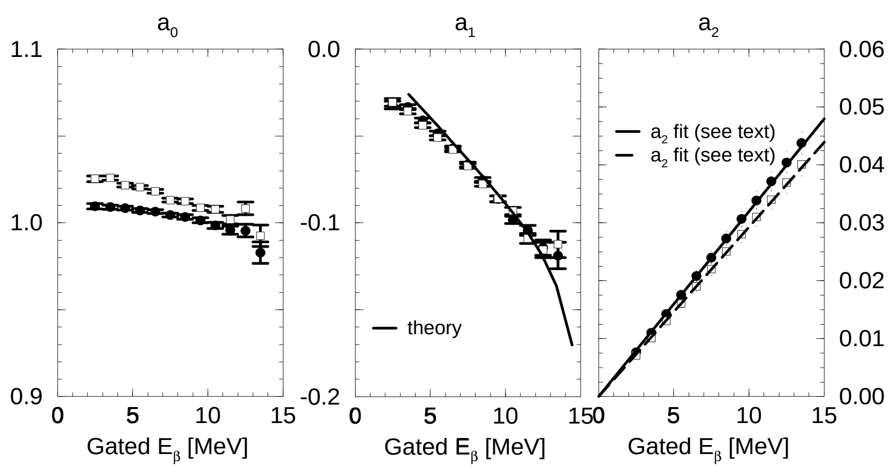

Fig. 1.2-1. Result for the coefficients a_0, a_1 and a_2 for the decay $^{8}\mathrm{Li}\rightarrow{}^{8}\mathrm{Be} + e^- + \bar{\nu}$ using Eq. 1. The fit for a_2 has been constrained to a linear polynomial. The solid (open) data involve the downstream (upstream) α-counter.

---

[2] Nuclear Physics Laboratory Annual Report, University of Washington (1996) p. 1.
[3] Nuclear Physics Laboratory Annual Report, University of Washington (1995) p. 27.
[4] Nuclear Physics Laboratory Annual Report, University of Washington (1996) p. 2.
[5] K.B. Swartz, *Measurement of the $\beta-\alpha$ Angular Correlation of Decay in ^{8}Li*, Ph.D. thesis, University of Washington, 1996.

1.3 The e-ν correlation in ^{32}Ar decay

E.G. Adelberger, M. Beck, A. Garcia* and H.E. Swanson

We are continuing to analyze the results of CERN/ISOLDE experiment IS332. The focus is on the lineshape of the delayed proton group corresponding to the superallowed $0^+ \rightarrow 0^+$ decay of ^{32}Ar. Two completely independent Monte Carlo analysis programs have been written - one is based on the CERN PAW package, the other uses Microsoft Fortran on the PC. In order to improve our analysis and minimize errors in the e-ν correlation coefficient a, due to uncertainties in the detector response function, we have made a study of the response function of Si detectors to ionizing fast particles (see Section 1.4). Once this response function is understood we will return to our extraction of the e-ν correlation coefficient.

We have an approved proposal for a new measurement of the e-ν correlation in ^{32}Ar decay (A. Garcia, spokesman). This new measurement will use a superconducting solenoid to “curl up” the beta particles so that they will not reach the proton detector. This will allow us to have larger detector solid angles improving the statistical precision of the result, and reduce systematic uncertainties that arise from the distortion of the superallowed proton peak by summing the betas. Design work on the apparatus is being carried out in collaboration with our Notre Dame colleagues.

* Notre Dame University, Notre Dame, IN.

1.4 Determining the response function of a silicon surface barrier detector

E.G. Adelberger, M. Beck, H. Bichsel and H.E. Swanson

In order to understand the response function of the proton detector in the ^{32}Ar delayed-proton measurement of the e-ν correlation (Section 1.3) we have calculated the α-particle response function of a Si-detector and compared it to data taken with a mono-energetic α-source. The model includes electronic straggling[7,8] in the α-source (thickness D_s) and in the detector deadlayer (thickness D_d), nuclear straggling[9] in the active volume of the detector, the source diameter d, and the solid angle between the source and the detector (square of side length l). The ionization efficiency of recoiling nuclei is calculated according to Lindhard *et al.*[3] with the parameterization of Smith and Lewin.[10] Ionization statistics are taken into account with W = 3.6 eV/electron-hole-pair and a Fano factor of 0.1. The electronic resolution was measured during the α-source measurement with a precision pulser. Nuclear straggling in the source and in the deadlayer are negligibly small.

The electronic straggling functions for α-particles traversing the Si deadlayer and Gd_2O_3 source were calculated[8] from photoabsorption and electron energy loss spectra.[11,12] The nuclear straggling function was computed with a Monte Carlo convolution of the nuclear single-collision cross section. After the two straggling functions were combined the result was folded with Gaussian electronic (FWHM = 5.2 keV) and statistical (FWHM = 2.5 keV) resolutions. The calculated lineshape is shown in Fig. 1.4-2. Its width is dominated by the straggling in the source and the deadlayer whereas the low-energy tail is caused by nuclear straggling in the active volume of the detector (Fig. 1.4-1).

The experimental lineshape of 3183 keV α-particles in a Si-detector (l=0.82 cm, D_d=58 nm) was measured with a d=0.5 cm $^{148}Gd_2O_3$ source. D_s=29 nm and D_d=58 nm were determined by analyzing spectra taken with the source translated and/or rotated with respect to the detector. Fig. 1.4-2 shows the comparison of the measured lineshape with the calculated response function. We find good agreement between the calculated response function and the measured lineshape. We will now use the model to determine the detector response to protons.

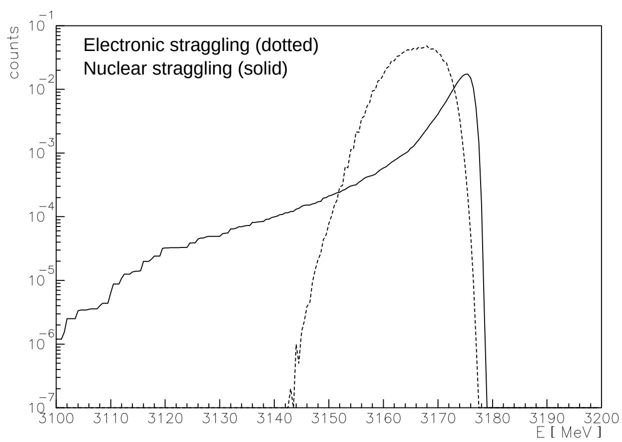

Fig. 1.4-1. Contributions to the response function.

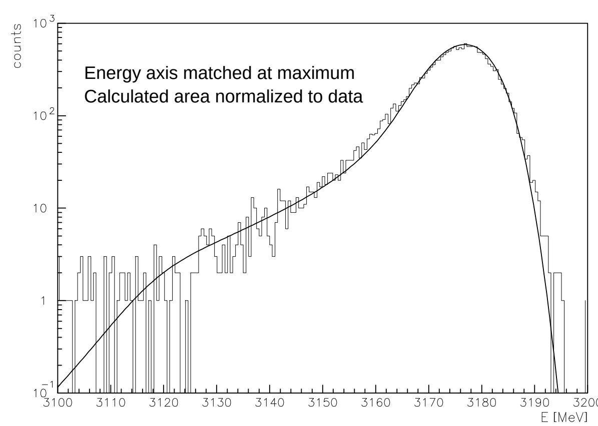

Fig. 1.4-2. Calculated response function and comparison with the measured lineshape.

---

[7] H.Bichsel and R.P. Saxon, Phys. Rev. A **11**, 4, 1286 (1975).
[8] H.Bichsel, Rev. Mod. Phys. **60**, 3 663 (1988).
[9] J.Lindhard *et al.*, K. Dan. Vidensk. Selsk., Mat-Fys. Medd. **33**,10 (1963).
[10] P.F. Smith and J.D. Lewin, Phys. Rep. **187** 203 (1990).
[11] P. Schattschneider, F. Foedermayer and D. S. Su, Scanning Microscopy, **2**, (1988).
[12] E. Hencke, Atomic Data and Nuclear Data Tables **54**, (1993).

1.5 Spin-decomposition of the GT strength in ^{37}Ca decay

<u>E.G. Adelberger</u>, S.E. Darden,[†] A. Garcia,[†] W. Haeberli,[‡] N.I. Kaloskamis,[†] E. Miller,[†] P.A. Quin,[‡] B.P. Schwartz[‡] and E. Yacoub[‡]

We[13] had previously noted significant discrepancies between the GT strength observed in ^{37}Ca decay (see references[14,15] for more recent experimental results) and shell model calculation using the Universal $2s-1d$ Hamiltonian. In an attempt to better understand the discrepancy and provide data that could be used to improve the shell-model Hamiltonian, we made an extensive study of the spins of the final states fed in ^{37}Ca decay. This work was done by studying the daughter ^{37}K levels as $^{36}Ar(\vec{p},p)$ resonances using the polarized beam at the University of Wisconsin tandem accelerator. Spins, parities, and widths of 17 ^{37}K levels were determined, and the isospin mixing of the lowest T = 3/2 level was inferred. We found that neither the Universal or the earlier CW shell-model interaction reproduced the results. However, the Universal interaction predictions would be considerably improved if the energy of the $J = 5/2^+$; T = 1/2 component of the GT giant resonance were lowered by about 2.5 MeV. This result should therefore point the way toward improvements in the shell model residual interaction.

As this work has recently been published[16] it will not be described in detail here.

[†] Notre Dame University, Notre Dame, IN.
[‡] University of Wisconsin, Madison. WI.
[13] E.G. Adelberger *et al.*, Phys. Rev. Lett. **67**, 3658 (1991).
[14] A. Garcia *et al.*, Phys. Rev. C **51**, R439 (1995).
[15] W. Trinder *et al.*, Phys. Lett. B **349**, 267 (1995).
[16] N.Kaloskamis *et al.*, Phys. Rev. C **55**, 630 (1997).

1.6 Beta decay of ^{40}Ti and the efficiency of the ICARUS ^{40}Ar neutrino detector

E.G. Adelberger, R. Anne,[†] M. Bhattacharya,[‡] C. Donzaud,[§] A. García,[‡] S. Grévy,[§] D. Guillemaud-Mueller,[§] N.I. Kaloskamis,[‡] M. Lewitowicz,[†] A.C. Mueller,[§] F. Pougheon,[§] M.G. Saint-Laurent,[†] O. Sorlin,[§] H.E. Swanson and W. Trinder[†]

The proposed large-volume liquid-argon detector ICARUS[17] has several advantages over existing solar neutrino detectors because it will detect neutral and charged-current neutrino interactions in a very symmetrical way. Neutral-current interactions will be characterized by single-track $e(\nu,\nu)e$ events, while charged-current $^{40}\mathrm{Ar}(\nu_{e,}e^-)^{40}\mathrm{K}^*$ interactions will produce multiple tracks because the $J^\pi = 1^+$ states fed in allowed neutrino capture emit several γ rays as they decay to the $^{40}\mathrm{K}\ J^\pi = 4^-$ ground state. Therefore the multiplicity and angular distribution of the event will signal its neutral or charged current nature. The neutral-current efficiency of ICARUS can be accurately calculated using electro-weak theory. However, the charged-current efficiency depends on the matrix elements for neutrino-capture transitions on ^{40}Ar to excited states of ^{40}K. A recent shell-model calculation[18] predicts a capture rate of 6.7 ± 2.5 SNU [1 SNU = 10^{-36} captures per target atom per second], where 2.2 SNU arises from the model-independent Fermi cross section and 4.5 SNU is expected from the model-dependent Gamow-Teller transition strengths, *B*(GT). An empirical calibration of the $^{40}\mathrm{Ar}(\nu_{e,}e^-)$ transition strengths, is therefore essential. We made such a calibration by studying the β^+ decays of ^{40}Ti and used isospin symmetry to relate the $^{40}\mathrm{Ar} \to {}^{40}\mathrm{K}$ transitions to the strengths of the mirror $^{40}\mathrm{Ti} \to {}^{40}\mathrm{Sc}$ transitions.

Very little was known about ^{40}Ti as it lies far from the valley of stability. Detraz *et al.*[19] observed β delayed protons from ^{40}Ti decay, but their statistics were rather poor. They obtained a half-life of 56^{+18}_{-12} ms and observed four delayed proton branches whose branching ratios summed to 43 ±6%, implying that about 60% of the decays were followed by γ rays, or by protons that were below their detection threshold. We produced ^{40}Ti at GANIL by projectile fragmentation of a 82.6 MeV/u ^{50}Cr beam on a 272.4 mg/cm^2 nickel target. The ^{50}Cr beam was produced in an ECR ion source using isotopically enriched feed material. The momentum analysis of the reaction products was performed using the ALPHA[20] spectrometer with a momentum acceptance of 0.6% around $B\rho = 715.6$ MeV/ec. Fragments of interest were then selected using the LISE3 spectrometer.

Our charged particle detection system consisted of 5 surface-barrier Si detectors, $D_1(150\mu\mathrm{m})$, $D_2(150\mu\mathrm{m})$, $D_4(500\mu\mathrm{m})$, $D_5(500\mu\mathrm{m})$ and $D_6(500\mu\mathrm{m})$. Each of the first two detectors (D_1 and D_2) provided energy loss and time-of-flight information which gave two independent identifications of the incoming fragments. The last three detectors (D_4, D_5 and D_6) formed a telescope used for implanting the fragments and detecting their subsequent β decays. A remotely-controlled carbon energy degrader of variable thickness was adjusted so that the ^{40}Ti ions were implanted in the center of D_5. Detectors D_4 and D_6 registered the β particles emitted by ions implanted in D_5. Five "70%-efficient" HPGe detectors, mounted close to D_5, detected β-delayed γ rays. A preliminary analysis of the data, which contains about 3×10^4 ^{40}Ti decays, yields a ^{40}Ti half-life of 53.7 ± 1.4 ms and we observe proton decays whose branches sum up to close to 100%. Analysis of the data is continuing.

[†] GANIL, BP 50-27, 14021 Caen Cedex, France.
[‡] University of Notre Dame, Notre Dame, IN.
[§] Institut de Physique Nucléaire, 91406 Orsay Cedex, France.
[17] ICARUS Collaboration, Proposal, ICARUS II, A second-generation proton decay experiment and neutrino observatory at Gran Sasso.
[18] W.E. Ormand, P.M. Pizzochero, P.F. Bortignon and R.A. Broglia, Phys. Lett. B **345**, 343 (1995).
[19] C. Détraz *et al.*, Nucl. Phys. A **519**, 529 (1990).
[20] M. Lewitowicz *et al.*, Phys. Lett. B **332**, 20 (1994).

1.7 Large helium cell for measurement of the spectrum of photons in ^{8}Be

K.A. Snover, D.W. Storm and J.P.S. van Schagen

Part of the Mass-8 test of CVC and search for second class currents involves measuring the distribution of isovector M1 transition strength to the broad 2^+ final state at 3 MeV in ^{8}Be. The initial states are formed by ^{4}He-^{4}He fusion, and the width of the final state is reflected in the photon spectrum. In order to determine the M1 matrix element accurately, the energy distribution of the emitted photons needs to be known. The spectrum can be measured with a detector at 90°, using a long gas cell with the windows shielded from the detector. In earlier measurements it was determined that a significant background was produced by scattered helium which subsequently interacted with the walls of the cell.

Consequently we built a large gas cell, long enough that the windows can be well shielded and large enough in diameter that He must be scattered through an angle greater than 45° to hit the part of the walls viewed by the detector. Preliminary design details were presented in last year's Annual Report.[21] At 45° the He has only one-half of the 34-MeV beam energy. The cell walls are lined with Ta, so that subsequent nuclear interactions are suppressed by the Coulomb barrier. We measured the rate for photon production on thick Ta by He of energies from 18 to 24 MeV and fit the energy dependence to an exponential to extrapolate to lower energies. By integrating along the beam, over the He-He scattering cross section, and over the photon production rate, we found that we should expect 4×10^{-4} photons from the wall for every photon produced in the resonant He-He interaction. Most of these wall-produced photons have energy below 7 MeV, so the problem of background from the wall should be solved. The windows are shielded with 6 inches of lead, which should attenuate the low energy photons by a factor of 1000. The background from the windows can be measured by running with H_2 in the target.

We have performed a preliminary measurement of the photon spectrum from the resonant states in ^{8}Be using this cell and the Seattle NaI detector. The spectrum, which peaks at about 14 MeV, appears to be clean above about 10 MeV. Work is in progress to analyze these data.

[21] Nuclear Physics Laboratory Annual Report, University of Washington (1996) p. 57.

1.8 Target and apparatus development for a planned ^{7}Be(p,γ) experiment

E.G. Adelberger, N. Bateman,[*] L. Buchmann,[*] J.-M. Casandjian, R. Hoffenberg, K.A. Snover, T.D. Steiger, J.F. Wilkerson and A. Zyuzin[*]

We are developing the target fabrication and the experimental apparatus for a measurement of the astrophysically interesting ^{7}Be(p,γ)^{8}B reaction in the energy range E_p = 0.3 to 1.0 MeV. The experiment is a collaboration in which the radioactive ^{7}Be target will be fabricated at TRIUMF and the cross section measurements carried out here at the NPL.

Much of the effort of the past year has been focused on target preparation and testing. The previous scheme[22] of Be and Al layers on a Cu backing has been abandoned in favor of a simpler design of a single Be layer on a conductive backing. A series of targets of 5-10 mm diameter of ^{9}Be have been produced at TRIUMF by a combination of chemistry and vacuum distillation using a procedure similar to that intended for the fabrication of the ^{7}Be targets. Testing of the targets has been carried out by heavy ion sputtering diagnostic tests in Vancouver, British Columbia, by (p,γ) resonance studies and by a search for characteristic γ lines from 2.4 MeV proton bombardment. The ^{9}Be(p,γ) reaction at $E_p \cong 1$ MeV has been used to characterize the ^{9}Be thickness of the targets, as well as the purity. The present results of this iterative procedure are targets of the desired thickness with an impurity/Be ratio of about 2/1. Efforts at further improvement are continuing.

A beamline (L45) has been identified as suitable for dedication to our experiment. An additional magnetic quadrupole lens has been obtained[23] and tested together with some rudimentary optics on L45. Design of the target box and components are now underway. The water-cooled target and rotating arm have been designed, as well as the Faraday cup and the LN_2 cold trap. Our goal is to have a working apparatus and preliminary measurements on a low activity ^{7}Be target by the end of this year.

---

[*] TRIUMF, Vancouver, BC, Canada.

[22] Nuclear Physics Laboratory Annual Report, University of Washington (1996) p 7.

[23] Long-term loan from the State University of New York, Stony Brook.

1.9 Measurement of the PNC spin-rotation of cold neutrons in a liquid helium target

E.G. Adelberger, J.H. Gundlach, B.R. Heckel, D.M. Markoff, S.D. Penn and H.E. Swanson

We have completed the first measurement of the parity nonconserving spin-rotation of cold neutrons transmitted through a liquid helium target. This parity-violating observable is sensitive to the pion exchange term in the nucleon-nucleon weak interaction. A determination of the pion coupling constant, f_π, will provide information on the neutral current contribution to the N-N weak interaction. Discrepancies remain between the experimental constraints on f_π, set by γ-ray circular polarization measurements in ^{18}F, and theoretical calculations.[24]

After tests of the entire apparatus were completed at NPL, the experiment was shipped to the National Institute of Standards and Technology (NIST) in Gaithersburg, Maryland. The apparatus was then reassembled on the Fundamental Physics beam line (NG-6) at the Cold Neutron Research Facility (CNRF) which provided a polarized cold neutron (wavelengths greater than 3.9Å) flux of 2×10^8 neutrons/cm^2/sec. The spin-rotation apparatus remained on the NG-6 line for three 6-week reactor cycles.

The apparatus consists of a crossed polarizer-analyzer system with magnetic field coils to preserve the neutron spin in transition to the low field region, and two target chambers separated along the beam axis by a 180 degree spin-rotating coil, the π-coil. The beam profile was measured at the entrance and exit of the magnetic field transition coils and at the entrance to the detector located immediately downstream of the analyzer. The neutron transmission from the polarizer to the detector was determined to be approximately 3%. The polarization product for this system was measured for various states of target configuration and π-coil settings.

During the second and third cycles, we optimized the running of the polarimeter and collected data. A description of the data acquisition system is presented in Section 1.10. To minimize false signals from magnetic field effects, we used two layers of passive magnetic shielding and two active magnetic field trim coils (one producing a uniform field, the other a gradient field) to reduce the residual magnetic fields inside the target region to less than 100μGauss. We have characterized the magnetic field drifts including changes in ambient fields from equipment, most notably the overhead crane. We were able to monitor and minimize magnetic field rotations with the use of our segmented ^{3}He ionization chamber, described elsewhere in this report (see Section 1.11). The active trim coils were set so that the background angular spin-rotations, on the order of a few milliradians, were identical within 1 mrad in all velocity separated regions of the detector. We use the segmented detector data to separate the geometry and velocity independent parity non-conserving rotation from background rotations. The cryogenic system which supports the liquid helium targets suffered from a number of complications. This included increasingly problematic vacuum cold leaks in the helium stack of the Oxford Instruments cryostat, cold shock created vacuum leaks in the target feedthrough tubes, and damage to the target helium transfer pump from ice entering the liquid helium reservoir. The loss of data acquisition time due to these problems was about 7 weeks.

Preliminary analysis of the data indicates a neutron spin-rotation in helium of $(-6.9\pm7.3)\times10^{-7}$ radians/cm, which is within a factor of 1.2 of statistical noise. Section 1.12 discusses the analysis program and the techniques used to extract the rotation signal from background reactor fluctuations and magnetic field drifts. This result, $\phi_{PNC}(\vec{n}+\alpha)$, in conjunction with the measured longitudinal analyzing power of polarized protons in helium, $A_L(\vec{p}+\alpha)$,[25] implies a range for the pion coupling constant of $6\le f_\pi\le55$, in units of 3.8×10^{-8}. (For comparison, the theoretical range is $0\le f_\pi\le30$.[26]) We have successfully shown that the spin-rotation measurement in the n-α system can be used to extract information on f_π.

[24] W. Haberli and B.R. Holstein, "Parity Violation in the Nucleon-Nucleon System," in *Symmetries and Fundamental Interactions in Nuclei*, W.C. Haxton and E.M. Henley, eds. World Scientific, 1995 p. 58.
[25] J. Lang *et.al.*, Phys. Rev. C **34**, 1545 (1986).
[26] B. Desplanques, J.F. Donoghue, and B.R. Holstein, Ann. Phys. (NY) **172**, 100 (1986).

1.10 NSAC - data acquisition for the neutron spin-rotation experiment

H. E. Swanson

The data acquisition system and apparatus for the neutron spin-rotation experiment were described in last years annual report.[27,28] The program NSAC functions to sequence external fields in the apparatus and to record signals from an array of neutron detectors. It was written in Microsoft Fortran 6.1 with simple real time extensions written in Assembler. NSAC was used throughout 1996 at NIST to obtain the data discussed in the accompanying article in this report (see Section 1.9). The program was upgraded to include the following capabilities:

Additional data-taking modes were added to measure the Polarization of the neutron beam and to scan the magnitude of external fields, to tune the polarimeter, and to investigate systematics. The neutron beam polarizations measured for each detector element are written to a file and are used to calculate the spin-rotation angle.

Online analysis routines were added to compute and display various combinations of asymmetries in the data. These greatly aided online monitoring of the experiment.

Multitasking capability was added to the target cycling program so that analysis could be performed at the same time as the somewhat lengthily process of filling and draining the targets.

Non-data-taking modes were added to cycle the mechanical parts of the fill system during cooldown to prevent them from freezing.

[27] Nuclear Physics Laboratory Annual Report, University of Washington (1996) p. 8.
[28] Nuclear Physics Laboratory Annual Report, University of Washington (1996) p. 55.

1.11 Design and testing of a ^{3}He ionization chamber for use in measuring the velocity profile of a cold neutron beam

E.G. Adelberger, B.R. Heckel, D.M. Markoff, S.D. Penn, and H.E. Swanson

We have designed, constructed, and tested a ^{3}He ionization chamber (IC) for use in the Neutron Spin Rotation experiment which ran from July-November 1996 (see Section 1.9). Unlike standard ionization chambers, our detector operates with a low density of ^{3}He and has multiple charge collection regions along the beam axis. This configuration allows us to calculate the beam's velocity spectrum from the absorption profile in the IC. The detector was originally built and tested in the summer and autumn of 1995. During the past year we have overhauled the gas handling and electrical systems. This final design was tested in July just prior to the experimental run. At standard operating voltage (1200 V) the detector channels registered a dark current of 0.2 pA compared to a typical signal current of 30 nA. Calculated currents differed from measured currents by only 2% where the majority of this error arises from an inability to accurately characterize the neutron beam.

Our experiment placed four important restrictions on the detector design. The incident cold neutron beam ($\lambda_N \approx 5$ Å) was split into two parallel beams separated by 1 cm. We required that the two beams be measured separately with no left-right crosstalk. Since our liquid He targets were frequently cycled, we needed to separately measure the upper and lower beam halves to ensure that the targets had properly filled/drained. Our detector noise had to be small compared to the typical signals of 30 nA. Finally we had to establish collection regions along the beam axis which had similar statistics and maximal velocity separation. To reduce our error in measuring φ_{PNC} it was essential to minimize longitudinal magnetic fields which also rotate the neutron spin. Using the fact that α_M, the rotation due to the magnetic field, depends on velocity, we required enough velocity separation in the IC to detect the spin rotation arising from a 40 μ Gauss B field, the limit of our static μ–metal shields.

The detector consisted of an alternating series of circular HV and grounded sensor plates. The plate separation was 3 cm, and the operating voltage was 1.2 kV. To reduce fringe fields an annular ring at half voltage was positioned midway between the HV and sensor plates. The first plate differed from the rest; it had a plate spacing of 1.5 cm, operated at 600 V and had no half voltage ring. Each sensor plate (5" OD) had a 1" wide outer annulus (grounded) and inner sensing plate (0.8 mm thick, 3" OD) which was divided into four quadrants. The quadrant plates were mounted on a quartz annulus with a separation of 1 mm. The plates defined four sensing regions with depths of 1.5, 3, 6, and 9 cm respectively. The plate stack was surrounded by an Al cylinder and filled with a gas mixture of 3 atm Ar and 0.5 atm ^{3}He. The ^{3}He density was chosen so that the percentage of the cold neutron beam absorbed in each region would be 30, 30, 30, and 10% respectively. The Ar density was chosen so that the proton range would be small compared to 1 cm, the separation of the left and right beams.

The detector was tested at the NIST Cold Neutron Research Facility with a full spectrum and a monochromatic beam. The full spectrum beam has a Maxwell distribution peaked at 5 Å with a high energy cut-off at 4.4 Å. Using this distribution, the predicted plate currents precisely matched our measurements, and there was no measurable left-right crosstalk. On the other hand, the monochromatic beam measurement yielded an unexpected result. The monochromatic cold neutron beam is created on the neutron interferometer beamline using Bragg reflection. Our measurements indicated that the assumed monochromatic beam was actually polluted by a second Bragg reflection which accounted for one third of the flux. Our findings were later supported by independent measurements.

Currently to measure the beam velocity profile at the CNRF one must scan through the neutron wavelengths using either a Bragg reflection system or a beam chopper for time-of-flight separation. Both processes are time consuming and are susceptible to reactor fluctuations. With our low density ^{3}He detector we have demonstrated that we could essentially take a snapshot of the beam velocity profile, a process which is both easy and independent of beam fluctuations. However since our detector has only four velocity sectors the profile is rather crude. We are currently collaborating with the NIST Neutron Interferometer Group to build a second detector with 10-15 absorption regions to test the practicality of measuring the CNRF beam profile in this manner.

1.12 Development of the data analysis code, DANSR, for the neutron spin-rotation experiments

E.G. Adelberger, B.R. Heckel, D.M. Markoff, S.D. Penn and H.E. Swanson

We have developed the code DANSR (Data Analysis for Neutron Spin Rotation) to analyze the data from the Neutron Spin Rotation experiment which was conducted from July - November 1996 (see Section 1.9). The code's basic functions are to read in the raw data files generated by the acquisition code NSAC (see Section 1.10), and to calculate the PNC spin rotation angle, φ_{PNC}, as well as several systematic values such as the magnetic rotation angle, α_{M} and the raw asymmetries. Since φ_{PNC} is known to be small (10^{-7} rads) compared to the total spin rotation ($\theta \approx 10^{-3}$ rads), the main thrust of the code is in developing methods to reduce systematic noise such as reactor fluctuations, magnetic field drifts, magnetic field spikes, and variations in the target conditions. I will explain the current strategies used in the code with the caveat that much of the analysis remains to be done.

During data acquisition NSAC repeatedly cycles the experiment through the states for the end coil field (±), data collection subcycles, pi coil field ($\pi = -1, 0, 1$), and target position ($T = 1, 2$), in order of most to least frequently cycled state. The two end coil states alternately measure the neutron spin projection along $\pm\hat{y}$, where the beam direction is along $\hat{z}$ and the initial polarization along $\hat{x}$. By switching between target positions in front of and behind the π coil, we alternate the sign (±) of our φ_{PNC} signal. For each system state NSAC writes out the integrated charge from the 16 detector channels (see section 1.11). We can denote $S_{i,\pm,\pi,T}$ as the channel readout for a given system state where we have integrated over subcycles. Let $N_{i,\pm,\pi,T}$ be the total number of neutrons of a given polarization which would be absorbed in an ideal, lossless system on channel *i*, in state $\pm, \pi, T$. Then, $S_{i,\pm,\pi,T} = N_{i,\pm,\pi,T}\left(1 \pm \mathrm{P}_{i,\pi,T}\sin(\theta)\right)/2$ where $P_{i,\pi,T}$ is the polarization product. If $N_{+,\ldots} = N_{-,\ldots}$ then the raw asymmetry $A_{i,\pi,T} = (S_{+} - S_{-})/(S_{+} + S_{-}) = P\sin(\theta)$, from which we can extract φ_{PNC} using quadratic smoothing as described below.

Unfortunately because of reactor fluctuations, $N_{+,\ldots} \neq N_{-,\ldots}$ on the 0.1 % level. To eliminate these fluctuations we assume that for a Left-Right plate pair $N_{L,+,\pi,T}/N_{L,-,\pi,T} = N_{R,+,\pi,T}/N_{R,-,\pi,T}$, and we calculate:

$$\Re_{\pi,T} = \frac{S_{R,+,\pi,T}\, S_{L,-,\pi,T}}{S_{R,-,\pi,T}\, S_{L,+,\pi,T}} = 1 + 2\left[P_{R,\pi,T}\sin(\theta_R) - P_{L,\pi,T}\sin(\theta_L)\right] + \mathrm{O}\left(\sin^2(\theta)\right)$$

If we further assume that $P_{i,\pi,T}$ does not depend on target state, then we can define

$$\varphi'_{\pi,\mathrm{T}} = \frac{\Re_{\pi,\mathrm{T}} - 1}{\mathrm{P}'_{\varphi,\pi}} = \frac{2\left[\mathrm{P}'_{\alpha,\pi}\alpha_{\mathrm{M}} + (-1)^{\mathrm{T}+1}\mathrm{P}'_{\varphi_{\mathrm{T}},\pi}\,\varphi_{\mathrm{PNC}}\right]}{\mathrm{P}'_{\varphi,\pi}} \text{ where } \mathrm{P}'_{\varphi,\pi} = \mathrm{P}'_{\varphi_1,\pi} + \mathrm{P}'_{\varphi_2,\pi}\,.$$

The combined polarization product and rotation angle due to the magnetic field, $P'_{\alpha,\pi}\alpha_M$, is a smooth background which is independent of target state. φ_{PNC} is then an oscillating signal on a background which slowly varies as the magnetic field drifts. Therefore we can extract φ_{PNC} via quadratic smoothing. For a series of target states, labeled *j*:

$$\varphi_{\mathrm{PNC},\pi,\mathrm{j}} = (-1)^{\mathrm{j}+1}\left(\varphi'_{\pi,\mathrm{j}} - 3\varphi'_{\pi,\mathrm{j}+1} + 3\varphi'_{\pi,\mathrm{j}+2} - \varphi'_{\pi,\mathrm{j}+3}\right)\Big/8$$

A first pass through our data has yielded a result of $\varphi_{\mathrm{PNC}} = (-6.9 \pm 7.3)\times 10^{-7}$ rad. This number is still quite rough since we have not eliminated corrupted data nor analyzed our systematics. We are also in the process of understanding the dependence of φ_{PNC} on several systematics such as α_M, *A*, and the count rate asymmetry $\aleph_{i,\pi} = (S_{i,\pi,1} - S_{i,\pi,2})/(S_{i,\pi,1} + S_{i,\pi,2})$.

1.13 Time reversal in neutron beta decay - The emiT experiment

S.R. Elliott, H.P. Mumm, A.W. Myers, R.G.H. Robertson, T.D. Steiger, T.D. Van Wechel, D.I. Will and J.F. Wilkerson

The emiT experiment is a search for a violation of time-reversal (T) invariance in the beta decay of free neutrons. The experiment utilizes a beam of cold (<10 meV), polarized neutrons from the Cold Neutron Research Facility at the National Institute of Standards and Technology (NIST) in Gaithersburg, MD. A sizable team of scientists has been assembled to perform this experiment from Los Alamos National Laboratory, NIST, the University of California at Berkeley/Lawrence Berkeley National Laboratory, the University of Michigan, the University of Notre Dame and the University of Washington's Nuclear Physics Laboratory.

emiT will probe the T-odd triple correlation (between the neutron spin and the momenta of the neutrino and electron decay products) in the neutron beta-decay distribution.[29] The coefficient of this correlation, *D*, will be measured by detecting decay electrons in coincidence with recoil protons while controlling the neutron polarization. Technological advances in neutron polarization and proton detection--in addition to an improved detector geometry--should allow emiT to attain a sensitivity to D of 3×10^{-4}. This level of sensitivity represents a factor of five improvement over previous neutron T tests, and may permit restrictions to be placed on several extensions to the Standard Model that allow values of D near 10^{-3}.

emiT is the first neutron T test to make use of a "supermirror" neutron polarizer. Thus, emiT achieves a polarization of 95±2%, as opposed to the 65-85% polarizations typical in previous experiments. The emiT detector consists of four plastic scintillator paddles for electron detection and four arrays of large-area PIN diodes to detect the protons. The PIN diodes have been extensively tested and shown to be efficient and economical detectors of low-energy (~ 30 keV) protons.[30]

The eight detector segments are arranged in an alternating octagonal array about the neutron beam so that each segment of one type lies at an angle of 135° relative to *two* segments of the other type. This geometry takes advantage of the fact that the electron-proton angular distribution is strongly peaked due to the disparate masses of the decay products. When compared to the 90° geometry used in previous experiments, this octagonal geometry results in an increase in signal rate which is the equivalent of a factor of seven increase in neutron beam flux.

The emiT experiment was installed on the NG-6 beamline at NIST in November of 1996. Roughly two months were spent carefully characterizing the neutron beam and performing the initial shakedown of the detector. A run commenced in early February 1997 which entailed collecting preliminary data under full running conditions. The detector is operating roughly as expected and electron-proton coincidences are being detected at rates up to 3 Hz. The reactor was down for scheduled maintenance during March, 1997. Hence the bulk of emiT's data collection will occur during April-July, 1997.

[29] J.D. Jackson, S.B. Treiman and H.W. Wyld, Jr., Phys Rev. **106**, 517 (1957).

[30] E.G. Wasserman, *Time Reversal Invariance in Polarized Neutron Decay*, Ph.D. thesis, Harvard University, 1994.

1.14 Detection of radio-frequency pulses associated with cosmic ray air showers

J.L. Rosner[*] and J.F. Wilkerson

As a result of work in the 1960's and 1970's[31,32] some of which has continued beyond then, it is recognized that air showers of energy 10^{17} eV are accompanied by radio-frequency (RF) pulses, whose polarization and frequency spectrum suggest that they are due mainly to the separation of positive and negative charges of the shower in the Earth's magnetic field.[33] The most convincing data have been accumulated in the 30-100 MHz frequency range. However, opinions have differed regarding the strength of the pulses, and atmospheric and ionospheric effects have led to irreproducibility of results. In particular, there may also be pulses associated with cosmic-ray-induced atmospheric discharges.[34]

A study is being undertaken of the feasibility of equipping the Auger[35] array with the ability to detect such pulses. RF pulses may be able to provide auxiliary information about primary composition and shower height. It is possible that the higher energy of the showers to which the array would be sensitive would change the parameters of detection. Before a design for large-scale RF pulse detection can be produced, it has been necessary to retrace some of the steps of the past 30 years by demonstrating the existence of the pulses for 10^{17} eV showers, and by controlling or monitoring some of the factors which led to their irreproducibility in the past.

A prototype detector has been set up at the CASA/MIA[36] site in Dugway, Utah. A trigger based on the coincidence of several muon "patches" was set to select 'large' showers with a rate of 30-50 per hour . A log-periodic antenna sensitive to 26-170 MHz was mounted about 30 meters to the east of the CASA boundary, at an elevation of about 10 meters to place it just above the lightning protection grid. A digital storage scope was used to register filtered and preamplified RF data on a rolling basis. These data were then captured and stored upon receipt of a large-event trigger.

A total of more than 5000 triggers, obtained under various conditions of filtering, preamplification, and noise reduction, have been acquired during runs in September 1996, December 1996, and February 1997. Preliminary results from initial analysis indicates that about 1 in 10 of these triggers may contain information on RF pulses from air showers. Shower sizes, core locations, and incident shower angles are being correlated with time, duration, and intensity of radio bursts. Detailed analysis of these data are in progress.

---

[*]Enrico Fermi Institute and Department of Physics, University of Chicago, Chicago, IL 60637.

[31] P.R. Barker, W.E. Hazen and A.Z. Hendel, Phys. Rev. Lett. **18**, 51 (1967); W.E. Hazen *ibid.*, **22**, 35 (1969); **24**, 476 (1970).

[32] H.R. Allan, in *Progress in Elementary Particles and Cosmic Ray Physics*, v. 10, edited by J.G.Wilson and S.G. Wouthuysen North Holland, Amsterdam 1971) p. 171, and references therein, V.B. Atrashkevich *et al.*, Yad. Fiz. **28**, 366 (1978).

[33] F.D. Kahn and I. Lerche, Proc. Roy. Soc. A **289**, 206 (1966); S.A. Colgate, J. Geophys. Res. **72**, 4869 (1972).

[34] R.R. Wilson, Phys. Rev. **108**, 155 (1967); R.A. Roussel Dupré, A.V. Gurevitch, T. Tunnell, and G.M. Milikh, Los Alamos National Laboratory Report LA 12601, MS, November, 1993.

[35] Auger Design Report, March 14, 1997. See http://www-td-auger.fnal.gov:82/.

[36] A. Borine et al., Nucl. Instrum. Methods A **346**, 322 (1994).

1.15 Construction of a new high-precision rotating torsion balance

E.G. Adelberger, J.H. Gundlach, B.R. Heckel, K. Mauldin, H.E. Swanson and P. Williams

We are constructing a continuously rotating torsion balance designed to test the equivalence principle with at least 20 times better sensitivity than our previous work[37]. Among other things, this will allow us to test whether the 600 km/s velocity of our region of the universe with respect to the rest frame of the cosmic microwave background is predominantly due to ordinary gravitation. The 600 km/s velocity divided by a Hubble time corresponds to an acceleration of about $1.7 \times 10^{-10}\ \mathrm{cm/s^2}$. Our new device will allow us to compare this acceleration for Be, Al and Ti test bodies with a sensitivity better than $2 \times 10^{-13}\ \mathrm{cm/s^2}$. This will be sufficient to detect any significant non-gravitational (i.e. equivalence-principle violating) component of the acceleration.

The new apparatus is located in the old cyclotron cave. This site has the advantage of being removed from traffic patterns, is thermally stable, and provides a strong topographic source for Yukawa interactions with ranges down to 1 m.

The turntable for the new instrument consists of a 25 cm diameter aluminum air bearing powered by a direct-drive eddy-current motor. A Heidenhain 36000-line shaft encoder is directly mounted to the turntable rotor. This system was manufactured by the Professional Instruments Company in Minneapolis. We developed a rotation-rate controller based on a TMS320 digital signal processor that digitizes the sine and cosine outputs of the Heidenhain, computes the turntable angle, and compares it to the desired angle which was set by the digital pulses of a Stanford precision programmable oscillator. This error signal is then used in a digital PID loop to drive the turntable motor. This device is extremely successful, the error signal of the unloaded turntable is less 100 picoradians per root Hz for frequencies below 2.5 Hz.

Signals from, and power to, the rotating apparatus are brought out via a 60-contact slipring assembly that is servoed to track the turntable so that the turntable does not provide the torque to rotate the sliprings.

The vacuum chamber is completed and will be attached below the turntable. The torsion pendulum will be suspended from a small motorized rotation and vertical translation stage that is mounted on a two-axis gimbaled platform. The autocollimator and its optics will also be suspended from this gimbaled platform.

A hermetic thermal shield consisting of double-walled aluminum cylinders that will have temperature-regulated water flowing in them has been completed. A μ-metal shield is mounted inside the shields.

We have designed a symmetric pendulum that holds 8 test bodies (4 each of 2 kinds of material - either Be, Al or Ti). The entire pendulum has vanishing q_{20} and q_{40} mass moments. The barrel-shaped test bodies themselves have vanishing q_{20} and q_{40} moments, and are located very reproducibly in conical seats in the pendulum. A prototype has been built from aluminum; the final pendulum will be machined from Be.

Currently we are testing the turntable with an old torsion balance that is temporarily suspended from a gimbal on the turntable. This setup will enable us to measure gravity gradients in the location of the final apparatus, so that the gravity gradient compensator masses can be rough-cut before the whole system is completed.

[37] Y. Su *et al.*, Phys. Rev. D **50**, 3614 (1994).

1.16 Design and testing of autocollimators for the Eötwash experiments

E.G. Adelberger, J.H. Gundlach, M.G. Harris, B.R. Heckel, S.D. Penn, G.L. Smith and H.E. Swanson

We have designed, built, and tested a new version of autocollimator for use in the Eötwash experiments. This new model features an improved construction and an updated optical system. Our tests on the new autocollimator indicate a fourfold improvement in sensitivity over the old model.

The Eötwash autocollimator is used to measure the angular deflection of our torsion pendulum. The autocollimator consists of a diode laser, an optical system, and a position sensitive detector (PSD). The laser is positioned at the focal point of a plano-convex lens. The laser light is reflected through a beam splitter to the lens, where the beam becomes parallel, and is then reflected off a series of mirrors and onto the pendulum's mirror. The light reflected off the pendulum returns along a similar path but passes through the beam splitter to the PSD.

In the old autocollimator we used a standard beam splitter which had two drawbacks. First we lost half our light with each pass through the beam splitter. This 75% light loss was very inefficient, and any spurious light reflected back onto the PSD added noise to the system. In addition half of the return beam was reflected back into the laser which is known to cause laser instability. In the new model we incorporated a polarizing beam splitter (PBS) which had an efficiency of > 98% for splitting the beam along its orthogonal polarizations. We also added a 1/4 waveplate between the PBS and the lens with its optical axis set at 45° to the normal of the optical plane. Thus by correctly aligning the laser polarization, nearly all of its light would be reflected to the lens while nearly all the return beam would be transmitted to the PSD. This eliminated our problems with reflections, back scattering, and light efficiency.

The autocollimator design was enhanced in several ways to provide a more accurate and rigid alignment and greater ease of use. The laser holder was altered to include a rotational mount with locking ring to allow to an easy change in polarization without changing laser position. In addition a heat shield was added to guard against temperature variations thereby increasing laser stability. Both the 1/4 waveplate and the lens were mounted in a disk-shaped holder and prevented from slipping by a slightly compressed O-ring. The 1/4 waveplate holder also had a locking ring rotational mount to allow easy and accurate alignment of the optical axis. This locking ring was extended to project slightly from the block so as to rigidly align the block with the spindle piece, which houses the lens and connects the autocollimator to the vacuum can.

The PSD holder was also fitted with a rotational mount and locking ring to set the detector angle. The PSD is a 1-D detector so it is important to keep its angular position fixed. However the complete PSD mount is composed of several pieces (mounting block, preamp box, and heat shield) which must sometimes be taken apart. Thus we also devised a way to remove one or all of these components without changing the rotational orientation of the PSD. The detector itself was mounted in a sliding bed with lock screws to allow for the small transverse motion to align the detector center on the optical axis. The PSD mount was also equipped with a scale to measure the detector angle.

Between the PSD mount and the block was the stage block, a spacer which during calibration can be replaced by a translation stage. The stage block was modified slightly to allow the stage and its adapter blocks to be inserted as a unit rather than in three pieces as before. Also the stage blocks were equipped with protruding rims to align them on the block.

An unfortunate consequence of the new design was that the focused spot on the PSD was too small. For best results the spot must be large compared to the gaps on the PSD. This problem was fixed by increasing the thickness of the stage block which placed the PSD slightly beyond the focal point.

A newer version of the autocollimator is currently being designed. This new model will include a longer focal length (from 20 to 30 cm), transverse adjustment for the laser, longitudinal adjustment for the PSD, a more massive laser mount (to better heat sink the laser), a more compact heat shield for the PSD, and the ability to swap positions of the laser mount and detector mount.

1.17 A short-range test of the Equivalence Principle

E.G. Adelberger, J.H. Gundlach, B.R. Heckel, G.L. Smith and H.E. Swanson

We developed the Rot-Wash torsion balance to extend our existing tests[38] of the equivalence principle (EP) in several ways.

1. to probe Yukawa EP-violating interactions with ranges down to 1 cm
2. to achieve high sensitivity for interactions that couple to charges such as *N-Z* for which our earth-attractor data was insensitive because the earth contains nearly equal numbers of neutrons and protons.
3. to "fill in" the gap (Yukawa ranges between 10^4 m and 10^6 m) where earth-attractor constants are not available because of the difficulty in calculating the horizontal component of a Yukawa force for these ranges (see reference. 1).

As these results should appear in Physical Review Letters[39] before this Annual Report is published, we reproduce below the abstract of our publication and refer the reader to that publication for details:

We rotated a 3 ton ^{238}U attractor around a compact torsion balance and compared the accelerations of Cu and Pb toward U. We found that $a_{Cu} - a_{Pb} = (0.7 \pm 5.7) \times 10^{-13}$ cm/s^2 compared to the 9.8×10^{-5} cm/s^2 gravitational acceleration toward the attractor. Our results set new constraints on equivalence-principle violating interactions with Yukawa ranges down to 1 cm and rule out an earlier suggestion of a Yukawa interaction coupled predominantly to N-Z.

It is amusing to note that if an acceleration of 5.7×10^{-13} cm / s^2 were applied to an object beginning at the time of Caesar and continued to the present day, the body would now be moving approximately as fast as the end of a minute hand on a clock.

[38] Y. Su *et al.*, Phys. Rev. **D** 50, 3614 (1994).
[39] J.H. Gundlach *et al.*, Phys. Rev. Lett. in press.

1.18 On the translation of multipoles for a $1/r$ potential

E.G. Adelberger and C. D'Urso

We outline an analytic method for calculating with high accuracy inner and outer multipoles of a $1/r$ potential about an arbitrary point in terms of known multipoles about a given point. This problem is frequently encountered in experimental gravitation where the multipole formalism is used to calculate torques and forces[40,41] on test bodies in the fields of attractors with realistic geometries. Many cases of practical interest deal with distributions that can be accurately approximated as a linear superposition of basic geometric shapes. To calculate the inner and outer multipoles of these distributions it is necessary to know the multipoles about the point of interest for each of the superposed shapes. We showed that if the inner and outer multipoles of these simple shapes are known about any one point then analytic solutions can be obtained for the multipoles of a superposed distribution about an arbitrary point.

Consider an arbitrary distribution of mass, charge, etc. that can be separated into two disjoint bodies. One body, the "object", is considered to be in the field produced by the other body, the "source". Integrating over this distribution, the object has inner and outer multipoles

$$q_{lm} = \int \rho_0(\vec{r}) r^1 Y^*_{lm}(\hat{r}) d^3r \qquad Q_{lm} = \int \rho_s(\vec{r}) r^{-(1+1)} Y_{lm}(\hat{r}) d^3r, \tag{1}$$

respectively, where Y^*_{lm} and Y_{lm} are spherical harmonics and the density functions, $\rho_0(\vec{r})$ and $\rho s(\vec{r})$, correspond to the object and source bodies, respectively. Assuming that both q_{lm} and Q_{lm} are known about a coordinate origin, O, we now wish to know the corresponding inner and outer multipoles about an arbitrary point, $P(r',\theta',\phi')$. To express the moments about P in terms of the moments about O we use relations found in D.A. Varshalovich *et al.*[42] The inner and outer multipole moments about P, respectively, take the following forms:

$$\tilde{q}_{lm} = \sum_{l',m'l,m} \sqrt{\frac{4\pi(2L+1)!}{(2l'+l)!(2l+1)!}} r'^{l'} Y^*_{l'm'}(\hat{r}') C(l',m',l,m,L,M) \delta_{L,l+l'} q_{lm}, \tag{2}$$

$$\tilde{Q}_{lm} = \sum_{l',m'l,m} \sqrt{\frac{4\pi(2l)!}{(2L)!(2l'+1)!}} r'^{l'} Y^*_{l'm'}(\hat{r}') C(l',m',l,m,L,M) \delta_{L,l+l'} Q_{lm}, \tag{3}$$

where C is a Clebsch-Gordan coefficient. These expressions provide analytic solutions for the multipole moments about an arbitrary point in terms of known moments about a given point. The equation for $\tilde{q}_{LM}$ is equivalent to one given in Reference 2.

Here we mention selection rules that are useful in understanding the effects on the multipole moments due to perturbations in the position of the objects. For small displacements the leading order terms in Eqs. 2 and 3 have $l' = 1$. As a result, a small translation of an object with moments q_{lm} and Q_{lm} induces new moments $\tilde{q}_{l+1,m'}$ and $\tilde{Q}_{l-1,m'}$ where $m' = m$ if the displacement is along $\hat{z}$ and $m' = m \pm 1$ if the displacement is in the $x-y$ plane. In second order in the displacement one induces new moments $q_{l=2,m''}$ and $Q_{l-2,m''}$ where $m'' = m$ for displacements along $\hat{z}$ and $m'' = m, m \pm 2$ for displacements in the $x-y$ plane.

These expressions allow one to calculate, without numerical integration, inner and outer multipoles of complex systems. Perhaps more importantly, one can study the effect of perturbations of systems whose unperturbed multipole moments are known and, for example, to center precisely objects in the field of a source using purely gravitational means. Rotations of the spherical multipoles are easily carried out using standard techniques of angular momentum algebra. We addressed the problem of translations.

---

[40] E.G. Adelberger *et al.*, Phys. Rev. D **42**, 3267 (1990).
[41] Y. Su *et al.*, Phys. Rev. D **50**, 3614 (1994).
[42] D.A. Varshalovich, A.N. Moskalev, and V.K. Khersonskii, *Quantum Theory of Angular Momentum*, World Scientific, 1988, p. 167.

2.0 NEUTRINO PHYSICS

2.1 The neutral current detector project at the Sudbury Neutrino Observatory (SNO)

M.C. Browne, T.H. Burritt, P.J. Doe, C.A. Duba, S.R. Elliott, J.E. Franklin, J.V. Germani, K. M. Heeger, R. Meijer Drees, A. Myers, A.W.P. Poon, R.G.H. Robertson, M.W.E. Smith, T.D. Steiger, T. Van Wechel, J.F. Wilkerson and S. Zsitvay.

SNO will detect Cerenkov light emitted from electrons or positrons produced by charged-current neutrino interactions. These measurements will provide a measure of the flux of electron neutrinos from the sun. Neutrinos of any flavor, however, can produce free neutrons in the heavy water by neutral current interactions. Thus the measurement of the neutron production is a measurement of the total flux of neutrinos from the sun. Since solar burning produces only electron neutrinos, a comparison of the total neutrino flux to the electron neutrino flux could provide strong evidence for neutrino oscillations and therefore neutrino mass. The neutral current detectors (NCD's) are ^{3}He filled proportional counters designed to detect such neutrons. These NCD's are made from CVD Ni tubing and endcaps. A quartz tube forms the high voltage and signal feedthrough to a Cu anode wire.

We have received about 300 acceptable 2-meter CVD Ni tubes from Mirotech in Toronto, Canada. The remaining 150 tubes should arrive by June 1997. Recent assay results from LANL of production tubing sampled from standard handling during counter production shows the Th contamination level to be approximately 1 ppt. This level is acceptable in terms of neutral current background.

The various parts needed to assemble endcaps are being fabricated. As they are produced, they are being shipped to IJ Research in Santa Ana, California and being assembled. Severe difficulties were encountered in the transition from prototype to production endcaps at IJ Research. Good solder seals between the silica insulator and the nickel parts were elusive. Although prototype endcaps had worked well, the initial production endcaps were not leak tight. A final assembly jig was delivered to IJ from UW which solved these glass-to-metal seal difficulties. Thus after a significant delay, IJ is beginning full production of endcaps and we received 25 finished endcaps in December. As of January 1997, they are metallizing all of the quartz feethroughs and preparing them for radioassay. Beginning in March, full production should be underway. We measured the temperature change that compromised the glass-to-metal seal on the endcaps. Previous estimates indicated that this temperature change could be as small as 40°C. The measurement indicates that it is actually closer to 100°C which is very good news for shipping logistics. The endcap delays led to a decision to store nickel tubes in the Index adit (northern Washington state) under 800 m.w.e. of rock to reduce cosmic-ray activation. The cleanroom in which the counters will be produced is now continuously monitored and is better than Class 1000 when in use. The production factory is ready to use once endcap production resumes.

The gas handling system for mixing the counter gas is operational. We have begun making counters and they work quite well. This initial batch of counters is intended to be studied underground at the Waste Isolation Pilot Plant facility in southern New Mexico to verify that they are low in radioactivity. The production cable has arrived from South Bay Cable in Idyllwild, California and looks very good both electrically and mechanically. Samples have been characterized optically by UBC and have been radioassayed by direct counting. All parts for the delay lines have been fabricated and assembled. These have all been tested to verify the impedance and testing for microdischarge characteristics under high voltage will soon begin. Using production cable, we have assembled 6 wet-end terminations, which will soon undergo long-term testing under water. Deep Ocean Engineering has delivered the Mark II ROV to Los Alamos for pool tests this summer and fall.

The microdischarge test system is working well and has been installed in the cleanroom. Microdischarge tests have been done for 115 endcap-days at 2200 Volts. Only 10 microdischarge events have been observed. Since the counters will operate at a lower voltage (~1800 V) and most microdischarge events can be identified on an event-by-event basis, this low rate indicates that the endcap electrical breakdown should not result in a significant background for the NC measurement. More details are given elsewhere in this report. Our present production schedule will have all detectors underground in Sudbury by early 1998, ready for deployment that year after a period of cooldown during which cosmogenic ^{56}Co decays away.

2.2 The SNO data acquisition system

Q.R. Ahmad, J.C. Beck, Y. Chan,* S.R. Elliott, M.A. Howe, M. Isaac.* F. McGirt,† R. Meijer Drees, A.W. Myers, T.D. Steiger, T.D. Van Wechel, J.F. Wilkerson and M. Wilson

Our group is responsible for providing the data acquisition (DAQ) system which will read out the signals from SNO's 9557 photomultiplier tubes. The electronics and DAQ system is designed to handle modest background rates in excess of 1 kHz and burst rates in excess of 1 MHz and to have essentially no deadtime, in case of a galactic supernova. The DAQ system is written in an object-oriented programming language (C++), supports the VME bus, and utilizes multiple VME embedded processors (Motorola MVME 167s) for control of the experiment.

The SNO DAQ system supports the readout of the 9557 individual channels via 19 custom 9u "SNO Crates" each containing 16 32-channel front end cards and a crate trigger card. Each SNO Crate is controlled via a SNO Crate translator/controller card that connects the SNO Crate backplane to a 6u VME card located in a standard VME crate, termed an interface crate.

The interface crate contains additional SNO translator/controller cards as well as VME embedded processors directing readout of each crate. Event information is shipped from these crates via VME-to-VME controllers to VME embedded processors located in the primary VME data crate which handle event building, data recording, and shipment of data to the surface. We are currently developing code using Metrowerks' CodeWarrior C++ compiler and the Symantec TCL 1.1.3 class library. The advances made in the general DAQ framework will be addressed in "Extensions to the SNO DAQ Software" (see Section 2.4). The UW is also responsible for testing the custom front-end electronics as they come off of the production chain, and the progress we've made towards the test-stand is discussed in the section "The SNO Electronics Production Testing System" (see Section 2.3).

The last year has seen considerable development on the monitoring side of the DAQ; we have now designed and prototyped the mechanism whereby "live" data can be shipped from a VME-resident cpu to a UNIX workstation running a TCP/IP socket manager called a "Dispatcher", from where it can be further distributed to analysis and visualization programs. The Dispatcher program, developed and in use at CERN, has been installed at NPL and has been extended for use with Macintosh computers. Several prototype analysis and visualization programs have been written, including an HTML interface for automatic updating of a Web page, an event display, an electronics calibration program, and an extended version of the CERN analysis program PAW, tailored for SNO, which can receive events from the Dispatcher and can show updating plots as the data arrives. Our group has also provided code to enable the official SNO offline analysis package (SNOMAN) to be able to hook up to the Dispatcher.

*Lawrence Berkeley National Laboratory, Berkeley, CA.

† Los Alamos National Laboratory, Los Alamos, NM.

2.3 The SNO electronics production testing system

Q.R. Ahmad, J.C. Beck, M.A. Howe, R. Meijer Drees and J.F. Wilkerson

At the time of writing, the design of SNO's data acquisition electronics is complete and the boards have been sent out for manufacture. When this is done (sometime in early April), all components will need to be checked for proper functionality before being used in the detector. Since there are large numbers of certain types of components, SNO is developing an automated system to perform most of this testing.

The University of Washington's SNODAQ group is responsible for writing the software that comprises this automated test system. It is designed to test the 350 Front-End Cards (FECs) which acquire all SNO data, and the 350 High-Voltage Cards (HVCs) which connect the FECs to the 9,557 photomultipler tubes of SNO. The system performs basic analog and digital tests, produces a log of all test results, and decides whether the card is working properly or not. If the card passes the ensemble of tests, then another automated routine will adjust the timing of the electronics for proper operation in the detector. If the card fails, it will be sent to another testing station with the testing log for repairs.

The software for this automated test system is comprised of routines for two programs that run on the Apple Macintosh computer. The SNODAQ application, written in C++, is the interface program for the SNO electronics. One can perform basic operations to the FEC and HVC, and program more complicated tasks with additional C++ routines. The Userland Frontier scripting language controls the flow of the testing and generates the log files with test results.

At the moment, the basic framework of this automated test system is in place. The code for the SNODAQ application has been modified to allow two-way communication between it and Frontier. We have written a group of Frontier scripts that performs a basic set of digital read and write tests on the FEC. These scripts have been useful in debugging the pre-production hardware. Routines which test the ADC pedestal and slopes for all 32 channels of the FEC have recently been added to the SNODAQ code. Soon work will begin on the automated timing setup routines. After that, testing of the electronics will take place at the TRIUMF accelerator facility in Vancouver.

All of the software written for this test system will also be useful for multi-card testing and the final assembly of the electronics on-site in Sudbury.

2.4 Extensions to the SNO DAQ software

Q.R. Ahmad, J.C. Beck, Y. Chan,* S.R. Elliott, M.A. Howe, M. Isaac.* F. McGirt,† R. Meijer Drees, A.W. Myers, T.D. Steiger, T.D. Van Wechel, J.F. Wilkerson and M. Wilson

The Sudbury Neutrino Observatory will use a data acquisition program that has been under development in a generic form for several years by Frank McGirt and John Wilkerson. This program has been undergoing extensive modifications here at NPL. It now has a more Macintosh-like interface and is much more extensible.

The SNO DAQ code is runs on Macintosh computers using C++ compiled with MetroWerks CodeWarrior. The object-oriented nature of C++ allows data acquisition hardware, crate controllers, and other hardware objects to be fully described and encapsulated into software objects which contain a complete interface to that particular piece of hardware. A large number of VME, Camac, and NuBus based hardware modules are supported.

In the original program, the job of collecting, processing, and storing data was done with task objects which were written specifically for each experiment to control the interactions between multiple hardware modules. In some cases, these tasks also had self-contained plotting packages. As a result, these task objects were quite complex and were written by people who were intimately familiar with both the hardware and the underlying framework of the code.

In an effort to simplify the writing of such tasks, the original program was converted to a data-flow model with a new user-interface that allows all objects to be visually represented on the screen as icons with input/output pads. In this model, each object is as simple and self-contained as possible and can either produce, modify, display, or store data packet objects. The flow of data is set up by drawing lines between input/output pads using the mouse. In this way, data analysis chains (i.e. tasks) can be built or modified in seconds simply by adding/removing objects and drawing or moving connection lines. Data processing objects are simple and reusable. For example, an object that does histogramming or plotting only has to be written once and can then be connected into any analysis chain.

While not all of the hardware modules yet support this data-flow model, a number of data process objects have been written. The list includes one and two dimensional histograms, a disk file object, a plotter object, specialized SNO data filters, and even TCP/IP objects to send and receive data over the network. As more of the hardware modules are converted and more processing objects are written, it will become possible to build up non-trivial data collection and analysis chains without writing any code at all.

*Lawrence Berkeley National Laboratory, Berkeley, CA.

† Los Alamos National Laboratory, Los Alamos, NM.

2.5 SNO data acquisition software development

Q.R. Ahmad, J.C. Beck, Y. Chan,* S.R. Elliott, M.A. Howe, M. Isaac.* F. McGirt,† R. Meijer Drees, A.W. Myers, T.D. Steiger, T.D. Van Wechel, J.F. Wilkerson and M. Wilson

The SNO DAQ group is responsible, among other things, for developing the software needed to understand and debug the SNO Front End Cards. Early last year the 32 channel pre-production Front End Cards [FEC32] were delivered to the SNO Electronics group at the University of Pennsylvania (UPenn). Given the necessity to understand the electronics thoroughly in order to write software for it we spent many months at UPenn working closely with the Electronics group. During that time we developed the essential software tools required to interface to the hardware. These tools were developed under our "Object Oriented Software Bus" (OSB) architecture, which has been outlined in last years' Annual Report.

The FEC32 resides in a custom SNOBus Crate, which has been designed to minimize the VME bus electronics noise. Two custom made translator hardware modules, XL1 and XL2 respectively, provide the link between the VME bus and SNOBus. The SNOBus Crate consists of a XL2, 16 FEC32s and a Crate Trigger Card. The XL1 resides in the VME Crate. In order to interface to the SNOBus Crate a software module called SNTR[SNO Translator] was developed. This enables the user to interface to any hardware members of the SNOBus Crate. We have used this software module to perform low level debugging of the pre-production cards. We have made the user interface intuitive and have made it flexible enough so that new tools could be added with ease. Recently the electronics group, after debugging the pre-production FEC32, has submitted the FEC32 for final production. The SNTR module will be used in our Test Stand System which is under development to test, verify and characterize all production electronics cards.

We have also developed another software module called SMTC [SNO Master Trigger Card] which interfaces to the Master Trigger Card. This is now being used at UPenn to debug the card. Recently we received the Master Trigger Card from UPenn and we are in the midst of integrating it into our system. Very soon we will have all the primary electronics components at NPL and that will no doubt help us shake down the Electronics/DAQ system.

In addition to writing software for debugging electronics we have also developed algorithms for taking data, building events and then writing those events to disk. Currently these software tools have been developed on 68K and Power PC stations. In the final system all primary DAQ activities will take place in embedded processors [eCPUs] which reside in VME. We are currently in the process of migrating these tools to eCPUs.

---

*Lawrence Berkeley National Laboratory, Berkeley, CA.

† Los Alamos National Laboratory, Los Alamos, NM.

2.6 Progress on the acrylic vessel for the Sudbury Neutrino Observatory

P.J. Doe and the SNO collaborators

December, 1996 saw the completion of the upper hemisphere of the acrylic heavy water containment vessel for the SNO. The upper hemisphere and chimney, comprising 60% of the total vessel, is now suspended in position from its 10 Vectran ropes. Construction of the lower hemisphere has begun. This represents a major milestone in the progress to a complete and operating observatory. Achieving this milestone proved to be far more difficult than anticipated; however, valuable lessons were learnt which are being applied to the construction of the lower hemisphere.

SNO Institute personnel and physicists are responsible for: 1) positioning and surveying the acrylic panels from which the vessel is built prior to bonding them together; 2) postcuring (heat treating) the bond joints; 3) finishing joints (sanding and polishing) after the panels have been postcured; 4) maintaining cleanliness throughout construction. The company contracted to build the vessel (Reynolds Polymer Technology, Inc.) is responsible for bonding the panels together.

The first four of the five rows of acrylic panels comprising the upper hemisphere were installed between November 1995 and April 1996. Problems were encountered while bonding the fifth and last row. These were attributed to unexpected technical difficulties and inadequate quality control of the bonding operations. To overcome this, a dedicated R&D team was formed from members of the collaborating institutes to develop techniques to carry out the necessary repairs to the bonds. In addition the QA/QC (Quality Assurance/Quality Control) program was reviewed and reorganized. For each of the construction activities listed above, an activity leader from the SNO institutes has been appointed. That person is responsible for developing the QA program for his activity and ensuring that it is rigorously adhered to. The activity leaders report to an overall QA activity leader for the vessel. These measures are an important component in ensuring the timely and successful completion of the acrylic vessel.

By December 1996 the upper hemisphere and chimney of the vessel were complete and the process of removing all the scaffolding, jigs and fixtures begun. In January 1997, the upper hemisphere was raised 45 feet on its construction platform and suspended in its final position from 10 Vectran ropes. The special jigs and fixtures for constructing the lower hemisphere were then erected on this platform and the bonding of the first row of panels of the lower hemisphere has begun.

The schedule calls for the completion of the acrylic vessel by 18 June 1997. Throughout this period, Peter Doe, as group leader for the acrylic vessel will continue to direct the various activity leaders and to function as activity leader for bonding and bonding R&D. Hardy Seifert, Visiting Scientist on the UW faculty from October 1996 to July 1997, has been working with Peter in Sudbury on the SNO bonding R&D team, and many of the SNO group at UW have spent some months on site at Sudbury working to overcome the thorny problems encountered with the vessel construction.

2.7 Development of a compact 20 MeV gamma-ray source for energy calibration at the Sudbury Neutrino Observatory

M.C. Browne, R.J. Komar,* N.P. Kherani,† H.B. Mak,# A.W.P. Poon, R.G.H. Robertson and C.E. Waltham*

We are developing a compact 20 MeV gamma-ray source for energy calibration at the Sudbury Neutrino Observatory (SNO). The gamma-rays are produced in the $^{3}\mathrm{H}(\mathrm{p},\gamma)^{4}\mathrm{He}$ radiative capture reaction. The design and the operational characteristics of the source can be found in our previous reports.[1]

We have built the final source to be used in the SNO detector. In Fig. 2.7-1, a photograph of the source is shown. The tritium target used in the source was fabricated at the tritium facility at Ontario Hydro Technologies in Toronto, Canada. The target fabricated was a scandium tritide thin film on a molybdenum substrate. Prior to the target fabrication, the substrate was chemically cleaned and etched to enhance film adhesion. A scandium film of ~10000Å was evaporated. To ensure a good tritium-to-scandium stoichiometric ratio, the scandium film was tritiated *in situ*. The substrate was heated up to 400°C by an internal heater installed in the evaporation system. Tritium was let into the system and was pumped by the scandium film. Once the scandium film had been saturated by the tritium, the temperature of the substrate was slowly brought down to anneal the film.

After the target fabrication and its mounting in the source, the source was brought to Queen's University in Kingston, Ontario for testing. A 12.7cm(Ø) x 7.62 cm BGO crystal with an active cosmic veto was used to detect the 20 MeV gamma-rays. A 12.7cm (Ø) x 5.1 cm liquid scintillator with active cosmic-ray veto was used to monitor the neutron production rate by pulse shape discrimination. The neutrons are produced from $^{3}\mathrm{H}(\mathrm{t},\mathrm{nn})^{4}\mathrm{He}$ and $^{3}\mathrm{H}(\mathrm{d},\mathrm{n})^{4}\mathrm{He}$ reactions. Analyses are being done on the data. Preliminary results of an eight-hour, 25 keV beam energy run show that in the energy window of 18 to 20 MeV, we see gamma-rays at 8.7σ above the background. In Fig. 2.7-2, a background subtracted energy spectrum for the eight-hour run is shown. This analysis indicates that the source generates ~1 gamma per second. Neutrons were also observed coming from the source.

In the near future, we plan to make a gamma-ray angular distribution measurement with this source here at NPL.

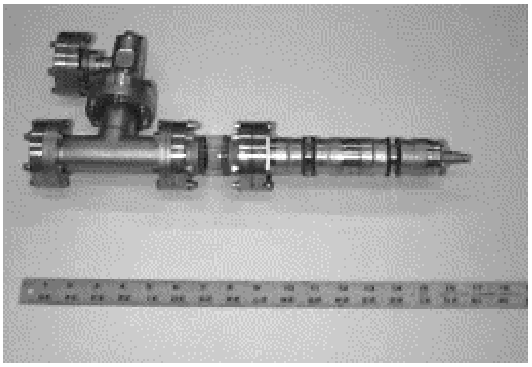

Fig. 2.7-1. A photograph of the $^{3}\mathrm{H}(\mathrm{p},\gamma)^{4}\mathrm{He}$ source. The ion discharge magnet is removed here in order to display the source body.

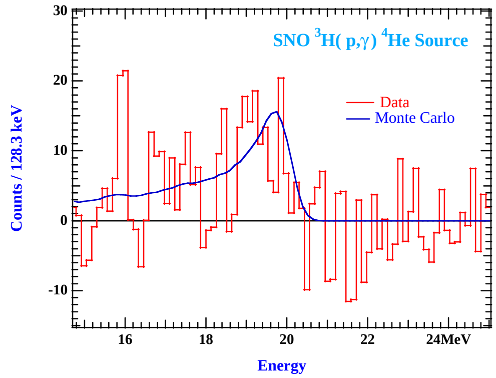

Fig. 2.7-2. Background subtracted energy spectrum of the eight-hour test run. The Monte Carlo spectrum is superimposed on the data.

---

* Department of Physics and Astronomy, University of British Columbia, Vancouver, BC, Canada V6T 1Z1.

†Ontario Hydro Technologies, 800 Kipling Avenue, Toronto, Ontario, Canada M8Z 5S4.

#Department of Physics , Queen's University, Kingston, ON, Canada K7L 3N6

[1]Nuclear Physics Laboratory Annual Report , University of Washington, (1994) p. 10; Nuclear Physics Laboratory Annual Report, University of Washington, (1995) p 22.

3.0 NUCLEUS-NUCLEUS REACTIONS

3.1 Preequilibrium particle emission and the GDR in Sn Nuclei

M.P. Kelly, J.P. Lestone J.F. Liang, K.A. Snover, A.A. Sonzogni and J.P.S. van Schagen

The proper analysis of GDR γ-ray spectra produced in heavy-ion collisions depends on the characterization of the hot nuclei produced in heavy-ion collisions. Our current GDR decay studies[1] involve 10 MeV/nucleon projectiles. We report the results of a study of preequilibrium particle emission in $^{18}O+^{100}Mo$ collisions in the region of 10 MeV/nucleon bombarding energy and the effects of this emission on the excitation energy of the fused compound system.

Measurements of light charged particles produced in $^{18}O+^{100}Mo$ collisions at 169 MeV and 200 MeV bombarding energy and measurements of evaporation residues for the same reaction from 100 MeV to 217 MeV bombarding energy were performed at the University of Washington Nuclear Physics Laboratory using the FN Tandem Van de Graaff as injector for the Superconducting Linear Accelerator. These studies allow us to accurately determine the average excitation energy and fusion cross section for compound nuclei formed in $^{18}O+^{100}Mo$ collisions.

Analysis of particle spectra for $^{18}O+^{100}Mo$ at 200 MeV bombarding energy indicate that on the average, 0.27 ± 0.06 protons and 0.45 ± 0.07 α-particles are lost due to preequilibrium emission. We infer from comparison with model calculations that 0.87 neutrons are lost as well. As a result, the average excitation energy of the fused system is decreased by approximately 20% relative to complete fusion. In addition, evaporation residue measurements show that the default fusion cross section often used in the statistical model code CASCADE[2] underpredicts the true (complete + incomplete) fusion cross section by nearly 20% at the same energy.

Results of statistical model calculations incorporating the experimentally determined fusion cross sections and excitation energies indicate that both the deduced GDR width and strength are significantly affected by the energy loss due to preequilibrium emission, while the deduced centroid energy remains relatively unchanged. In fact, it was found that if one neglects the effects of preequilibrium emission in $^{18}O+^{100}Mo$ collisions at 200 MeV bombarding energy, one determines both a GDR width and a strength that are 15%-20% lower than those deduced from a proper analysis which accounts for preequilibrium emission. A more detailed account of these studies is being submitted to Physical Review C.

[1] Nuclear Physics Laboratory Annual Report, University of Washington (1996) p. 25.

[2] F. Puhlhofer, Nucl. Phys. A **280**, 267 (1977).

3.2 Quasi-elastic and fusion barrier distributions for $^{40}Ca+^{46,48,50}Ti$

J.F. Liang, J.P. Lestone, M.P. Kelly, A.A. Sonzogni and R. Vandenbosch

It has recently been suggested that fusion information can be derived from quasi-elastic scattering at near-grazing angles.[3] Since fusion excitation functions were measured and barrier distributions derived for $^{40}Ca+^{46,48,50}Ti$,[4] an experiment to obtain quasi-elastic excitation functions was performed to compare the different barrier distributions results. The quasi-elastic events were detected with a set of Si detectors, placed at angles close to the grazing angle. Energy and time of flight information was used to distinguish between the different classes of events. The quasi-elastic barrier distributions were obtained by using the relation:[1] $D_{qel}(E) = -d/dE\left(\frac{d\sigma_{qel}}{d\sigma_{Ruth}}\right)$. The results can be seen in Fig. 3.2-1, together with the fusion results. A good agreement between them is seen.

Because of these results and those of references 1 and 3, one concludes that this technique can provide barrier distributions which closely resemble those from fusion data. This can be usefully exploited when trying to probe fusion enhancement with radioactive beams, where the beam flux is too small to be used in fusion cross section measurements at near-barrier energies.

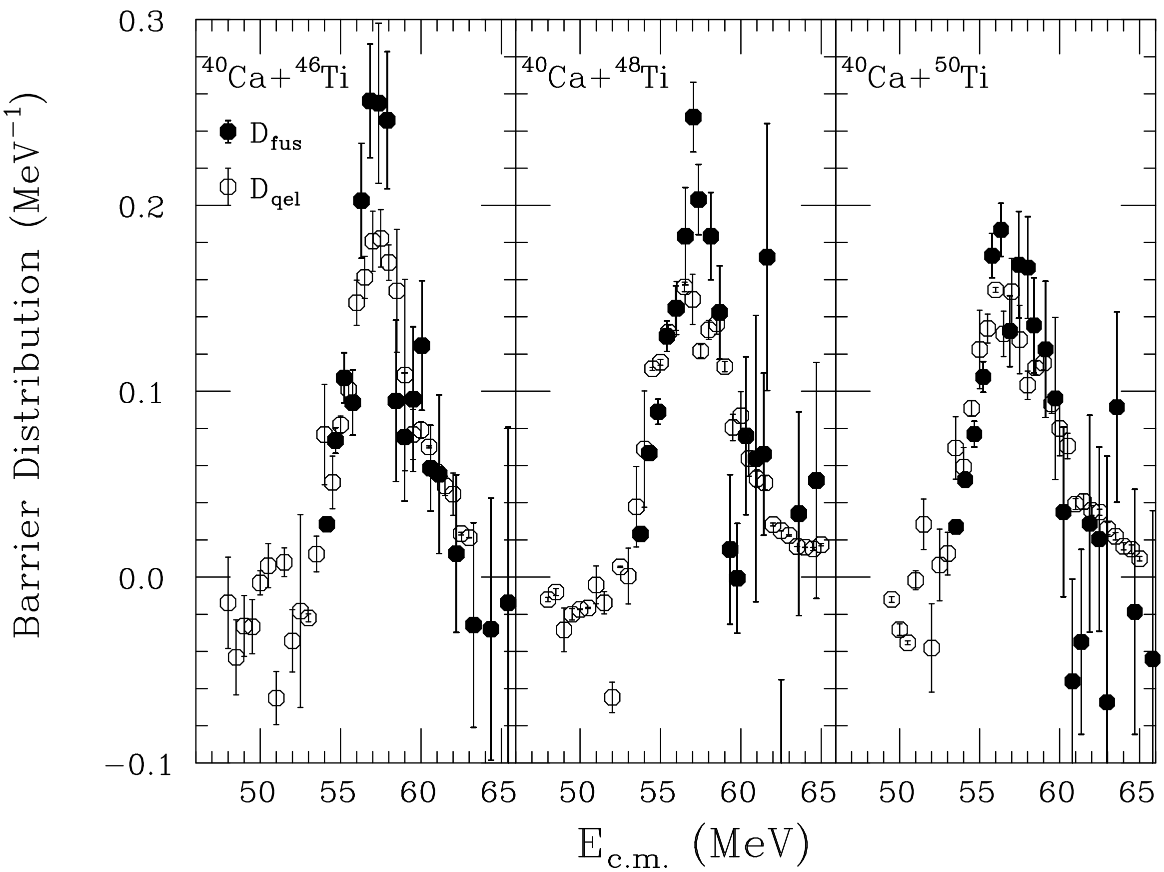

Fig. 3.2-1. Fusion and quasi-elastic barrier distributions for $^{40}Ca+^{46,48,50}Ti$.

[3] H. Timmers *et al.*, Nucl. Phys. A **584**, 190 (1995).
[4] Nuclear Physics Laboratory Annual Report, University of Washington (1996) p. 27.
[3] H. Timmers *et al.*, Instituto Nazionale di Fisica Nucleare, Laboratori Nazionali di Legnano, Annual Report (1995) pp. 88-90.

3.3 Projectile mass dependence of fission fragments anisotropies for heavy-ion induced fission on ^{232}Th at near-barrier energies

J.F. Liang, J.P. Lestone, M.P. Kelly, A.A. Sonzogni and R. Vandenbosch

Fission fragment angular distributions and angular correlations were measured for ^{16,18}O + ^{232}Th at near barrier energies. A brief description of the experimental technique can be found in Section 3.4 of this report. The folding angle distributions were used to separate a transfer-fission component. The percentage of transfer-fission to total fission was similar for both oxygen isotopes (~8-12% at near barrier energies).

The anisotropy results can be seen in Fig. 3.3-1, together with those of ^{19}F+^{232}Th,[5] ^{11}B,^{12}C+^{232}Th (see Section 3.4). It can be seen that for a given bombarding energy relative to the Coulomb barrier, the anisotropy increases smoothly with projectile size. No discontinuity in the fission dynamics, due to the mass asymmetry of the system, can be seen in this plot.

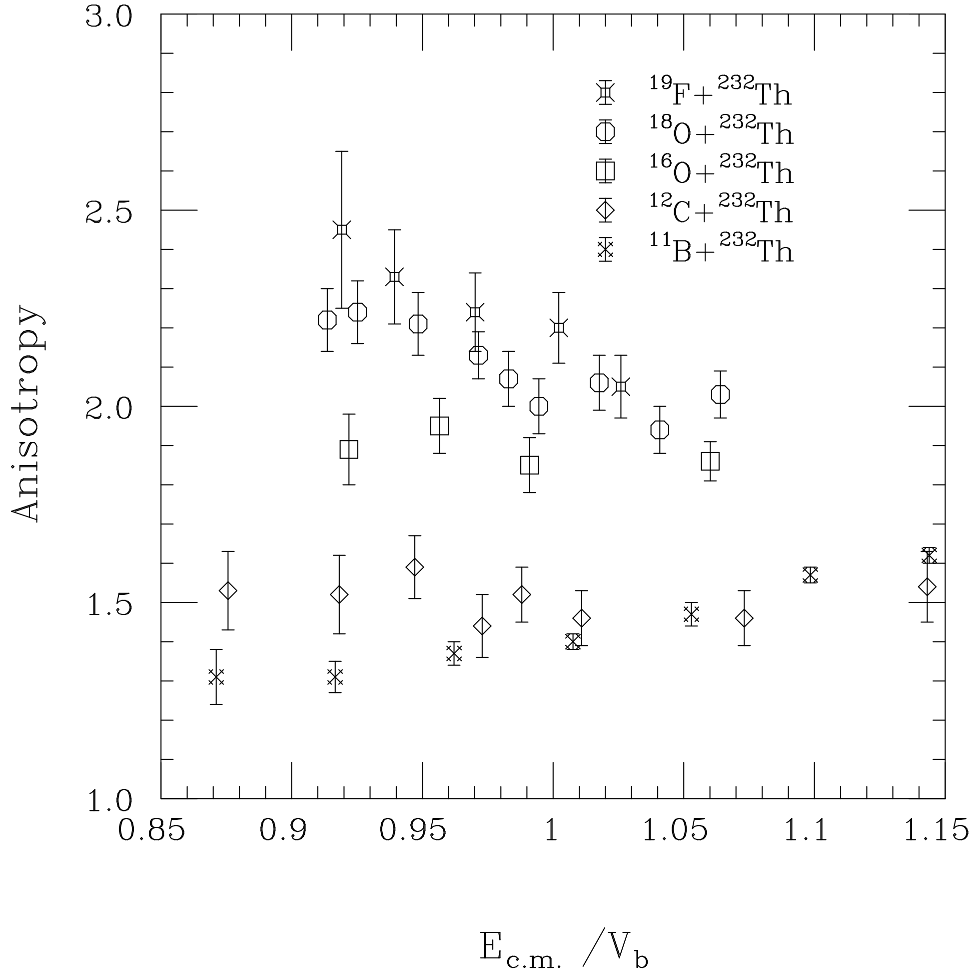

Fig. 3.3-1. Fission fragment anisotropy as a function of $E_{c.m.}$ / V_b for ^{11}B, ^{12}C, ^{16,18}O and ^{19}F+^{232}Th.

[5] N. Majumdar *et al*., Phys. Rev. C **51**, 3109 (1995).

3.4 Fission fragment anisotropies in the ^{11}B, $^{12}C+^{232}Th$ reactions

M.P. Kelly, J.P. Lestone, D.J. Prindle, A.A. Sonzogni and R. Vandenbosch

Majumdar *et al.*[6,7] have recently published measurements of the anisotropies of fission fragments following fusion reactions with ^{11}B, ^{12}C, ^{16}O and ^{19}F projectiles on ^{232}Th. These measurements show unexpected peaklike structures in the anisotropies as a function of center of mass energy in the near- and sub-barrier energy regions. The ^{16}O and ^{19}F measurements are made difficult by the presence of a significant yield of fission following transfer reactions at near- and sub-barrier energies. However, for reactions involving ^{11}B and ^{12}C projectiles on Th, the transfer-fission yield is small enough that the anisotropy of fragments following full momentum transfer can be obtained by simply measuring the singles fission fragments at all but the lowest beam energies.[1,8]

We have measured the angular distribution of fission fragments in the $^{11}B+^{232}Th$ and $^{12}C+^{232}Th$ reactions, using beams from the University of Washington superconducting linac. The target consisted of a $225\mu g/cm^2$ layer of $^{232}ThF_4$ evaporated onto a 100 $\mu g / cm^2$ Ni foil. Fission fragments were detected with Si surface barrier telescopes and identified using energy and time-of-flight information. Folding angle distributions were obtained by observing fission fragments in Si telescopes and the complementary fragments in a large area position sensitive Si detector. Our folding angle distributions contain a single peak and confirm that the fission yield in ^{11}B, $^{12}C+^{232}Th$ reactions is dominated by fission following complete fusion. Fig. 3.4-1 compares our fission fragment anisotropies to those of other authors. Our anisotropies vary smoothly with center of mass energy and give no hint of the peaklike structures reported in References 1 and 2. In view of our results we feel that the conclusions drawn in Reference 1 should be viewed with caution.

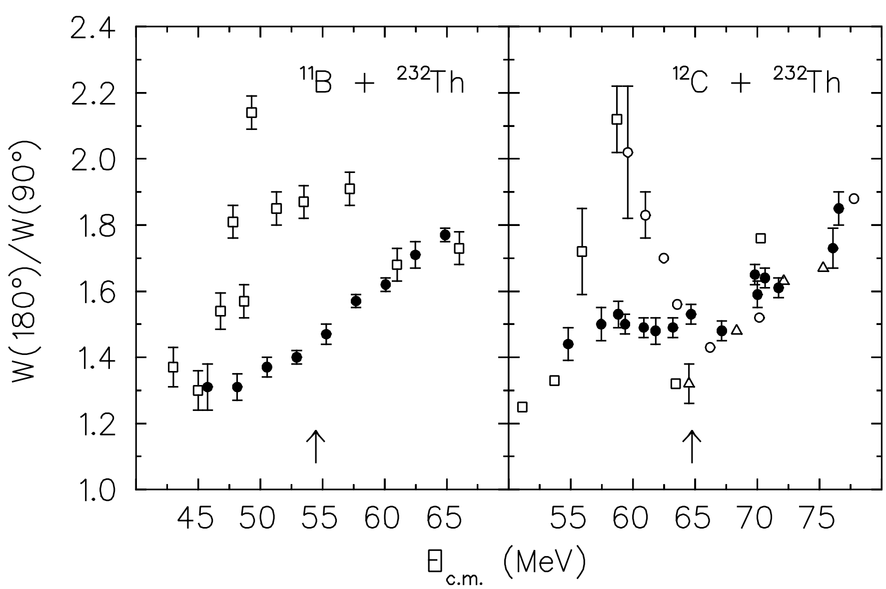

Fig. 3.4-1. Fission fragment anisotropies for the ^{11}B, $^{12}C+^{232}Th$ reactions. The solid circle shows the present work; (open squared);[1,2] (open circles);[4] and (open triangles).[5] To avoid over crowding of this figure only representative error bars have been shown for the $^{12}C+^{232}Th$ data of Majundar *et al.*,[2] Karnik *et al.*[9] and Ramamurthy *et al.*.[10] The up arrows show the positions of the B+Th and C+Th fusion barriers.

---

[6] N. Majumdar *et al.*, Phys. Rev. Lett. **77**, 5027 (1996).
[7] N. Majumdar *et al.*, Phys. Rev. C **53**, R544 (1996).
[8] J.P. Lestone *et al.*, Phys. Rev. C. **55**, R16 (1997).
[9] A. Karnik *et al.*, Z. Phys. A. **351**, 195 (1995).
[10] V.S. Ramamurthy *et al.*, Phys. Rev. Lett. **65**, 25 (1990).

3.5 Search for an entrance channel dependence of fission anisotropies

M.P. Kelly, J.P. Lestone, A.A. Sonzogni and R. Vandenbosch

In recent years several authors claim to have seen an entrance channel dependence of fission anisotropies [$A = W(180°) / W(90°)$] for target projectile combinations across the Businaro-Gallone (BG) ridge in the mass asymmetry degree of freedom.[11,12] To remove any effects due to the difference in fissility of different compound nuclei, it is necessary to study reactions that form the same compound nuclei with different entrance channel mass asymmetries. At above barrier energies, Vandenbosch *et al.*[13] found no entrance channel dependence of the fission anisotropies for ^{248}Cf compound nuclei formed in the two reactions ^{12}C+^{236}U and ^{16}O+^{232}Th which span the BG ridge. We present here a study of these two reactions at near- and sub-barrier energies. Fission fragment cross sections, angular distributions and folding angle distributions were measured using ^{12}C and ^{16}O ions from the University of Washington superconducting linac. In the ^{16}O+^{232}Th reaction, corrections due to transfer fission were made using our fission fragment folding angle distributions. Our ^{12}C+^{236}U folding angle distributions are consistent with the fission yield being dominated by fusion-fission events. To remove the influence of the differing amounts of angular momentum brought in by the projectiles and the different fusion barriers (V_B) for the ^{12}C+^{236}U and ^{16}O+^{232}Th reactions the quantity $4(A_{exp}-1)K_0^2/<J^2>$ has been estimated as a function of the center of mass energy relative to the fusion barrier $E_{c.m.} / V_B$ using the present experimental results and those of other studies[3,14] (see Fig. 3.5-1). The mean square spin of the compound nuclei $<J^2>$ was estimated as a function of the center of mass energy using calculations that reproduce our measured fission cross sections. Values of $4(A_{exp}-1)K_0^2/<J^2> \neq 1$ indicate a departure of the experimental anisotropies from the values predicted by the transition state model. Our analysis suggests the anomalous behavior of anisotropies increases smoothly as the center of mass energy drops through the region of the fusion barrier independent of the entrance channel mass asymmetry.

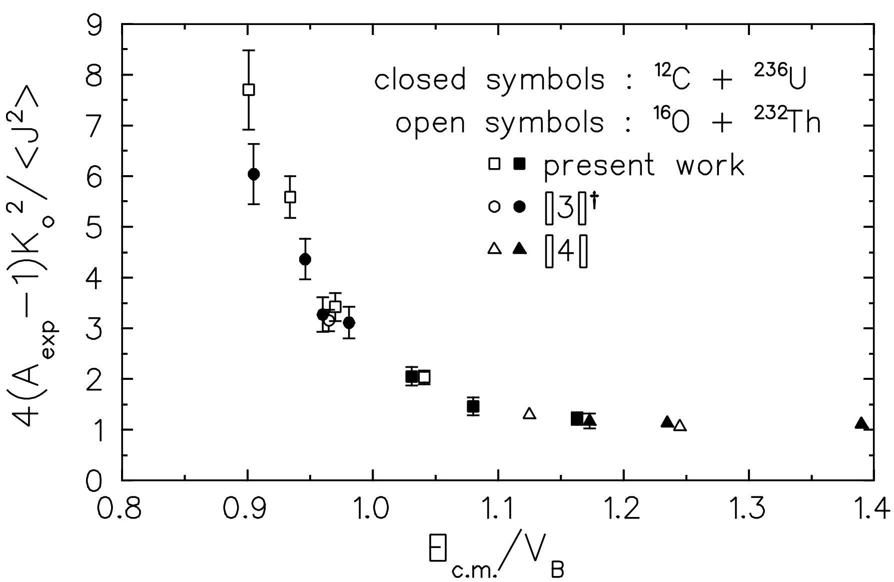

Fig. 3.5-1. $4(A_{exp}-1)K_0^2/<J^2>$ as a function of $E_{c.m.} / V_B$. † The ^{16}O+^{232}Th point of Reference 4 has been corrected using the transfer fission measurements of Lestone *et al.*[15]

---

[11] V.S. Ramamurthy *et al.*, Phys. Rev. Lett. **65**, 25 (1990).
[12] N. Majumdar *et al.*, Phys. Rev. Lett. **77**, 5027 (1996).
[13] R. Vandenbosch *et al.*, Phys. Rev. C **54**, R977(1996).
[14] T. Murakami, *et al.*, Phys. Rev. C **34**, 1353 (1986).
[15] J.P. Lestone *et al.*, Nucl. Phys. A **509**, 178 (1990).

3.6 Influence of target spin on sub-barrier fission fragment anisotropies

M.P. Kelly, J.P. Lestone, A.A. Sonzogni and R. Vandenbosch

Liu *et al.*[16] recently observed that the sub-barrier fission anisotropies in the ^{11}B+^{237}Np reaction are substantially lower than the corresponding anisotropies in the ^{16}O+^{232}Th reaction. It is claimed that this entrance channel effect is due to the Businaro-Gallone ridge in the mass asymmetry degree of freedom. This conclusion is, however, not supported by a similar comparison of ^{12}C+^{236}U and ^{16}O+^{232}Th fission anisotropies (see Section 3.5). Another possible explanation of the large differences in the ^{11}B+^{237}Np and ^{16}O+^{232}Th anisotropies is the 5/2 spin of ^{237}Np and the 3/2 spin of the ^{11}B. At beam energies well above the fusion barrier the angular momentum brought in by the projectile in sufficiently large that the spin of the target and/or projectile can be neglected. At sub-barrier energies where the fusion spins are smaller it is possible for target/projectile spins to have a noticeable effect. To test this possibility we measured the fission anisotropy for the three reactions ^{12}C+^{235,236,238}U, as a function of center of mass energy (see Fig. 3.6-1). Measured folding angle distributions for all three reactions confirm that the fission yields are dominated by fusion-fission events. At above barrier energies the three different ^{12}C + U reactions have comparable anisotropies. At sub-barrier energies the ^{12}C+^{236,238}U reactions have anisotropies of ~1.6, while the fission anisotropies for the ^{12}C + (7 / 2 spin)^{235}U reaction decrease with decreasing center of mass energy to values well below 1.6. This is strong evidence for an influence of target spin on sub-barrier fission anisotropies. The magnitude of our observed sub-barrier target spin effect requires a preferential reaction with the tips of the deformed target nucleus at low energies and some remembrance of the K of the target ground state.

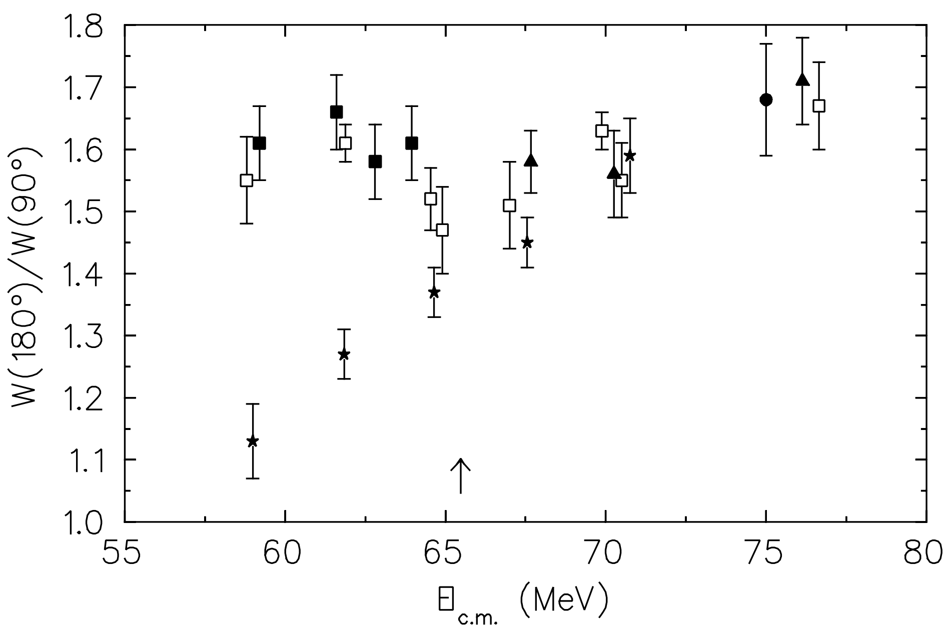

Fig. 3.6-1. Fission fragment anisotropies of the three reactions ^{12}C+^{235}U,^{236}U and ^{238}U. The open squares, closed triangles and stars show the present results with ^{238}U,^{236}U and ^{235}U targets respectively. The solid squares and circles show the ^{236}U target results of Murakami *et al.*[17] and Vandenbosch. *et al.*[18] The up arrow shows the position of the C+U fusion barrier.

[16] Z. Liu *et al*., Phys. Lett. B **353**, 173 (1995).
[17] T. Murakami *et al*., Phys. Rev. C **34**, 1353 (1986).
[18] R. Vandenbosch *et al*., Phys. Rev. C **54**, R977 (1996).

4.0 ULTRA-RELATIVISTIC HEAVY IONS

4.1 Event simulation of high-order Bose-Einstein and Coulomb correlations

J.G. Cramer and D.D. Weerasundara

Last year we reported[1] the initial development of a new Monte Carlo event generator program for simulating the high-order multiparticle correlations between pions produced in ultra-relativistic heavy ion collisions. The program uses a new Monte Carlo elimination algorithm that employs the multiparticle correlation formalism developed in a recent paper[2] to impose Bose-Einstein and Coulomb correlations of up to 6th order on the $\pi^{\pm}$ particles of a simulated event.

Tests of a preliminary version of this code in event simulations showed an unexpected "Bose-Einstein cooling" effect in the generated particle spectrum, with increasing correlation order producing a dramatic decrease of the particle spectrum's inverse-slope or "temperature" parameter. Further, the 2-particle correlations extracted by analyzing the simulated events showed a tendency toward runaway to Bose-Einstein condensation as the correlation order used in the simulation was increased from 2 to 6. Since no such runaway effect is apparent in NA49 data (which should contain true BE and Coulomb correlations up to order 250 or so), there was a puzzling discrepancy between theoretical simulation and experimental data.

The root of these problems was recently discovered to be the basic *ansatz* that the full multiparticle correlation of a "candidate" particle with its nearest neighbors in momentum space is proportional to the probability of acceptance or "wave function collapse" of that particle. This is discussed in another article (see Section 4.2) in which it is shown from quantum mechanical arguments that a new "reduced correlation function" must be used to determine the acceptance or rejection of candidate particles in the rejection algorithm.

An improved Monte Carlo event generator program **sim_hbt_10** has been developed and is now debugged and running. It includes several significant improvements over the old code: 1) it simulates Bose-Einstein effects in the rejection algorithm using partially-coherent reduced correlation functions generated by *Mathematica*; 2) it uses Coulomb correlation functions obtained from 6-dimensional Monte-Carlo integration of Coulomb wave functions over the source (see Section 4.3) to take into account the finite source size; 3) when *N* particles are used in the BE correlation it now includes about *2N-1* particles in the Coulomb correlation; 4) it explicitly includes the effects of the pion "halo" from long-lived resonances decaying well beyond the surface of the primary pion freezout source; and 5) it explicitly includes the effects of mis-identified "contaminant" particles.

The first calculations with this new code indicate that the unphysically strong Bose-Einstein effects described above are no longer present. In the new calculations there is no apparent tendency toward BE condensation runaway in the system as the correlation order is increased. We are continuing these investigations. We will soon use the new code to produce a library of simulated events under various conditions of source multiplicity, size, resonance fraction, and contamination that approximate the conditions of experiment NA49 and the planned STAR experiment.

[1] Nuclear Physics Laboratory Annual Report, University of Washington (1996) p. 37.

[2] J.G. Cramer and K. Kadija, Phys. Rev. **53**, 908 (1996).

4.2 Wave function collapse: Schrödinger's Cat and HBT simulations

J.G. Cramer

In an ultra-relativistic collision between heavy nuclei leading to the emission and detection of a large number (*M*) of pi mesons, the quantum mechanics of Bose-Einstein statistics requires that when the measurement of the system is made by the detector (e.g., the NA49 time projection chambers) the full *M*-pion wave function of the event must collapse to a fully symmetrized *M*-particle state. On the other hand, in a cascade-type Monte-Carlo simulation that attempts to include Bose-Einstein effects (see Section 4.1) the particles can only be produced and accepted sequentially, one at a time. This is the quantum-mechanical equivalent of making a new measurement each time a particle is produced.

Parts (*a*) and (*b*) of Fig. 4.2-1 illustrate the difference between these two quantum mechanical situations, with horizontal lines representing measurements and downward arrows representing created particles. This difference leads to a version of the Schrödinger's Cat paradox: repeated measurements of the cat's condition (by repeatedly peeking into the cat box) lead to a different quantum condition from that which would have existed if the cat was left unobserved until the final measurement. In computer simulations we are forced to "peek into the cat box" with the production of each new particle, thereby distorting the quantum result.

This qualitative difference between the simulation and the actual quantum condition has two important consequences: 1) it affects the choice of the correlation function used in selecting candidate particles; and 2) it introduces an order-asymmetry in particle treatment that must be "annealed out" by the destruction as well as creation of particles.

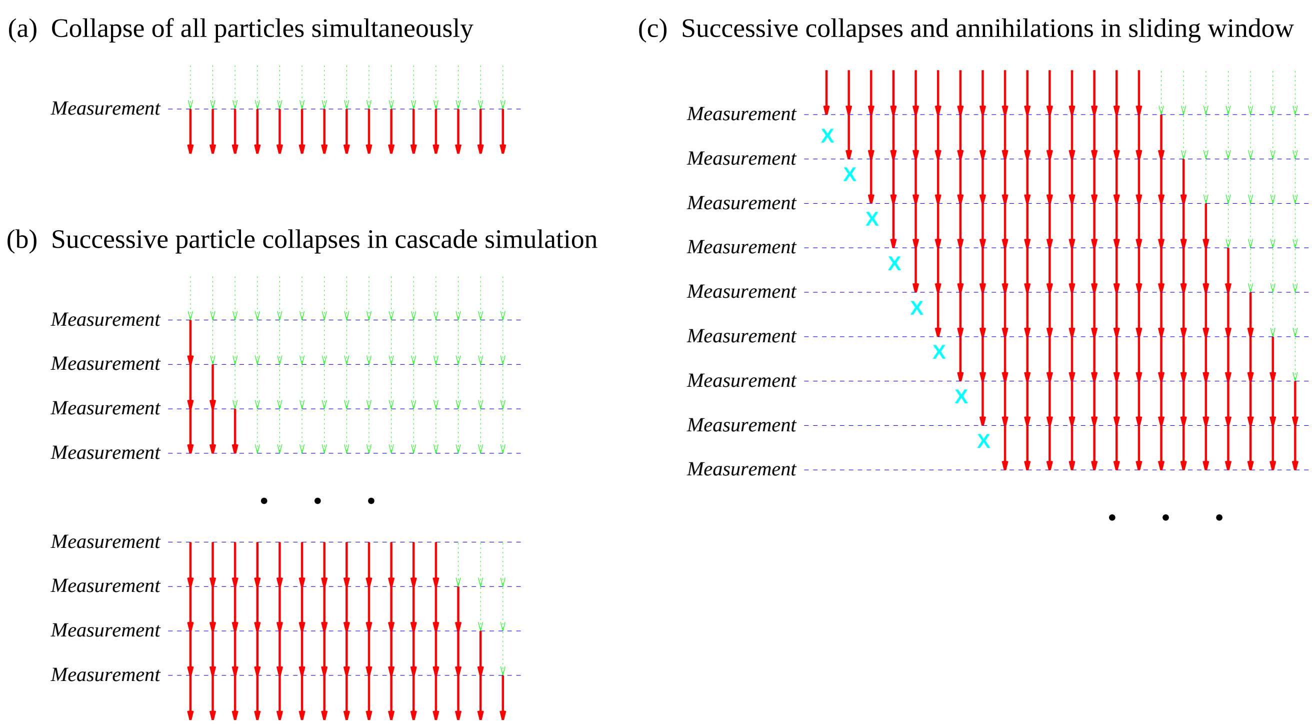

Fig. 4.2-1. Comparison of wave function collapse modes.

First let us consider the choice of the correlation functions. The multiparticle momentum-space correlation function R_M of order M (i.e., the correlation between M identical particles) is defined by the relation:

$$R_M(\vec{p}_1,\ldots\vec{p}_M) = \frac{\rho_M(\vec{p}_1,\ldots\vec{p}_M)}{\rho_1(\vec{p}_1)\ldots\rho_1(\vec{p}_M)}, \tag{1}$$

where $\rho_M(\vec{p}_1,\ldots\vec{p}_M)$ is the inclusive probability density for M particles expressed as a function of the three-momenta $\vec{p}_i$ of the correlated particles, and $\rho_1(\vec{p}_i)$ is the single particle probability density of the *i*th particle.

This function can be interpreted as the relative probability of measuring a particular momentum-space configuration $(p_1, p_2,\ldots p_M)$ of the M particles. If we were able to collapse the full wave function of an M particle event with a single measurement, then R_M could be used to select among full M-particle candidate events in a Monte-Carlo rejection algorithm. This, however, is not computationally feasible.

In Monte-Carlo simulations, in effect, we "measure" or select candidate particles one at a time in the presence of other pre-existing previously measured particles. In this circumstance it is not appropriate to use R_M as the probability of the resulting momentum-space configuration because it include contributions from pre-existing particles that do not "connect" with the candidate particle. The relative probability of a new momentum space configuration with the new particle added is the difference between new M particle configuration and the old M-1 particle configuration. This leads to a "reduced correlation function" S_M, as defined by:

$$S_M(i, j, k\ldots, M) = 1 + R_M(i, j, k\ldots, M) - R_{M-1}(j, k,\ldots, M), \tag{2}$$

where i is the index of the candidate particle and $j,k \ldots,M$ are the indices of its M-1 nearest neighbors. Using the reduced correlation function in selecting among candidate particles insures that the spurious probability enhancements from clusters that are distant or of opposite charge do not influence the correlation generated. We note that the when all particles have the same momentum, the reduced correlation function reaches its maximum value of S_M (*max*) = M! - (M-1)! + 1, which has the values 2, 5, 19, 97, and 601 for M = 2, 3, 4, 5 and 6, respectively. Simulations of Bose Einstein effects should use this distribution function in accepting or rejecting particles.

To deal with the second problem mentioned above, that of annealing out the order-asymmetry in particle treatment, we have devised a "sliding window" technique illustrated in part (*c*) of Fig. 4.2-1. For an event of multiplicity M, we first pre-fill the momentum space with M-1 uncorrelated particles. The generation of the Mth particle and succeeding ones then proceeds by "killing" one old particle as each new particle is accepted. In effect, each new particle is only correlated with particles within a "sliding window" of width M-1. This procedure is repeated for 2M+1 steps, so that a total of 3M particles have been generated. However, only the last M particles generated are retained in the event.

We have implemented both of these procedures in a new program and are currently testing them. The initial results are very encouraging and indicate that Monte-Carlo simulation leading to a good approximation of a state with a fully symmetrized M particle wave function is feasible.

4.3. Finite Coulomb size and finite resolution effects in NA49 mixed-charge pion correlations

J.G. Cramer

In ultra-relativistic 160 GeV/nucleon heavy ion collisions between lead nuclei at CERN, the size of the pion source produced is large enough (6-8 fm) that the pointlike Coulomb interaction between pions (i.e., a Gamow penetrability) must be modified to take into account the finite size of the source of pions. Therefore, it is important to determine the Coulomb radius of the source before generating the Coulomb corrections used in performing Hanbury-Brown-Twiss analysis on experimental data from experiments like NA49.

Partly to investigate this issue, an analysis of the $\pi^+\pi^-$ correlations has been made by the NA49 collaboration from data measured with the NA49 vertex TPCs.[3] The $\pi^+\pi^-$ correlation offers the advantages that it is an enhancement at low relative momentum (while the $\pi^-\pi^-$ correlation is a suppression) there is no Bose-Einstein effect between non-identical particles to modify the Coulomb effects, and the attenuation of the Coulomb effect by pions from resonances are about the same in $\pi^+\pi^-$ and $\pi^-\pi^-$ Coulomb correlations.

The effect of the finite source size on the Coulomb correlation between charged pions can be calculated by integrating the two-particle Coulomb wave function of the pions over the spatial distribution of the source. The programs **pipibig** and **pipipm** were written by Pratt[4] to calculate the finite-size Coulomb effects for $\pi^-\pi^-$ and $\pi^+\pi^-$ correlations, respectively. The programs as written, however, did not allow for the uncertainty in momentum determination in experimental data, which smears out and reduces the strength of the Coulomb effects at low relative momentum. We have therefore modified the Pratt programs to include the resolution effects.

A sample of the $\pi^+\pi^-$ correlation data of Appelshauser was fitted with the modified **pipipm** program, varying the Coulomb radius and the resolution width to obtain an optimum fit. The results are shown in Fig. 4.3-1, which plots the ratio of experimental data points to values from the **pipipm** calculation, with the parameters R_{Cou} = 6.7 fm and Δp = 6.0 MeV. A perfect fit would be a raio of 1.0. As can be seen, the deviations are very small.

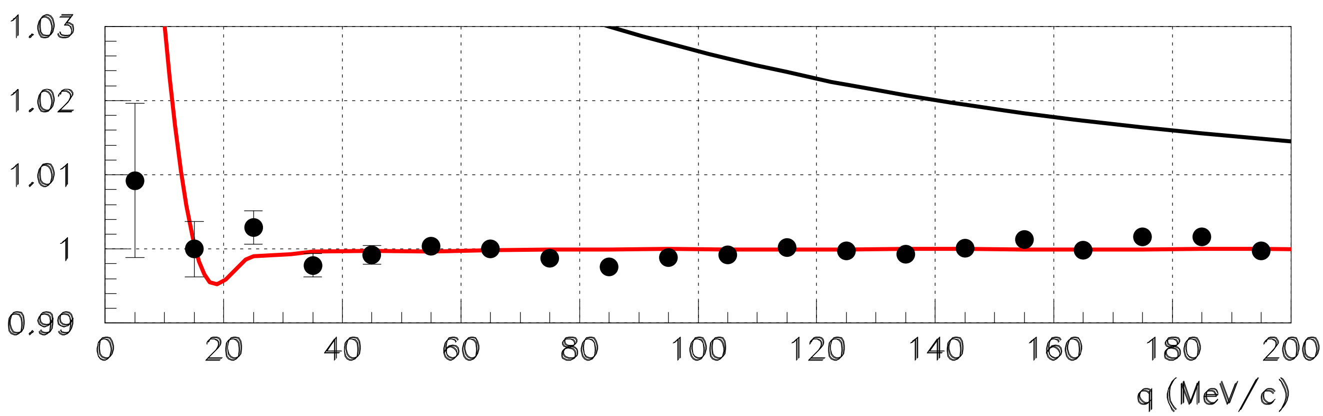

Fig. 4.3-1. Ratio of $\pi^+\pi^-$ correlation data to calculated finite-size Coulomb correlation. The curve through the points is the Coulomb correlation without resolution smearing. The upper line is the Gamow penetrability.

---

[3] H. Appelshauser, Ph.D. thesis, University of Frankfurt, Germany (1996).

[4] S. Pratt, private communication (1992).

4.4 Phase space filling systematics and superradiance in ultrarelativistic heavy ion collisions

J.G. Cramer

Collisions of ultra-relativistic heavy ions produce a spatial volume that is for a time densely populated with Bose-Einstein particles, i.e. pions. It is therefore interesting to consider whether the number density in position-momentum phase space is large enough to produce the dramatic phenomena associated with Bose-Einstein statistics: superradiance, stimulated emission, lasing, and Bose-Einstein condensation.

Bertsch[5] has shown that under the assumptions of a simple but plausible model for heavy ion collisions the filling factor $< f >$ for cells of volume $\hbar^3$ in position-momentum phase space for a given collision event is:

$$< f > = \sqrt{\frac{\pi}{2}} \frac{dN_{\pi^-}}{dy} \frac{(\hbar c)^3}{R'_\ell R'_s R'_o T^3} \tag{1}$$

Here N_{π^-} / dy is the multiplicity of π^- particles per unit rapidity, R'_ℓ R'_s, and R'_o are the longitudinal, side, and out radii of the pion source, respectively, using the NA35 convention for source radii, and T is the characteristic "temperature" or (inverse-slope parameter) of the transverse mass distribution of the pions. Replacing dN_{π^-} / dy with the charged particle multiplicity dN_{ch} / dy and using the commonly accepted NA44/NA49 convention for source radii (R'(NA35) = R(NA49)/$\sqrt{2}$), expression becomes:

$$< f > = \frac{\sqrt{\pi}}{8} \frac{dN_{ch}}{dy} \frac{(\hbar c)^3}{R_\ell R_s R_o T^3} \tag{2}$$

Experiments using HBT interferometry on a number of colliding heavy ion systems over a wide range of particle masses and collision energies have revealed certain systematics for the colliding systems: (1) the characteristic temperature T ranges between 150 and 190 MeV; (2) the side and out radii are approximately equal, while the longitudinal radius is perhaps 20% larger; (3) defining the transverse radius R_t as the average of R_s and R_o, over a wide range of multiplicities $R_t \cong 0.9[dN_{ch} / dy]^{1/3}$. If we accept this relation and take $R_\ell / R_t \cong 1.2$, then the phase space filling factor becomes $< f > \cong 0.24[\hbar c / T]^3$. For a typical mid-range temperature of T = 170 MeV, $< f > \cong 0.38$. This value scales as $[(170\text{ MeV})/T]^3$ at other temperatures.

This value of $< f > \cong 0.38$ is an extremely large filling factor. It is to be compared with Bertsch's value for the onset of superradiance which is $< f >_{crit} \cong$ 0.11 to 0.13. However, $< f > \cong 0.38$ is probably an overestimate because not all of the pions come directly from the source. It is estimated that about 25% of the pions observed in a lead-lead collision at CERN come from long-lived resonances that decay well away from the collision point and would not participate in the phenomena of Bose-Einstein statistics. Correcting for this resonance fraction gives $< f > \cong 0.28$, still more than twice the calculated value of $< f >_{crit}$.

This estimate indicates that heavy ion collisions over a wide range of conditions produce Bose-Einstein systems which have number densities leading to superradiance and stimulated emission. We are investigating experimental analysis techniques for observing these effects.

[5] G.F. Bertsch, Phys. Rev. Lett. **72**, 2349 (1994).

4.5 Coulomb radii for STAR single event physics?

J.G. Cramer

The STAR detector at RHIC will begin operation in 1999. One analysis theme of the new detector will be a program of "event-by-event" physics, in which events exhibiting some unusual characteristic are grouped in an ensemble that is then subjected to further analysis, in search of unusual physics. It is expected that each Au+Au collision at RHIC will produce several thousand charged pions, and it remains an open question whether this particle multiplicity is sufficient to gain some indication of the characteristic source size of a single event through correlation analysis.

Last year we examined the question of whether two-particle or three-particle Bose-Einstein correlations provide the best indicator of single-event source size[6] and showed that two-particle correlations are always statistically superior. Now we are considering a similar comparison of $\pi^+\pi^-$ vs $\pi^-\pi^-$ correlations as indicators of single-event source size. In the RHIC environment it is expected that the size of the source will be at least twice as large as that found in the lead-lead collisions at CERN, i.e., in the range of 12 to 16 fm. For sources of this size, the like-charge Bose-Einstein momentum-space correlation for $\pi^-\pi^-$ and $\pi^+\pi^+$ is forced into the small relative momentum region where it is strongly suppressed by Coulomb repulsion.[7]

On the other hand, mixed-charge $\pi^+\pi^-$ correlations offer several distinct advantages for estimating single-event source size: 1) The number of opposite-charge pairs is n^2 vs. $n(n\text{-}1)$ like-charge pairs, giving slightly better statistics; 2) the $\pi^+\pi^-$ Coulomb correlation is a strong enhancement which is guaranteed to have better statistics than the like-charge correlation at the lowest relative momentum; 3) the $\pi^+\pi^-$ go to well separated parts of the TPC, so there is no need for a low-q cut when the tracks merge and are unresolved; and 4) while the $\pi^+\pi^-$ Coulomb correlation is somewhat suppressed by Coulomb size effects (see Section 4.2), that suppression is less severe than that of the like-charge Bose-Einstein correlation. Fig. 4.5-1 compares the predicted $\pi^+\pi^-$ correlation for Coulomb radii of 0 (Gamow), 6 fm, 12 fm, and 18 fm. We take this as an indication that size estimation from single event $\pi^+\pi^-$ Coulomb correlations may be possible. In the coming year we will use the simulation code **sim_hbt_10** (see Section 4.1) to investigate this question further.

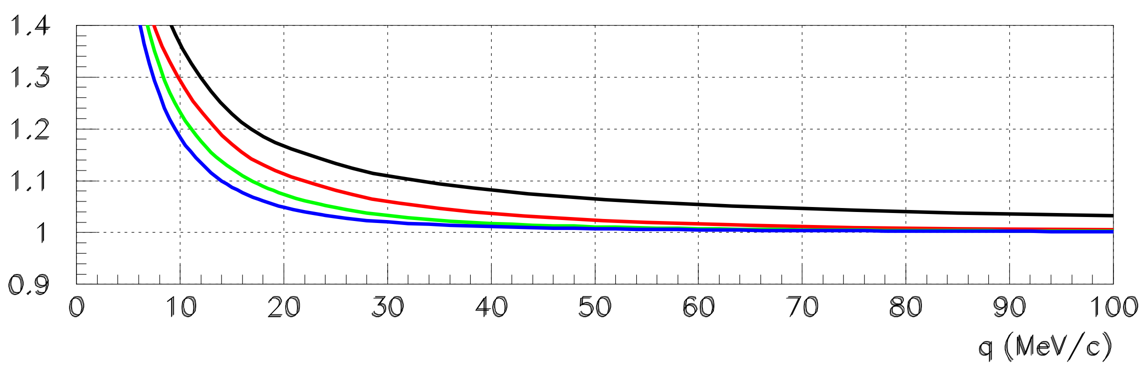

Fig. 4.5-1. Comparison of $\pi^+\pi^-$ correlations with R_{Cou} = 0 (high), 6, 12, and 18 fm (low).

[6] Nuclear Physics Laboratory Annual Report, University of Washington (1996) p. 38.
[7] J.G. Cramer, Phys. Rev. C **43**, 2798 (1991).

4.6 Application of SControl to the STAR TPC gas system

J.G. Cramer and M.A. Howe

The time projection chamber (TPC) for the STAR detector is nearing completion at LBL and will be transported by air to Brookhaven for installation at RHIC in October-November of this year. One critical component of the STAR TPC is the gas system, which supplies a mixture of helium and ethane to the TPC and monitors gas purity, pressure, temperature, and other relevant parameters.

We are adapting the program **SControl**[8,9] developed as the NA49 slow control monitor and alarm console for use with the STAR gas system. The project involves developing a version of **SControl** that will operate on a Sun workstation and linking the TPC gas system console, a PC running under Windows 95, the EPICS system which is the NA49 standard for slow control, and **SControl** as the top-level system communicating with the PC and the overall EPICS system.

We plan to test this system during the cosmic ray tests of the STAR TPC, which will be in progress from May-September, 1997.

[8]Nuclear Physics Laboratory Annual Report, University of Washington (1996) p. 45.
[9]Nuclear Physics Laboratory Annual Report, University of Washington (1995) p. 57.

4.7 Event-by-event physics at the SPS and RHIC

S. J. Bailey,* D.J. Prindle, J.G. Reid, C. Reynolds, T.A. Trainor and D.D. Weerasundara

Event-by-event physics in nuclear collisions has been an active field of research for more than a decade. Jet production in p-p and e-e collisions and flow in heavy-ion collisions have been extensively studied at LEP, CSPS, TEVATRON, BEVALAC and AGS among other facilities. Jets and flow are large-amplitude and/or large-scale effects which are detectable despite the rather small particle multiplicities per event from these collision systems. Multiplicities have been limited by small system size (p-p, e-e) or low energy densities (heavy ions). Both jet and flow phenomena are manifestations of symmetry reduction or increased correlation with respect to a nominally thermalized system of produced particles.

With the recent availability of a 158 GeV/nucleon lead beam at the CERN SPS one obtains (due to larger system size and increased energy density) substantially increased event multiplicities which can provide sensitivity to smaller-amplitude symmetry reductions over a finite scale interval. This increased statistical power permits event-by-event study of global thermodynamic variables and the possibility to extend this analysis program beyond global or large-scale variables to a scaling analysis approach. This additional analysis capability is needed to explore fully so-called soft or nonperturbative QCD phenomena.

NA49 event-by-event analysis has proceeded on two complementary fronts: large-scale or global event-variable analysis -- based primarily on a thermodynamic approach, and scaled correlation analysis of momentum space which attempts to extend the event-by-event concept over a range of scales limited only by event multiplicity. There is also a flow analysis program underway.

Examples of global variables are $< P_t >$, K / π ratios, m_t-spectra slope parameters and some measure of the width of the rapidity distribution about the CM (for each species). These quantities all measure in some way the ‘boundedness’ of the phase-space distribution in momentum and flavor composition. One looks for deviations of the distributions of these variables from an event-mixed or other reference population or for correlations among global variables.

With the larger collision systems and energies at SPS and RHIC, event multiplicity (statistical power) becomes sufficiently great to extend global-variable analysis by using more detailed measures of the correlation content of the phase-space distribution. At the SPS the total pion multiplicity for 158 GeV/nucleon Pb-Pb collisions is more than 1000, making it worthwhile to pursue a more detailed analysis for this particle species. At RHIC, multiplicities of 5000 or more in the STAR acceptance are expected.

The UW group has pioneered a scaled correlation analysis technique for extracting all available information from a multiparticle distribution. The basic measure of this technique is scaled dimension transport, an elaboration of standard entropy-based topological measures on point sets. This technique has been applied to the STAR detector trigger algorithm production, jet-finding and electromagnetic calorimeter analysis, and NA49 event-by-event analysis (see Section 4.8). In the last case a population of anomalous events at the part-per-mil level has been detected in a sample of 200k events, illustrating the sensitivity of this model-independent approach.

* Now at Harvard University, Cambridge, MA.

4.8 Scaled correlation analysis applied to NA49 main TPC data

D.D. Weerasundara and T.A, Trainor

QCD theory predicts the formation of color deconfined quark matter in the ultrarelativistic heavy ion collisions at the CERN SPS, RHIC and LHC energies. Event-by-event analysis of multiparticle distributions produced in these collisions is widely recognized as a promising way to look for the formation of color deconfinement. We have developed a multiparticle event-by-event scaled correlation analysis based on Renyi entropy[10] to extract as much information as possible to search for rare phenomena produced in these collisions.

The NA49 experiment provides an ideal test bed to further develop this correlation analysis. As part of the preparation for the large-scale DST production of NA49 data, we have analyzed ~200,000 events of main TPC (MTPC) data during 1996, using the large scale production computing facility (SHIFT) at CERN. The production of this DST sample serves two purposes. First it tests the robustness of the event reconstruction software, helps to develop calibration data bases and refine the DST production scripts. Secondly and most importantly, it provides a sufficiently high-statistics data sample to develop and test various physics analysis software.

In order to have a manageable data volume (a few gigabytes) for the physics analysis, we have created from these DSTs, a set of mini-DSTs containing a minimal set of essential information relevant to our correlation analysis, which is being carried out at the UW-NPL HP-UX computer facility (see Section 4.13).

We have performed scaled correlation analysis on the transverse mass spectra extracted from particle trajectories reconstructed using the MTPC-only data. For this analysis, we assume all the measured charged particles to be pions. For each event, scaled correlation analysis generates a set of measurements, namely, rank-q Renyi entropy (S_q, q = 1,2,3), scale derivative of entropy: information (I_q) and scale derivative of information: dimension lowering (Δd_q) as a function of scale for scales in the range [-4,2]. For the calculation of I_q and, Δd_q, we generate for each run (*i.e.*, a set of ~10k events), a reference entropy $\bar{S}_q$ as a function of scale by taking the ensemble average of the measured event entropy for that run period. Subsequently, an event space is formed in polar coordinates (r,θ,ϕ) by taking Δd_q at three different scale points (x,y,z). Each point in this space represents an event. r is a measure of deviation from the reference and (θ,ϕ) represents the "shape" of this deviation.

In order to look for events with highly correlated structure, we compare real data to a set of Poisson events with constant m_T slope and track multiplicity distribution identical to that from real data. Comparison of Poisson and real data yields a set of anomalous events in real data at the 1 part per mil level. We find that the distribution from this special class of events exhibit a higher yield in the range $0.6 \le m_T \le 1\mathrm{GeV}/\mathrm{c}^2$, compared to normal events from real data as well as Poisson events.

The fact that we have used MTPC-only data limits our ability to select high quality tracks; hence the physics interpretation of the observed signal remains ambiguous. Reconstruction of global tracks that combines information from all four TPCs will allow us to use high quality tracks in our analysis. However, we conclude that from the present results that scaled correlation analysis of multiparticle distributions proven to be a powerful tool to search for rare events in NA49 data.

---

[10] Nuclear Physics Laboratory Annual Report, University of Washington (1996) p. 36.

4.9 STAR trigger interval review

J.G. Reid and T.A. Trainor

On June 6-7, 1996 the STAR current trigger effort was reviewed and approved intact. Our contribution to this was primarily the recently developed level-2 algorithms using scaled correlation analysis. However, the level-1 autocorrelation techniques that have been in place since 1995 were also discussed.

The STAR trigger relies on data coming from five different sub-detector systems. First, there are vertex position detectors which consists of 48 Cherenkov radiators. Second, there is a central trigger barrel consisting of 240 scintillator slats placed cylindrically about the interaction region covering $-1 < \eta < 1$ and $0 \le \phi \le 2\pi$. Third, and most important because of its fine segmentation in η, is the multiwire proportional counter which is about 8000 TPC anode wires covering $-1 < |\eta| < 2$. Fourth, two hadron calorimeters operating collectively as a veto calorimeter. Finally, there is an electromagnetic calorimeter (1200 EM modules) covering η from -1 to 1. Our trigger studies rely most heavily on scaled correlation analysis of data from the CTB and MWCs giving a total coverage in η from -2 to 2.

The most significant problem encountered in the level-2 trigger was the trigger processor time constraint. The scaled correlation analysis we have developed requires the data set of interest to be sampled using binning systems of a range of sizes (we call this range the scale window). Also, to avoid aliasing effects we need to resample the data set several times at each bin size. Due to this sampling and resampling of the data, our analysis is very CPU time intensive. Since the time constraint for the level-2 trigger in STAR is 5ms we were forced to develop a subset of the full analysis that maintains most of the discriminating power, but is several orders of magnitude faster.

To meet these runtime challenges we performed the full analysis on simulated data and identified a few points in the scale window where we expect most of the data's correlations to be. Rather then looking at the entire scale window we concentrate on three main points. We also turned down the resampling at each scale level, allowing in some noise, but not enough to overwhelm the final results. Finally, after some code optimization we were able to meet the timing requirements.

In performing the full scale window analysis on simulated data sets we discovered the negative effects of charge integration in the MWCs (as opposed to hit counting). We found that the charge integration method suffers from Landau fluctuations which degrade the trigger quality significantly. Our analysis showed conclusively that to maintain trigger integrity we must implement hit counting in favor of charge integration in spite of the extra expense.

4.10 DCC simulations

J.G. Reid, T.A. Trainor and D.D. Weerasundara

Among the proposed phenomena associated with QCD symmetry restoration the disoriented chiral condensate (DCC) serves as a paradigm. If chiral symmetry restoration occurs within the highest energy-density regions of the collision volume the distinction among pion species is predicted to be lost there. In the subsequent cooling process this symmetric state may decay preferentially into a particular isospin state over some finite volume, resulting in nonstatistical deviations of the neutral pion fraction from its usual value (1/3) in some regions of phase space.

The observability of the DCC phenomenon hinges on both the thermodynamic trajectory of the collision process and the observability of the soft-pion component of the particle spectrum. Observable DCC effects seem to depend on significant departure from an equilibrium thermodynamic trajectory (during the cooling phase) according to current model calculations. And manifestation of a DCC in particle spectra is expected to occur only for transverse momenta near or below the pion mass. In general, neutral and charged pions are not observed with the same detector components, there are significant low-momentum detection thresholds, and phase-space acceptance overlap for these two species may be incomplete, giving rise to the possibility of significant systematic error. Nevertheless, theoretical and experimental studies of this phenomenon are being vigorously pursued.

An initial event-by-event DCC analysis (CERN experiment WA98) utilizes the total yields of neutral and charged particles for each event, distributed on a 2D scatter plot. This distribution shows a significant linear correlation corresponding to correlated variations of the two species with total event multiplicity. The event-by-event signal of interest is the degree of deviation from the correlation axis. This deviation is equivalent to a variation in the N_γ / N_{ch} ratio, or the neutral particle fraction, as a global event variable. Excessive fluctuation (beyond counting statistics) of this deviation from the correlation axis could be an indication of an anomalous neutral-to-charged pion ratio resulting from DCC formation. No statistically significant DCC signal has been observed in a preliminary analysis.

In order to evaluate the optimum analysis procedure for a DCC search, and indeed to determine whether DCCs are observable at all with the available experimental apparatus and conditions, we have undertaken a simulation program using scaled correlation analysis as the diagnostic measure. Fig. 4.10-1 summarizes the preliminary results of this study for the STAR detector at RHIC.

While about 5000 particles fall into the acceptance of STAR, of these only about 1400 pions lie in the “soft-pion” region of the p_t spectrum (and about 700 neutral pions detectable only by the electromagnetic calorimeter). We have examined the observability of several DCC scenarios having different scaling behavior. The outcome of this study will be a characterization of the sensitivity limits of the STAR detector in terms of DCC scaling structure and amplitude.

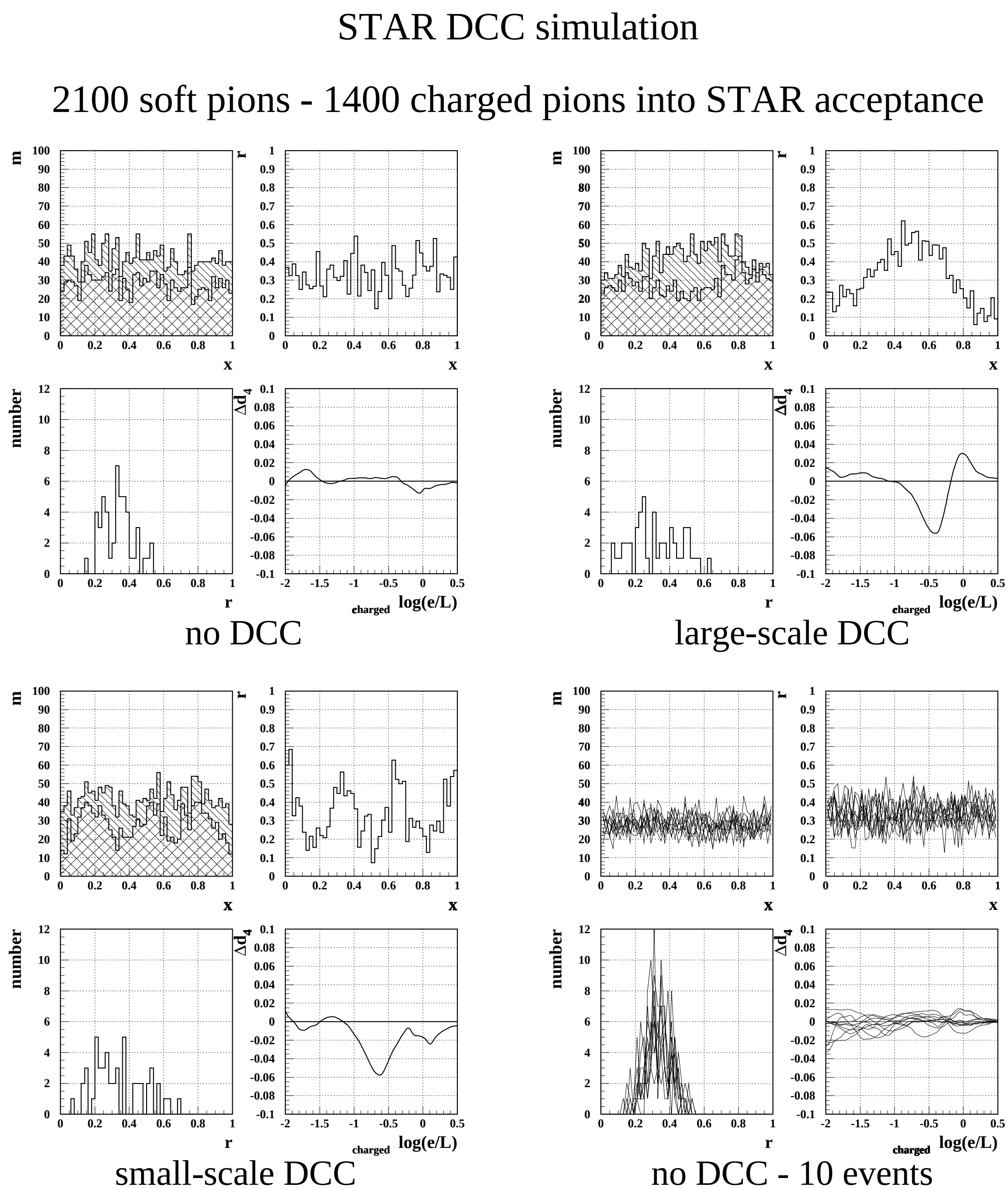

Fig. 4.10-1. DCC simulations showing charged and neutral pion single-event multiplicity m distributions on an arbitrary parameter x with no DCC structure, large-scale structure and small-scale structure. In each case the neutral pion fraction r is also plotted on x. The frequency distribution on r is plotted, and the corresponding dimension transport Δd(e) is shown. At bottom right is an ensemble of 10 events without DCC structure to provide a measure of statistical fluctuations.

4.11 Human face recognition by scaled correlation analysis

Q.R. Ahmad, J.G. Reid and T.A. Trainor

We have been developing a very general analysis system for use in the STAR trigger as well as for data analysis in STAR and NA49. Since the analysis is a general method of identifying relative correlations in data sets it can be easily applied to the problems of image analysis and comparisons. One exciting application we have begun to explore is human face recognition. However, since we are using a scaled analysis we can also probe the more difficult problem of identifying smaller scale correlations in the faces in our data set, namely looking for correlations between the similar expressions (i.e., smiling, frowning) as made by different people. This problem is also being approached using neural network methods so we can compare our results to a standard approach, and try to better understand the true nature of our analysis and neural network methods.

The data we used in this preliminary study was a set of 24 images taken by CCD camera. There are pictures of five different people in this data set, each person making five different expressions (except one person who only makes four). Our goal in analyzing this data was two-fold. First, we wanted to be able to distinguish between the people in the images, so if we were given another photo of a member of the ensemble we could identify which one it was. Second, we examined the small scale region to see what correlations were apparent.

We were very successful in distinguishing between the members of the ensemble. After analyzing the data and forming a phase space we found the data for each individual to lie clustered in a region of the space. Identifying individual's expressions as being similar was inconclusive and we have decided to postpone this analysis until we have a larger data set to work with. Unfortunately, the neural network analysis is still incomplete, so we have yet to do the analysis system comparison.

The face recognition analysis could also benefit from a larger data set, and in the future we would like to get a significant amount of data (~1000 images of ~50 people). A system of masking off everything in the image but the person's face would also be beneficial. Some measures were taken to do this in the existing data set, cropping the photos above the neck and having the subjects wear shower caps to make their hair look more uniform, but much more could be done here. Our results from this study were very exciting and we plan to pursue it further in the future.

4.12 NA49 distortion corrections and system geometry

T.A. Trainor, D.D. Weerasundara, and the NA49 Collaboration*

System geometry of the NA49 TPC system consists of: 1) an idealized mechanical representation of the system (geometry data base), 2) corrections to this idealization required by mechanical, electronic and other functional departures from the ideal (distortion correction data base and parametrizations), 3) determination of the effective time dependent drift speed,[11] 4) determination of the large scale alignment of the system with a multitarget tracking procedure[12] and 5) confirmation of the accuracy and consistency of the system geometry with global tracking across the enter TPC system.

The geometry data base contains an idealized mechanical representation of the TPC system. To complete the conversion from the raw data to the space points in the survey system, a measured system of distortions, represented parametrically or in supplementary data bases, must be removed from the transformed data. Knowledge of these distortions can be inferred from laser tracks, grid pulser calibration data and straight tracks in the TPC system. The distortion system in the horizontal and vertical planes are substantially different.

Vertical distortions have three sources: 1) spatial equivalent of time offsets in the pad electronics ranging up to 500 μm for which a correction data base is obtained with a grid pulser system; 2) mechanical distortion of the top plate and the individual sectors and pad-plane PC boards ranging up to 500 μm: correction data base obtained from straight track residuals; and 3) large-scale spatial drift speed variations across the TPC volume ranging up to 1 mm near the TPC walls and caused by electric field inhomogeneity arising from top plate deformations: correction data base obtained from tracking residuals, electric field calculations, reconstructed event vertex systematics and laser data.

Horizontal distortions have two sources: 1) mechanical misalignments of pad-plane PC boards during gluing operations ranging up to 100μm -- correction data base derived from straight track residuals and 2) effective charge transport of up to 1 mm near sector boundaries and electric field inhomgeneities near the top plate - parametric correction derived from reconstructed event vertex systematics.

Assuming that the internal representation space of for each subdetector is made distortion free to an acceptable degree, a multitarget alignment procedure[13] is performed to determine the positions and the orientations of various subdetectors with respect to each other and to an absolute reference system. The final system geometry has been completely determined and the NA49 experiment has begun the large-scale DST production from 1995 experimental run data.

* CERN, Geneva, Switzerland.

[11] Nuclear Physics Laboratory Annual Report, University of Washington (1996) p. 42.

[12] Nuclear Physics Laboratory Annual Report, University of Washington (1996) p. 43.

[13] Nuclear Physics Laboratory Annual Report, University of Washington (1996) p. 43.

4.13 Large volume NA49 data analysis at UW-NPL

C. Reynolds, R.J. Seymour, T.A. Trainor and D.D. Weerasundara

URHI group recently upgraded its offline computer system with the addition of three new HP 9000/780 model C180 unix boxes, one 5 slot 2500-XT DLT tape robot, one single slot 2000-XT DLT tape drive and three 9 gigabyte Seagate ST19171WD SCSI disks. Fig. 4.13-1 shows a schematic diagram of the hardware configuration of the new system. These three machines use NFS to share 12 gigabytes of internal disks and the 27 gigabyte logical disk giving a total disk capacity of 39 gigabytes in addition to the existing ~18 gigabyte disk capacity. The three HP machines provide cpu power (3x17.2SPECfp95 and 3x10.8SPECint95) comparable to that of a ~10x200MHz Pentium Pro processor farm. The HP C180, being a 64-bit machine, can handle very large (~100 gigabytes) of disk volumes, the three 9 gigabyte disks are mounted as a single 27 gigabyte logical disk volume which enables us to handle files with large data volumes. This is another advantage over Pentium Pro (32-bit) machines which cannot handle disk volumes with tens of gigabytes.

NA49 higher level offline data analysis is one of the several computation-intensive research projects (see Section 4.1) that utilize this system. The NA49 experiment produces ~10 terabytes of raw data (~one million events) per year. A factor of 10 data reduction is achieved at the first level DST production (on the SHIFT computer facility[14]) yielding one terabyte of reconstructed data. Another factor of 10 in data reduction is achieved by creating miniDSTs which contain selected information relevant to higher level physics analysis. This results in ~100 gigabytes of miniDST data volume that fits onto 10 DLT tapes. We estimate that we could analyze ~1 million miniDST events with the scaled correlation analysis (see Section 4.8) in ~30 days on our local offline computer facility.

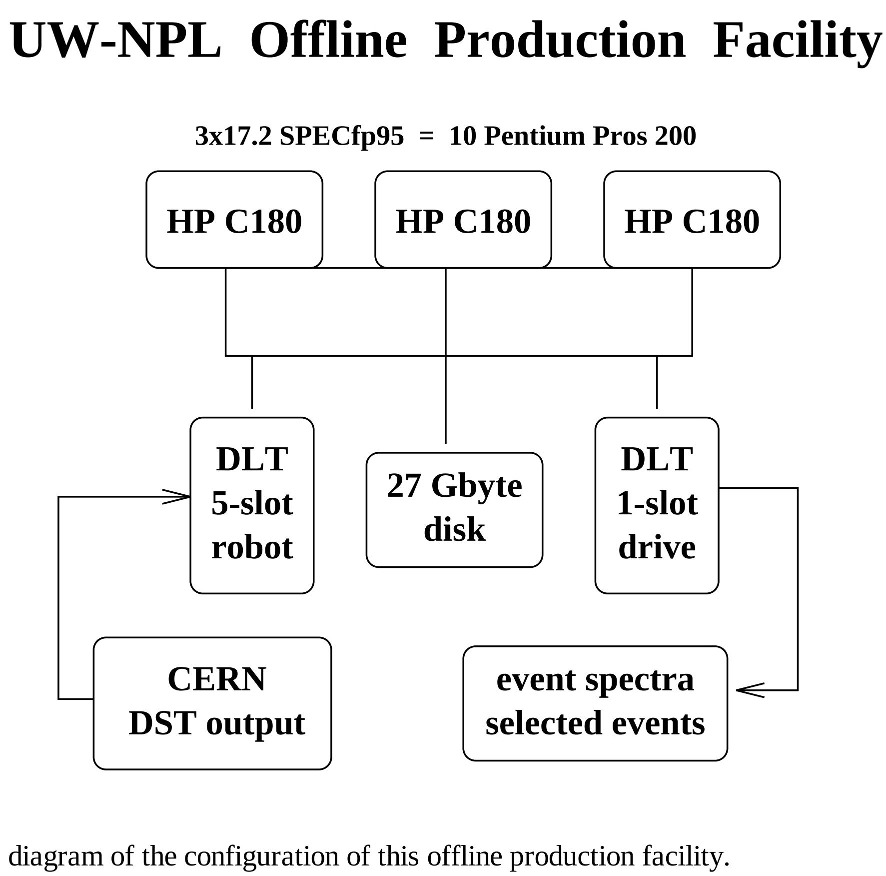

Fig. 4.13-1. Schematic diagram of the configuration of this offline production facility.

[14] http://wwwinfo.cern.ch/pdp/serv/shift.html.

4.14 Anomalous event generation for EbyE physics

D.J. Prindle, J.G. Reid, T.A. Trainor and D.D. Weerasundara

Coupled to any event-by-event analysis program are the problems of significance and interpretation. By what criteria can we conclude that a class of events is anomalous, and by what means can we interpret the physics content of these anomalous events? Standard significance criteria such as the χ^2 probability distribution may not suffice in the present context because of the complex and nonlinear nature of the problem. This is an area where new statistical concepts are needed.

The standard use of Monte Carlo event generators coupled to GEANT modeling of the experimental apparatus is not practical for event-by-event analysis, where the number of simulated events needed is typically an order of magnitude larger (~1M), and the computation time/event is also ten or more times larger (1-5 hrs) due to additional model complexity and larger collision system size. There is simply not enough computation power presently available to pursue this standard approach for event-by-event analysis. We are therefore exploring alternatives to these methods, including elimination of GEANT modeling for all but a small subpopulation of events and direct analysis of event-generator output for correlation content.

In order to anticipate what observable effects may arise in event-by-event analysis there are now several Monte Carlo collision model codes which permit one to explore a model parameter space which includes some anomalous dynamics in order to map out the corresponding fluctuation content of produced events. These "calibrations" should prove valuable for the interpretation problem.

Shown here are simulations using the VENUS MC simulation code to generate Pb+Pb collision events at 158 GeV/nucleon. A critical energy density (ced) control parameter is varied, causing observable changes in the variance content of the rapidity distributions. The variance content is analyzed quantitatively using scaled dimension analysis. The critical energy density parameter controls the percolation of prehadronic droplets in VENUS.

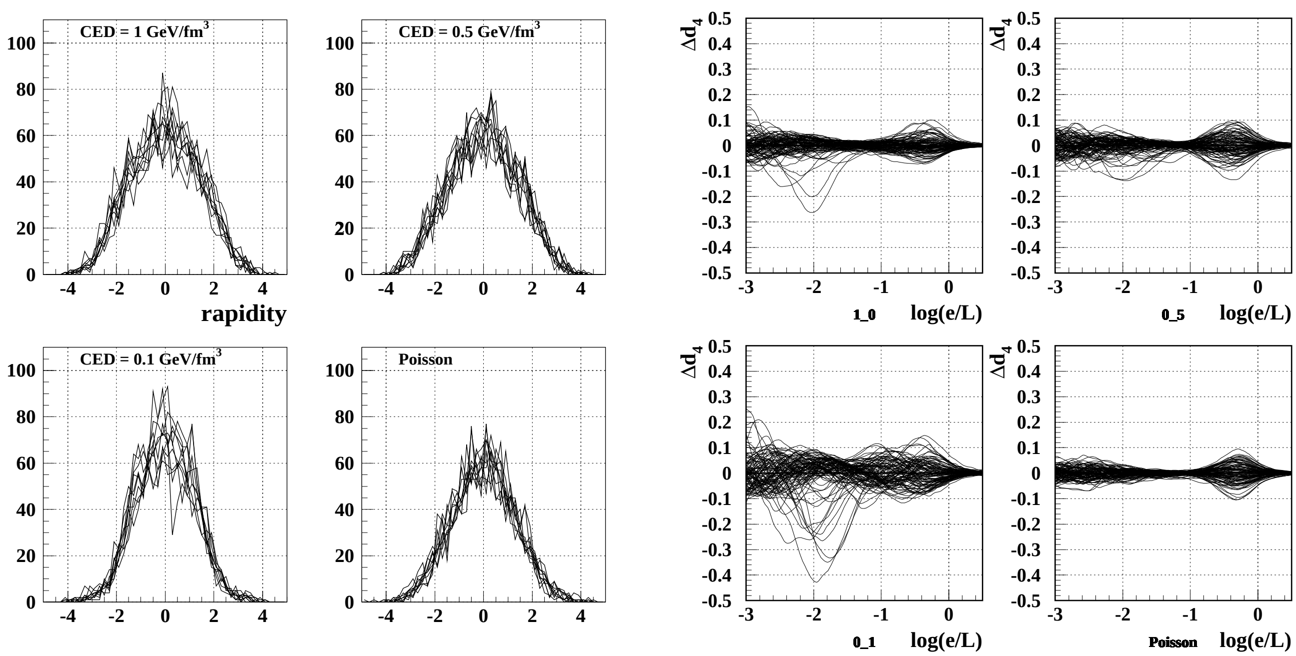

Fig. 4.14-1. Rapidity (left) and scaled dimension transport (right) distributions for three values of critical energy density in VENUS and a Poisson control simulation.

4.15 NA49 TPC cluster shape analysis

T.A. Trainor

There are typically 40k - 80k found "blobs" of contiguous charge in a TPC volume produced by each Pb + Pb event in the NA49 TPC system. Of this number typically 25-35% are "golden" clusters: idealized charge depositions in a pad plane by a hadron. Typically 10-15% more are "merged" clusters: produced by hadrons but requiring some further intervention (or rejection) prior to tracking. The remainder are associated with noise processes or are produced by energetic delta electrons and should be rejected from further cluster or tracking analysis. Until recently the standard cluster-finder algorithms for NA49 used a 1Dx1D approach, in which the charge distribution is searched first in the time direction and then in the pad direction for contiguous occupied pixels.

There has been a need for a precise method to categorize clusters, to reject electron and noise clusters and to provide the optimum processing for merged clusters. This article summarizes a recent extensive study of clusters or contiguous aggregates of charge on pad planes found with a new fully 2D cluster finder (DIPT, D. Irmscher, GSI) and categorized by newly-defined cluster morphology measures primarily based on determination of two orthogonal eccentricity components of the cluster charge distribution.

Application of these morphology measures has enabled a detailed sorting of clusters into four categories, as noted above. This sorting seems to be very effective, false positives and negatives having negligible statistical power. Furthermore, these measures permit an indication of the best approach to deconvoluting merged clusters (e.g., orientation of the major axis of a merged cluster and estimate of centroid separation in the case of bimodal clusters). We have demonstrated that using these measures merged cluster deconvolution by algebraic inversion of the morphology measures rather than by two-gaussian fits is practical. This method easily overcomes the Rayleigh limit, and reduces the two-track resolution from a typical 1-1.5 cm down to 3 mm or less.

Although cluster finding by 2D search, categorization by morphology measures and final deconvolution of select clusters according to these measures may increase the cluster analysis time by a factor of 2-3, this cost should be more than offset by the improvement in cluster quality and elimination of a substantial number of unwanted clusters (~50% of total) produced by noise and delta electrons. 2D cluster finding should offer a substantial improvement in physics quality of the tracking output, and may in fact substantially reduce the overall tracking analysis time because of the decreased combinatorics in the track finding process.

The results of the present study indicate that, contrary to established belief, even in the highest track density regions each contiguous charge region on a pad plane tells its own story very well, and can be fully analyzed independent of *a priori* tracking information in order to extract cluster centroid and charge, cluster identity, merge status and merge geometry.

5.0 ATOMIC AND MOLECULAR CLUSTERS

5.1 Fragmentation of C_{60} in collisions with hydrogen

C.H. Cooper,* B. Henry, J.F. Liang, R. Vandenbosch and D.I. Will

We are studying the collision dynamics of C_{60}, buckyballs, with hydrogen gas using the technique of reverse kinematics. We use an ion source described in last year's Annual Report.[1] We accelerate the ions using the injector deck of the tandem-linac facility. The beam collides with hydrogen in a windowless gas cell.[2] An important feature of reverse kinematics is that all of the reaction products are focused in the forward direction, and their energy in the lab system is proportional to the number of carbons in the reaction product. We energy analyze the reaction products in electrostatic deflectors, and hence determine the distribution of fragment yield as a function of their mass number.

The principal question we wish to address is the mechanism of making products such as C_{46} , C_{48} ,C_{50}, C_{52} , C_{54}, etc. Are they the result of extraction of carbon chains such as C_6, C_8 etc., or are they the result of successive emission of smaller fragments such as C_2? (This is analagous to the competition between nucleon and intermediate mass fragment emission in heavy ion induced nuclear reactions). The only way to get a definitive answer to this question is to perform a coincidence experiment. We place two analysis deflectors downstream from the target. The first deflector has a low electric field and deflects the light reaction products. A second deflector is placed downstream from this deflector and analyzes the heavy fragments. Channeltron detectors are placed behind the deflectors and the time relation between these two detectors are used to identify complementary reaction products from a single collision. In our first preliminary experiments we have identified C_2, C_4, C_6 and C_8 fragments in coincidence with C_{44} and with C_{50} fragments. The relative yields of different heavy fragments in coincidence with a particular light fragment have also been determined for several light fragments. The heavy fragment yield distribution in coincidence with C_8 fragments is shown in the Fig. 5.1-1. We have also shown that there are C_2 fragments in coincidence with light products such as C_8, C_{10}, etc. A typical scenario consistent with these observations is that C_{60} fragments into C_8 and C_{52} and then the excited C_{52} emits further C_2 fragments to make C_{44}.

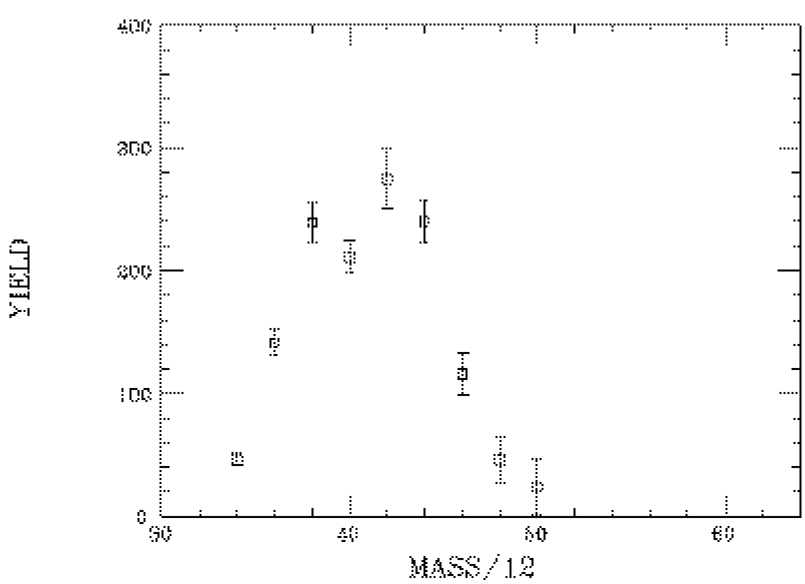

Fig. 5.1-1. Heavy fragment yield distribution in coincidence with C_8 fragments.

---

* Now at Sante Fe, NM.

[1] Nuclear Physics Laboratory Annual Report, University of Washington (1996) p. 50.

[*] Now at Sante Fe, NM.

[1] Nuclear Physics Laboratory Annual Report, University of Washington (1996) p. 50.

[2] Nuclear Physics Laboratory Annual Report, University of Washington (1996) p. 51.

5.2 Alkali carbide fragmentation : a new path to doubly-charged negative ions

C.H. Cooper,* B. Henry, J.F. Liang, R. Vandenbosch and D.I. Will

Previous experimental and theoretical work on alkali carbides has indicated that, for a sufficiently large number of carbon atoms, chains of the form AC_n^- might fragment into doubly negative anions C_n^{2-}.[1,2] We report here the results of an experiment in which doubly negative C_9 ions have been observed following collisions of CsC_9^- ions with H_2 and He. CsC_9^- ions were produced by sputtering cooled graphite with 3 kV Cs^+ ions. The negative ions were accelerated to 18 keV and mass separated with a 90 degrees magnetic analyzer. The mass-selected ions were further accelerated to 48 keV. The accelerated ions impinged on H_2 or He gas in a windowless gas cell operated typically at about 0.2 mtorr. The product ions were analyzed with an electrostatic deflector and counted with a Channeltron detector. In reverse kinematics the electric rigidity of a singly charged ion is proportional to the mass of the ion. An overview of the negative ion mass spectrum is shown in the inset to Fig. 5.2-1, where the dominance of C_9^- is apparent (note the logarithmic scale). The discriminator on the signal from the Channeltron detector was set to suppress contributions of ions lighter (and hence less energetic) than C_4^-.

C_9^{2-} ions are expected to show up halfway between C_4^- and C_5^-. A longer scan in this mass region is shown in the main body of Fig. 5.2-1. A peak at the expected position is readily apparent. The yield of this peak, relative to the neighboring C_4^- and C_5^- peaks, is reduced by almost an order of magnitude when hydrogen is substituted for helium as the collision gas. The yield of C_9^{2-} ions relative to C_9^- ions is quite small, typically about 10^{-4}. This ratio is comparable to that observed in sputtering of graphite. [3]

Further confirmation of the identification of this peak as C_9^{2-} can be obtained by examining the dependence of the yield of this peak relative to the neighboring C_4^- and C_5^- ions as a function of the Channeltron pulse height threshold. The C_9^{2-} ions have approximately twice the energy of the neighboring C_4^- and C_5^- ions. Thus one would expect the yield of the C_9^{2-} peak (relative to the C_4^- and C_5^- peaks) to increase as the threshold level for recording an event is increased. This was observed.

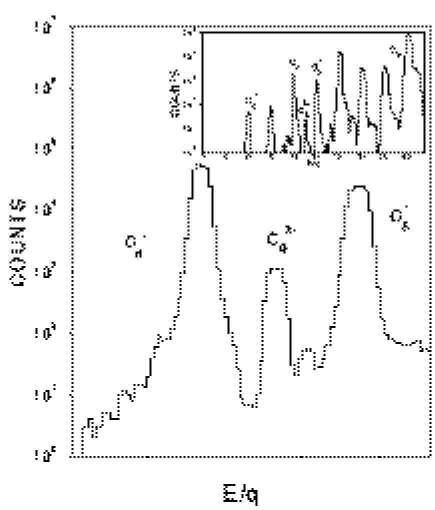

Fig. 5.2-1. Negative ion E/q spectrum in the vicinity of C_4^-, C_9^{2-}, and C_5^- for 48 keV bombardment of He with CsC_9^-. The inset gives an overview of the negative ion spectrum over the whole range from C_1^-- to C_9^- for 48 keV bombardment of H_2.

CsC_9^-. The inset gives an overview of the negative ion spectrum over the whole range from C_1^-- to C_9^- for 48 keV bombardment of H_2.

---

[*] Now at Sante Fe, NM.

[1] R. Vandenbosch and D.I. Will, J. Chem. Phys. **104**, 5600 (1996).

[2] R.N. Compton, private communications.

[3] S.N. Schauer, P. Williams and R.N. Compton, Phys Rev. Lett. **65**, 625 (1990).

6.0 ELECTRONICS, COMPUTING AND DETECTOR INFRASTRUCTURE

6.1 Electronic equipment

G.C. Harper, A.W. Myers and T.D. VanWechel

Along with the normal maintenance and repair of the Nuclear Physics Lab's electronic equipment, projects undertaken by the electronics shop this year included the following:

a. Last year, 3 light pulsers were manufactured to support the new 3-spectrometer setup and beamline for high energy gamma ray experiments (see Section 6.7). This year several modifications/improvements were made to these light pulsers.

b. The SNO neutral current detector preamp reported in last years report as being fabricated on hybrid circuits and tested satisfactorily have gone into full production. We currently have approximately 30 completed, tested preamplifiers and 25 completed but not tested at high voltage. An additional 70 will be completed by 5/1/97 (see Section 2.3).

c. The motherboard for the emiT preamplifier, detector and associated circuitry reported in last years report has been completed. These assemblies are currently in use at NIST for the emiT experiment (see Section 1.13).

d. We have stuffed (placed components on) thirteen shaper/ADC boards for use in the emiT experiment. These are currently in use at NIST in the emiT experiment (see Section 1.13).

e. We have modified a VME crate for use at NIST in the emiT experiment. We removed the switching power supply and replaced it with several Power One linear power supplies.

f. We built a 24 Bit coincidence regulator (see Section 1.2).

g. We built 2 Quadrature oscillators for the gravity group.

h. We built a Temperature controller which was mounted into a NIM module.

i. We built several 8-channel log amplifiers for use at Los Alamos National Laboratory. These are being used for initial testing for the SNO experiment.

j. We built two 8-way splitters for use in testing the shaper/ADC boards in emiT.

k. We designed a power supply box to distribute low voltage power for the SNO preamplifiers.

l. We made a power distribution box to supply power for the SNO DEV. TEST RACK. We used Power One and Condor linear power supplies to provide the following power: +5VDC @ 50 A, -5VDC @ 18A, +12VDC @ 16A, +24VDC @ 2.4A and -24VDC @ 2.4A. The +5VDC is also providing +1.2VDC @ 3A. The +12VDC is also providing +8VDC @10A. The -5VDC is also providing -2VDC @ 3A.

m. We are in the development phase of SNO NCD Front End electronics (see Section 6.5).

n. We have upgraded our electronics shop capabilities by adding a reflow batch oven. This oven complements our surface mount Pick and Place machine and our surface mount rework/reflow station. The addition of the oven greatly reduced the amount of time required to populate a circuit board. As an example, to populate one board (mentioned in item d.) and flow each component individually took approximately 3 days. To populate one board and flow the entire board utilizing the batch reflow oven takes only about 6 hours. Of this 6 hours, all except approximately 4 minutes was used to place the components. The oven only takes about 4 minutes to reflow the entire board.

6.2 VAX-based acquisition systems

M.A. Howe, R.J. Seymour, D.W. Storm and J.F. Wilkerson

We now have three VAXstation 3200-based data acquisition systems. They consist of digital Qbus-based VAXStation 3200s running VMS v4.7a using VWS/UIS as the “windowing” software. Each VAXstation supports a BiRa MBD-11 controlled CAMAC crate. Our primary system is attached to a dozen dedicated 200 MHz Tracor Northern TN-1213 ADCs. Those ADCs and other CAMAC modules are coincidence-gated by a UWNPL-built synchronization interface, which includes monitor (Singles) and routing-Or capabilities. The system also has a bank of 32 10-digit 75 MHz scalers.

Our principal VAXStation's small BA-23 cabinet is cabled into a second BA-23 CC expansion cabinet. That, in turn, has an MDB-11 DWQ11 Qbus-to-Unibus converter driving our old PDP 11/60's Unibus expansion bay. The system's Qbus peripherals include a CMD CQD-220/TM SCSI adapter for a Seagate ST41650 1.38 gigabyte disk and a TTI CTS-8210 8mm tape drive, a DEC IEQ11 IEEE-488 bus controller, and a DEC DRV11-J. The Unibus bay contains a DR11-C, our Printronix lineprinter controller and a Unibus cable to the MBD-11.

The other two acquisition systems consist solely of each VAXstation 3200's BA-23 using an Able Qniverter to provide a Unibus cable direct to a stand-alone MBD-11. Unlike the “principal” system, these do not control non-CAMAC-based equipment.

All three systems run acquisition software based upon TUNL's XSYS, with major modifications to their DISPLAY program.

One of this year's modifications to the acquisition systems consisted of adding a 1 gigabyte removable Iomega Jaz drive to the principal system. This is used to avoid the delays and system load caused by taping event files and histograms directly to 8mm tape during an acquisition run. Data are recorded directly to the Jaz drive. When the 1 gigabyte disk fills (in about a half-day), it is ejected and replaced with an empty one. Acquisition is resumed, and the full disk taken to a second offline VAXstation which is used to record the data on an 8mm tape. We have found that older non-Digital SCSI controllers, such as the CMD 220, accept the Jaz drive without problem. Digital's built-in SCSI controllers, such as the VAXstation 3100's and the Alpha 3000/400's are not able to accept the Jaz drive. Of the three acquisition systems, only the principal system has a SCSI adapter, the rest have Aviv ESDI controllers.. Hence we have had to swap both drives and disk controllers when we wished to use the Jaz drive on a different acquisition system. In light of that, and to increase a second acquisition system's disk capacity above ESDI's 660 Mbyte limit, we have added an Aviv QS6 caching SCSI controller and 4 gigabyte drive to that second system. At the moment that Aviv controller "sees" the Jaz drive, but considers it "offline". We are working on this with the controller manufacturer.

6.3 Data analysis and support system developments

J.G. Cramer, M.A. Howe, R.J. Seymour, D.W. Storm, T.A. Trainor and J.F. Wilkerson

Our offline computing and analysis facility shares resources via a building-wide thinwire ethernet. The facility is comprised of:

- Our VMS cluster, consisting of five VAXstations 3100s, five 3200s and a single Alpha 3000/400. The cluster shares seventeen gigabytes of disk space.

- The Ultra-Relativistic Heavy Ion's group of Hewlett Packard Unix systems, consisting of a pair of HP 9000/710s, four 9000/712/60s and the newest arrivals, a trio of 180 MHz PA-8000 C-180 workstations. The C-180s are running HP-UX v10.20, the rest run versions ranging from 9.01 to 9.05. We have added both a 2000XT DLT single-drive system and a five-cartridge DLT 2500XT tape library for processing NA49 tapes.

  The nine machines use NFS to share nineteen disks with a total capacity of fifty-two gigabytes. This doubling of last year's disk capacity was achieved by adding three 9-gigabyte Seagate drives to one of the C-180s. Those disks are mounted as a single 27-gigabyte "logical volume" to allow us to copy an entire 20-gigabyte NA49 DLT tape to the disk for analysis.

  We traded in our two one-year-old dual-processor J200s for their replacement by the three C-180s. We had planned to simply upgrade the J200s when the PA-8000 chipset became available, but HP offered a full-value trade-in towards the C-180s instead. Installation involved upgrading a trio of delivered C-110s to C-180s with "motherboard swap kits" which arrived with them.

  Benchmarks were run to compare their performance with the "old" J200s, with disappointing results compared to an advertised performance ratio of 2.75. Our first runs showed only a ratio of 1.8. Using the SPEC organization's website, we applied and tuned the compiler switches which HP had used for benchmarking. This eventually achieved ratios ranging from 2.3 to 2.9.

  Once again, three of the HP systems traveled to CERN for the NA49 run.

  One of the 9000/710s also serves as the lab's World Wide Web server (www.npl.washington.edu).

- The SNO and emiT group's collection of twenty-two networked Macintoshes, including a number of Power Computing 200 MHz PowerPC Mac "clones". The clones seem to have problems driving AAUI-to-thinwire ethernet adapters on long cable segments. They also have a Sun SparcStation 20 running SunOS v1.4 to provide CADENCE circuit layout facilities to our electronics shop, plus two Sun SparcStation 2s from the SSC equipment distribution.

- Desktop Intel-based PCs continue to spread throughout the building.

- Other systems in the building include: two VMS VAXstation 3200s providing Email and CPU cycles for the Institute for Nuclear Theory and the Physics Nuclear Theory group, a Sun Sparc 5 for developing the Slow Controls software for STAR, a VAXstation 3200 serving as the Linac's control and display system, nine PDP-11s built into the Linac for cryogenics, vacuum and resonator control, and four PCs serving as controllers for the rest of the accelerator systems' interlocks, safety and vacuum systems.

6.4 SNO NCD electronics

M.C. Browne, K.M. Heeger, A.W. Myers, R.G.H. Robertson, T.D. Van Wechel and J.F. Wilkerson

The SNO neutral-current electronics is designed to extract pulse information from the ^{3}He proportional detectors in order to provide the information required for SNO physics analysis. Pulses generated in each detector string are first amplified by a current preamplifier. The amplified signal is then sent to both an energy measurement system and a digitization system.

The design of the SNO neutral current preamplifiers has been finalized with improved stability resulting in a reduction of pulses originating from high voltage induced micro discharges inside the preamplifiers. The construction and testing of these amplifiers is now progressing routinely. The configuration of the front end electronics has changed slightly from that reported last year,[1] the primary difference being that rather than having 96 logarithmic amplifiers, one for each channel (a "string" of detectors), there are now 8, one for each multiplexer output. A 2-channel prototype multiplexer system is being evaluated.

The 96 amplified signals from the detector array are distributed to the eight multiplexer sections, with 12 channels each. Each section consists of a box containing a front end card and 12 delay lines, all mounted in an 88-inch-high relay rack. The front panel of each box has inputs from the NCD preamplifiers, outputs to the energy measurement system, and the multiplexed output to the digitizer. The input of each channel has two 50-ohm output buffers. One drives a delay line and a fast discriminator, and the other drives the energy measurement system located in a separate rack. The delay line, approximately 150 ns long, allows time for the multiplexer to open as well as providing a record of pretrigger baseline. When the fast discriminator of a channel is triggered, the multiplexer switch for that channel is turned on for 20 us. The multiplexer is followed by a logarithmic amplifier to handle the signal dynamic range with 8-bit digitizers. The digitizer is one channel of two four-channel digital scopes. The scopes will digitize a 20 us record at a sampling rate of 500 MS/s, each time the system is triggered. We are presently evaluating the scopes manufactured by Tektronix and LeCroy. The digitized data from the scope will be interfaced via GPIB bus.

Besides the development of the SNO NCD front-end electronics, progress has been made in testing the electrical properties of some of the neutral current detector components. A high-voltage test stand with a scope based data acquisition system has been set up to test the endcaps and delay lines for microdischarges. The reliable operation of this test system using the latest current preamplifiers has been demonstrated during the construction of clean neutral current detector prototypes. The fabrication of all delay lines has been completed.

After construction, the neutral-current proportional detectors will be stored underground for several months to reduce the background from cosmogenic activation. In preparation for this cooldown phase, an eight channel multiplexed data acquisition system based on commercially available components has been assembled. Eight signal readout channels are multiplexed into one digitizer followed by a current integrating ADC. This electronics system will be used during the initial cooldown period to monitor the performance of the proportional detectors. When the SNO NCD front end electronics system is in production it will replace the temporary data acquisition system. The cooldown period for the neutral detectors will start at the end of April 1997.

[1]Nuclear Physics Laboratory Annual Report, University of Washington (1996) p. 19.

6.5 A custom VME-based data acquisition system for the emiT experiment

M.C. Browne, A.W. Myers, T.D. Van Wechel and J.F. Wilkerson

The emiT board is a VME-based data acquisition system which contains both shaping and peak-detect ADC capability. The board was designed for the proton segment of the emiT experiment. Over the past year, the board has undergone rigorous testing of both the prototype analog and digital portions. A production run of acquisition boards was ordered, received, populated, tested, and implemented into emiT. We have also made advances in reducing noise induced into the acquisition board, and continue to work towards increased resolution and reliability.

The board is operated via an Altera 7192 field programmable gate array (FPGA). The FPGA is programmed with both the VME interface logic, as well as the overall board command logic. The prototype Altera programming was verified this past year by demonstrating successful operation under the IEEE VME standard. The digital portion of the prototype board was then tested to verify operational modes and characteristics.

Upon successful completion of prototype testing, we began population of a production run of emiT boards. This revision implemented discriminator outputs to allow for timing analysis of the proton detectors. Minor fixes were included in this revision as well. Populated production boards were tested for resolution and characterized to ensure similar board to board parameters such as conversion and threshold levels. Several revisions of Altera programming were developed. A more robust board operation mode, an additional scalar, and several board monitor functions were also added.

Tested production boards were shipped to NIST for implementation into the emiT experiment. We then shifted our emphasis to support maintenance of acquisition hardware. Boards which became inoperable were shipped back to UW for repair. Information obtained from failure modes was then used to modify acquisition boards. Part of this process was a continual effort to reduce noise and improve resolution. To this effect, we refit a standard VME backplane with non-switching power supplies, increased board filtering, and are currently exploring additional protection of on-board buffers.

The emiT board will be used in the future as a template in the design of the neutral current detector electronics for the Sudbury Neutrino Observatory.

6.6 Triple NaI detector set-up for measurement of high-energy γ-rays

J.F. Amsbaugh, J.H. Gundlach, M.P. Kelly, B. Krouse, C.E. Linder, K.A. Snover, D.W. Storm and J.P.S. van Schagen

The construction of the R-45 beamline and a triple NaI-spectrometer set-up in Cave 2 is finished. The beamline features a new and improved vacuum system. The long beamline from the scattering chamber to the beam dump is doubled in diameter so that scattered beam from the target intercepts the interior lead liner further downstream, reducing this source of background in the detectors. A second pumping station and gate valve now allows separate venting and pumping of scattering chamber and beam dump. Pumping is provided by two 360 l/sec turbomolecular pumps (TMP). One 20 cfm mechanical pump backs both TMP (with appropriate isolation valves, trap, etc.), and a second provides roughing for the entire experimental area. Vacuum pressure measurement is done with hot cathode ion, pirani, and thermocouple gauges. A 80486 Personal Computer-based programmable controller[2] provides flexible system control and graphic programming interface. It also runs a pushbutton and status light panel for normal user operation. This controller can provide integration with our LINAC control computer, but this feature is not implemented. Ultimate vacua are about 4×10^{-7} Torr.

A center post was mounted on the 13' by 14' platform[3] which is used as support for different kinds of scattering chambers and as a pivot around which the three spectrometers can rotate. An angle circle was inscribed on the floor to indicate the angle of the detector with respect to the beam axis.

Three NaI detectors have been assembled on the platform: the 10" by 15" Seattle NaI, a 10" by 11" NaI(Tl) spectrometer on loan from the University of Illinois and the OMEGA II spectrometer, with a 11.5" by 15" NaI(Tl) crystal, on loan from Ohio State University. Each NaI-detector is surrounded by a plastic Compton-suppression shield and Pb shielding to suppress background γ-rays and cosmic radiation. Each spectrometer rests on a cradle which is bolted to a cart that is electrically isolated, hence ground loops are avoided. The carts consist of welded 3" by 3" aluminum I-beams. The High Voltage power supply and voltage divider box for the plastic scintillator PMT's are mounted on the cart, together with a NIM bin in which electronic modules for e.g. the stabilization system are placed. These units are also electrically isolated from the cart frame.

Each detector can move over the platform by floating on four Air-Go 12" by 12" air-pads mounted underneath the cart. The air-pads are located such that sufficient mechanical stability is obtained while detectors can be placed as close as possible to each other. The radial motion of a detector cart is constrained along a 3" by 1.5" boxbeam which is bolted to one of the pivots at the bottom of the center post. To restrict the side-to-side motion when the distance of the detector to the target has to be changed, cam-followers with eccentric studs are used to guide the cart. The radial position of the detector can be fixed by clamping the cart to the boxbeam while hinges and pivots still allow the detector to rise when the air-pads are activated.

This set-up will be used for the study of high-energy γ-rays emitted in heavy ion (fusion) reactions to investigate the width of the Giant Dipole Resonance at different excitation energies and the study of the radiative $^4\mathrm{He}(\alpha,\gamma)^8\mathrm{Be}$ reaction to test CVC and test the existence of second class currents.

[2] Nuclear Physics Laboratory Annual Report, University of Washington (1993) p. 89.
[3] Nuclear Physics Laboratory Annual Report, University of Washington (1996) p. 58.

6.7 Electronics for triple NaI-detector set-up

A.W. Myers, K.A. Snover, H.E. Swanson, J.P.S. van Schagen and T.D. Van Wechel

A new electronic set-up to process signals from the three NaI-spectrometer (see Section 6.6) has been developed. It can be functionally separated in the following parts: energy and timing signals for the NaI crystals, timing signals from the plastic anti-coincidence shield and gain stabilization of the NaI-spectrometers.

Each of the photomultiplier tubes used to read out a NaI-crystal is powered separately using a LeCroy Model 1454 High Voltage Mainframe. This unit can be controlled in remote mode. The anode signals are summed in a passive impedance-matched summing box and then split off for timing and energy measurement.[4] For the digitization of the energy signal we use a Silena 4428/Q charge integrating ADC. This device has a true differential $Z_0 = 100\Omega$ input stage and separate gates for each channel. To be able to reject pile-up events, two channels are daisy-chained for each detector so the same energy signal can be integrated over different time intervals. The signal is sent to Counting room 4 through Belden-M 9207 100Ω twin-ax cable.

The timing signals are processed in the traditional way using Timing Filter Amplifiers and Constant Fraction Discriminators. Two thresholds are employed. A low threshold is set at ~400 keV to monitor the 'true' count rate with a scaler. The high threshold can be adjusted to the specific needs of the experimenter and will generate the NaI-crystal trigger. This trigger is used to generate the long and short integration gates for the Silena 4428/Q. A master event is formed by the logic OR of the NaI-triggers. This master gate is used to open gates for the QDC, ADC's and TDC used in the data acquisition. To distinguish which of the detectors have fired, the NaI-crystal sets a bit in a coincidence register designed to be used with a DSP Model 612 dual I/O register.

Signals from the photomultipliers connected to the plastic Compton-suppression shield are summed in an active mixer box and send to the counting room. Also here two thresholds are implemented., a high threshold (optimum efficiency) and a low threshold (optimum resolution). For each threshold, a logic AND is formed with the NaI-crystal trigger. The output is used to set bits in the coincidence register upon which the NaI energy signal can be routed into different spectra.

The gain of the detectors is stabilized using a LED pulser which generates two different amplitude signals. The system consists of two feedback loops. The light output of the high-amplitide LED signal is stabilized using a PIN diode and a Williams & Harris Gain Stabilizer. The pulser trigger sets a bit in the coincidence register. The energy signal will then be routed to a separate spectrum which is monitored by a computer program which stabilizes the NaI gain by feedback to the PMT supply voltage provided by the 1454 High Voltage Mainframe. Depending on whether the voltage has to be increased or decreased the program cycles through the PMT channels in different directions. To optimize the response times, different feedback gains are employed depending on the magnitude of the voltage correction.

Currently we are testing which type of LED to use to achieve optimum stability. We have tested a LED emitting in the blue but several instabilities were encountered. Tests with a LED emitting in the green have been restricted by their light output.

[4] The bases for the Seattle detector have also dynode outputs. These are summed in an active mixer box and used for the timing signal.

6.8 A precision generating voltmeter for reading deck voltage

J. F. Amsbaugh

The ion source deck voltage determines the beam energy in studies of cluster size dependence. Voltage measurement repeatability, linearity and relative accuracy are more important than the absolute accuracy. The resistive divider of the voltage regulation circuitry in the 300 kV power supply provides this. It is also measured with a second divider built of resistors with known voltage-current characteristics. Since the two are inconsistent, a different physical measurement is desirable.

A generating voltmeter (GVM) measures the charge induced on an electrical conductor (stator) as it is exposed to and shielded from an electric field, thus an absolute voltage measurement requires well-known physical electrode geometry. Relative measurements require mechanical stability. Usually, the induced current through a resistor to the stator as the rotor spins provides the signal. Three problems occur, the resistor current depends on rotor angular velocity, the stator voltage perturbs the electric field, and this voltage causes charge leakage though the stator supports. The new GVM design avoids these problems.

A two opening rotor, 4.5" diameter, is spun by an audiocassette motor at 2400 rpm. Each opening is a quarter of a circle. This rotor is grounded via the motor bearing and housing. The motor is mounted in an iron shield. Four 100 cm^2 stator segments, about an eighth sector each, are etched on G-10 printed circuit card leaving as much copper as possible on both sides for a ground plane. This stator mates to the can flange and to a 23" by 38" by 1/4" aluminum plate which acts as a large area ground plane. This assembly sits on the floor about one meter underneath the deck. The planes of the rotor and stator differ by about 0.12" which distorts the electric field as does the edge effects of the rotor opening, limiting absolute accuracy error to $\geq 0.5\%$. The use of one stator and one rotor opening eliminates errors caused by the tolerances of rotor openings and stator areas.

A reflective IR sensor detects rotor-opening edges and determines that the rotor opening is either exposing or shielding the stator. A second detects rotor phase selecting one rotor opening. These IR detectors generate logic signals that are gated with a minimum rotor speed. These signals operate a low noise dual switched integrator, Burr Brown ACF2101. This chip features FET switches for hold, reset, and output selection, and a low bias current (100 fA) Op-Amp with a precision 100 pF integrating capacitor. An external integrating capacitor is added so output range is approximately 0-3.5 volts for deck voltage range 0-350kV. The stator is connected directly to the integrator input. For 3/4 of a revolution the hold and reset switches ground the stator and integrator. When the rotor opening is centered over the stator, both switches are opened and the integrator keeps the stator at virtual ground minimizing charge leakage from the stator. When the next rotor edge is detected the stator is completely shielded by the rotor and the select output logic signal switches the charge integrator voltage to a sample and hold amplifier, which has < 0.1 mV droop per cycle. The output of the S/H amplifier is measured with a 5-1/2 digit voltmeter. The bench tests of drift, 0.2% in 24 hours and linearity, residuals $\leq \pm 0.1\%$, are consistent with specifications of the test voltage sources and measurement equipment.

The ion source deck has a resistor string biased beam acceleration tube with a gridded lens in the last electrode. The center electrode, at about half the deck voltage, is connected to field grading electrode located half way between the deck and the floor. As the grid lens voltage is varied the electric field at the GVM is perturbed. The high resistance of the beam tube resistors and capacitance of the mid-voltage grading ring forms a several second time constant. Experimenters use the GVM but there are still some inconsistencies to be resolved in the three measurement methods.

6.9 Mass 8 apparatus electron detector additions

J. F. Amsbaugh

The electron acceptance of the Mass 8 apparatus[5] has been increased by the addition of two new electron counter telescopes at 0° and 180°. Each telescope consist of a ΔE trigger, a veto and an energy scintillation counter, using NE104[6] plastic scintillator. The energy counter is an 18.33-cm diameter cylinder 12.5 cm long with a 45° conical lightguide coupled to a R-1250 5-inch photomultiplier (PMT) tube.[7] Surrounding this is a 1 cm thick veto scintillator coupled to two R-329 2-inch PMTs, with a 10.83-cm diameter entrance aperture. The veto entrance aperture, being smaller than the energy counter diameter, will veto events where the electron is likely to scatter out of the energy counter. In front and overlapping the entrance aperture is the ΔE trigger counter, a paddle of 1.5-mm thick NE104 coupled to a R-1450 0.75-inch PMT with two 0.125-inch thick lightguides.

The scintillation elements of the new counters were scaled from the previous electron detector design to preserve the angular acceptance. The new detectors are positioned behind the Breskin α counters increasing the distance to the source location. The photomultiplier tubes used are also the same. This was an attempt to have similar detector response for all the electron energy counters, however the light collection efficiency difference between the larger scintillators with lightguides and the smaller directly coupled ones were ignored. The scintillators are wrapped in aluminized Mylar, black 5 mil polyethylene plastic, then made light tight with a minimum of vinyl tape. A plastic fiber optic cable is coupled into the energy scintillator with a dab of optical cement for use with a light pulser gain stabilizer. The three detectors are assembled as a removable unit on a mounting bracket and frame.

The α counter back plate was redesigned with an electron exit window and mounting holes for the bracket of the electron telescope. The exit window should put as little material in the electron path as possible and yet withstand one atmosphere pressure differential, as the α counter is operated at a few Torr and is also evacuated. A hydrostatic test of 0.005-inch thick, 8-inch diameter Kapton window glued to 6061-T6 aluminum with Armstrong A-12 epoxy failed at 30 psig when the epoxy to aluminum bond broke where the bond width was the smallest. The epoxy joint was 0.5$\pm$.06 inches wide on clean as machined aluminum. Before the test to failure, deflection was measured to 20 psig over a few pressure cycles. The creep at 15-20 psig was also measured overnight. Results indicated that two Kapton thickness glued to sandblasted aluminum would have a deflection of about half the thickness of the back plate and not interfere with $\alpha$$ counter wire planes. The measured equilibrium deflection was 0.555 inches on the first of the new back plates installed on the apparatus. Neither windows has failed during several runs in the last year.

---

[5] Nuclear Physics Laboratory Annual Report, University of Washington (1994) p. 19.
[6] NE Technology, Sighthill, Edinburgh, Scotland.
[7] All PMTs from Hamamatsu Corporation, 2875 Moorpark Avenue, San Jose, CA.

6.10 A new computer system for the NPL

E.G. Adelberger, D.W. Storm and J.F. Wilkerson

We recently submitted a proposal to the DOE for capital equipment funds to upgrade our computer system. The proposal has three parts: 1) more powerful computers for major computations and data analysis; 2) a new data taking system; and 3) personal computers for faculty desks and graduate student offices. The computational computers would be two DEC Alphastations 500/500 or an equivalent. These would supplement our existing DEC Alpha 3000/400 and HP computers, which are presently near saturation.

The data taking system would be built around the system that is being developed for SNO by Wilkerson and coworkers here and at LANL. This system will use Pentium based computers which will be interfaced to CAMAC, VME, and IEEE data taking interfaces. Device drivers that have already been developed for SNO will be used. Using PC's, the system will be portable and can be taken to remote sites where we do experiments. It will also be faster and more flexible than the existing data-taking system used in the laboratory. The proposal includes hardware for two such systems.

Approximately 20 PC's are included in the proposal. These will provide each faculty member, computer professional, and graduate student office with a modern personal computer, with appropriate software for doing routine computations, producing papers and reports, and making illustrations. The new computers will replace the aging vax-stations and dumb terminals presently in use. Besides functioning as stand-alone computers, they will be able to emulate X-terminals for operating the new DEC Alpha computers or the existing HP machines.

We plan to implement this proposal over a two year period.

7.0 VAN DE GRAAFF, SUPERCONDUCTING BOOSTER AND ION SOURCES

7.1 Van de Graaff accelerator operations and development

D.T. Corcoran,* G.C. Harper, C.E. Linder, A.W. Myers and T.D. Van Wechel

On 3/19/96 a Pelletron terminal pick-up pulley was found to have lost its tire. It was replaced, and the two remaining pick-up pulleys that were still original were also replaced at this time, for reasons of preventative maintenance. One of these replacement pulleys threw its tire before 4/3/96, requiring the tandem to be shut down once more for repair. At this time an idler pulley in the LE mid-section was also found to have bad bearings and replaced. On 11/6/96 the lower HE end pick-up pulley had to be replaced again. This time the tire was intact but the ball-bearing was damaged. On 1/23/97 the HE chain drive motor had to be replaced due to a seized bearing. On 2/25/97 another idler pulley in the LE mid-section was replaced because of a totally destroyed bearing.

The problem of tank spark damage to the pelletron charging resistors, high voltage charging supplies, and RG-8/U cables at the low energy end that was mentioned last year has apparently been eliminated by the fixes listed at that time, plus the additional fix of shortening of some insulating stand-offs and rerouting a high-voltage cable.

The thoriated tungsten corona points mentioned in last year's report have run all year without having to be replaced. Ultimate life of these points is still unknown.

The tandem terminal ion source was installed once for developmental purposes. Its history is covered in a separate section.

During the year from March 1, 1996 to February 2, 1997 the tandem pellet chains operated 3075 hours. Additional statistics of accelerator operations are given in Table 7.1-1.

Table 7.1-1. Tandem Accelerator Operations
March 1, 1996 to February 28, 1997

Activity	Days Scheduled	Percent
A. Cluster Ion Physics Research, Ion Sources Alone	57	16
B. Nuclear Physics Research, Tandem Alone		
Light Ions†	95	26
^{3}He Terminal Ion Source	0	0
C. Nuclear Physics Research, Booster and Tandem Coupled		
Light Ions	6	2
Heavy Ions	49	13
Subtotal	207	57
D. Other Operations		
Tandem Development	20	5
Tandem Maintenance	79	22
Unscheduled Time, working days	17	5
Unscheduled Time, weekends or holidays	46	13
Subtotal	162	45
Total	369††	102††

† Light = ^{4}He and below.
†† Greater then 365 (100%) since some days of cluster research were done during tandem maintenance.

* Now at InControl, 6675 185th NE, Redmond, WA.

7.2 Booster operations

J.F. Amsbaugh, D.T. Corcoran,* G.C. Harper, M.A. Howe, D.W. Storm, D.I. Will and J.A. Wootress†

During the period March 1, 1996 to Feb 28, 1997, the booster was operated for 55 days. This is less than the 69 days operated last year. The month of August was spent overhauling the three resonator systems which had been inoperable because of various failures of equipment inside their cyrostats. All resonators are presently operable, and an energy of 218 MeV was obtained for an ^{18}O beam.

Beams ranged in mass from ^{4}He to ^{40}Ca, and included ^{12}C, $^{16,18}O$, ^{7}Li, and ^{11}B, as well.

We continue to operate the low beta resonators at an average field of 3.0 MV/m and the high beta ones at an average of 2.4 MV/m.

The helium compressors continued to run with no failures this year. Our oldest compressor now has run for 89k hours, and the other two have run for 58k hours in one case and 30k hours in the other case.

* Now at InControl, 6675 185th NE, Redmond, WA.
† Retired.

7.3 Tandem terminal ion source

G.C. Harper, C.E. Linder, A.W. Myers and T.D. Van Wechel

The terminal ion source was not scheduled for use in an experiment during the last reporting period. It has been, however, scheduled for a three week run using $^{3}He^{+}$ in March of this year. Requests have been made for different ion species and lower terminal voltages for future runs. In response to these requests part of this year has been devoted to development work on the source optics.

A spherical, double-focusing electrostatic deflector was designed and built for use with the terminal source to provide mass independent deflection. This project was motivated by requests for experiments using other ion species, in particular $^{1}H^{+}$ for the $^{7}Be(p,g)^{8}B$ experiment. An electrostatic deflector with a bending radius, R, of 14 cm was specified. The radius chosen was equal to that of the deflection magnet so that it could be mounted in the same space in the foil stripper box as that occupied by the deflection magnet. The deflection angle of 60° was of course also retained.

The foci for a 60° spherical electrostatic deflector occur at $\sqrt{3}R$ from the deflector edges, much closer than the 3.46R for a double-focusing deflection magnet with the same bending angle. The beam profiles at various points along the trajectory are necessarily different for the two configurations. The apparent object for the electrostatic deflector is close to the source canal whereas for the magnet the virtual object is outside of the source region. Since the foci are much closer, the beam reaches a much larger diameter as it passes through the electrostatic deflector due to its larger divergence. Because the beam exiting the electrostatic deflector forms a waist before reaching the accelerator tube, it is diverging at the tube entrance rather than converging like the beam exiting the magnet.

Tests of the deflector both inside and outside of the tandem indicated that it was not double-focusing and consequently produced an elliptical beam profile at the image. In tests conducted outside of the accelerator the horizontal size of the beam measured about twice that of the vertical size at the theoretical image point. When tested in the accelerator the ion beam in the vertical plane was divergent to the extent that it interfered with transmission by striking and loading down the beam tube. Poor transmission was seen at all terminal voltages when using protons with the electrostatic deflector.

Concurrent with development of the electrostatic deflector, a new gradient scheme was developed for the high energy tube that would theoretically allow operation down to 50 kV terminal voltage. In practice it was found that satisfactory operation was extended down to 800 kV, a substantial reduction from the 1.8 MV achieved with the previous gradient scheme. This test was made using $^{3}He^{+}$ and the deflection magnet to ensure that the ion beam transported was at least cylindrical. It is believed that reducing the beam diameter and removing the halo with a small aperture may improve transmission at lower terminal voltages. Beam transport with a reduced diameter will be tested later this year. In addition, further studies of the electrostatic deflector will be made.

7.4 Cryogenic operating experience

M.A. Howe, D.I.Will and J.A. Wootress*

The booster linac is cooled by liquid helium which is thermally shielded by liquid nitrogen.[1]

The following table summarizes our maintenance for 1996 January 1 to 1996 December 31:

Item	In Use	Major Services	Times Performed
Refrigerator			
Cold Box	97%	warm/pump/purge	2
Main Dewar	100%	warm/pump/purge	0
Top Expander	~7500 Hrs[2]	warm/pump/purge	8
	~130 RPM	valve rod and valve seals	1
		wristpin, crank, and cam follower bearings	2
		flywheel bearings and belts	2
		main seals	3
Middle Expander	~7500 Hrs[3]	warm/pump/purge	6
	~100 RPM	valve rod and valve seals	1
		wristpin, crank, and cam follower bearings	1
		flywheel bearings and belts	1
		main seals	2
Wet Expander	3843 Hrs	warm/pump/purge	5
	~50 RPM	main seals	1
Distribution System	99%	warm, pump, purge lines	7

This final table shows screw compressor history here as of 1997 March 6:

Item	Total	1996	Status	Maintenance
RS-1	88,600 hours	8609 hours	running	none
RS-2	55,958 hours	0 hours	phases shorted	core removed 1993
RS-2a	29,544 hours	8782 hours	running since 1993	none
RS-3	22,752 hours	0 hours	shorted to ground	core removed 1990
RS-3a	57,905 hours	8783 hours	running since 1990	none

Mean RS compressor pump core lifetimes are as follows: all five cores listed above, 51,270 hours; those four cores operated to minimize starts (RS-1, RS-2, RS-2a, RS-3a), 58,399 hours.

* Retired.

[1] Nuclear Physics Laboratory Annual Report, University of Washington (1996) p. 65.

[2] This time is estimated due to the failure of the elapsed time hour meter for this engine.

[3] This time is estimated due to the failure of the elapsed time hour meter for this engine.

7.5 Improvements to the linac control system

M.A. Howe

A terminal ion source was added to the tandem recently. A full description of the ion source, its installation, and operating experience can be found elsewhere in this report (see Section 7.3). In order to control the source a new page was added to the linac control system (CSX). When the terminal ion source is in place the regular tandem terminal page which shows steering and foil controls is replaced by the new ion source page by either modifying the CSX initialization data file or by entering a simple typed command.

The new page shows a rendering of the ion source, with the extraction electrodes, einzel, gas bottle, and deflector shown in typical CSX schematic form. All of the relevant control values are shown as both set-point dac values and read-back adc values. All dac control parameters can be controlled from either the touch screens, console knob boxes, portable knob box, or the keyboard. The on/off parameters, such as the gas valve can only be controlled from the touch screens. Also shown and controlled on the page are the horizontal and vertical steerers. Other things displayed are the terminal voltage and gas valve position. In addition, the ion source turns pink when the extraction current indicates that a plasma has been formed.

The terminal ion source parameters are fully integrated into CSX and can be logged and restored.

8.0 OUTSIDE USERS

8.1 Targetry for RFQ production of radionuclides from ^{3}He irradiation of ^{16}O, ^{14}N, ^{12}C, ^{10}B and ^{9}Be*

K.A. Krohn,* J.M. Link,* W.G. Weitkamp and D.I. Will

The positron emission tomography (PET) radiochemistry group at UW, Fermi National Accelerator Lab, Science Applications International (San Diego), and the Biomedical Research Foundation (Shreveport) are jointly developing a radionuclide production system using a radiofrequency quadrupole (RFQ) accelerator. When compared to cyclotrons this system has advantages which include smaller size and weight, simpler operation and maintenance, and minimal shielding. An initial RFQ project for an 8 MeV ^{3}He beam (1992 NPL Progress Report) was never completed. The new design for the RFQ being built at Fermilab calls for a high current (7.5mA particle, peak), pulsed (167 μsec, 120Hz) beam of higher energy (10.5 MeV) $^{3}He^{++}$. The collaborative responsibility of the investigators at UW is to design targetry and chemical systems capable of producing ^{11}C, ^{13}N, ^{18}F, and ^{15}O in sufficient amounts for PET and compatible with the beam characteristics of the RFQ.

Data previously collected at NPL on radioisotope yields, neutron yields and windows, when critically evaluated, led to this increase in design energy. We knew from cross section measurements that to achieve useful yields of PET radionuclides from 8 MeV $^{3}He^{++}$ would require ~300 μA_e with at most 1.0 MeV loss in the entrance window. For the target window to tolerate this power (150 watts), the beam must be spread over 30 cm^2 of window (Havar). We have not had an opportunity to test a window under the power load presented to the proposed targets, and the manufacturer could not guarantee this window thickness and area free of pinholes. Assembling targets with such thin material without tearing or wrinkling is also difficult. Thermal calculations suggested it would be difficult to achieve sufficient cooling in gas targets (or solid targets with gas cooling) to maintain target window integrity during high current irradiations.

Specification of the appropriate energy for the RFQ involves trade-offs between energy, current and cost to produce clinically useful radioisotope yields with robust machine and targetry performance. To help determine the optimal targetry conditions, further cross section and yield experiments were performed at NPL this past year. The results are shown in Figs. 8.1-1 and 8.1-2. These results as well as those from NPL experiments done in previous years were used to develop Table 8.1-1 below which gives the minimum mCi required for clinical PET and the current required to deliver this yield for the different nuclear reactions. One of the problems of the 8 MeV RFQ was that many of the nuclear reactions were (^{3}He, alpha) where the product nuclide is an isotope of the target element, thus yielding low specific activity radionuclides of limited usefulness in radiopharmaceutical production. By increasing the energy of the ^{3}He beam, we can lower the current on target and gain access to new reactions producing high specific activity radionuclides (on ^{14}N to produce ^{15}O and on either ^{10}B or ^{9}Be to produce ^{11}C). From these tables we conclude that sufficient ^{18}F, ^{13}N, ^{11}C and ^{15}O can be made with 9 MeV (200 μA_e) reaching the target material. For the ^{11}C, ^{13}N and ^{15}O targets at the higher energy, the current on target can be reduced and the robustness of the target windows will improve. A ^{3}He beam at 10 to 10.5 MeV on a 0.3 mil Havar window provides a good compromise. It is likely that this window can be operated at an energy deposition in the window of about 1.5 MeV and a current of < 200 μA_e in most cases, thus not increasing the power deposited in the window but doubling its strength.

Neutron measurements on these targets showed that the neutron flux was reasonably low for the higher energies, with the exception of ^{3}He on ^{9}Be which had a neutron flux approximately ten times the flux from the other nuclear reactions. The angular dependence of the neutron flux from these reactions was measured and is presented in Fig. 8.1-3. As expected, neutrons from irradiation of N and O were isotropic, those from C and Be were forward scattered. At lower energy the relative amount of forward scattering increased.

---

*Imaging Research Group, University of Washington, Seattle, WA. This research was supported jointly by the DOE Division of High Energy Physics and the Office of Health and Environmental Research as a subcontract through Fermilab.

Table 8.1-1. mCi Requirements for PET and ^{3}He Current Required from the PET RFQ

Radionuclide	mCi EOB* in tgt (Required for PET)	μA_e at 8 MeV	μA_e at 9.5 MeV	μA_e at 10 MeV
$^{16}O(^{3}He,p)\ ^{18}F$	600	360	215	180
$^{12}C(^{3}He,alpha)^{11}C$ (low SA)	1000	180	120	100
$^{10}B(^{3}He,pn)^{11}C$ (high SA)	440	140	90	80
$^{9}Be(^{3}He,n)^{11}C$ (high SA)	440	110	90	80
$^{12}C(^{3}He,pn)\ ^{13}N$	100	310	120	90
$^{16}O(^{3}He,alpha)\ ^{15}O$ (low SA)	800	340	220	190
$^{14}N(^{3}He,pn)\ ^{15}O$ (high SA)	200	170	90	70

Assumes a 1.0 MeV window at 8 MeV machine beam and 1.5 MeV windows at the higher energies and irradiation times of 1 hr for ^{18}F and ^{11}C, 20min for ^{13}N and 10 min for ^{15}O. (*EOB = End of Bombardment)

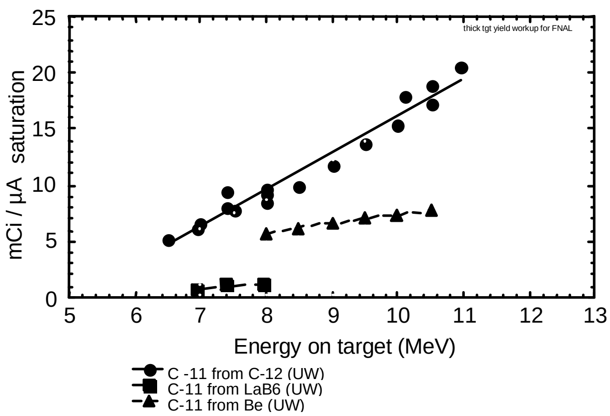

Fig. 8.1-1. ^{11}C yields from different nuclear reactions.

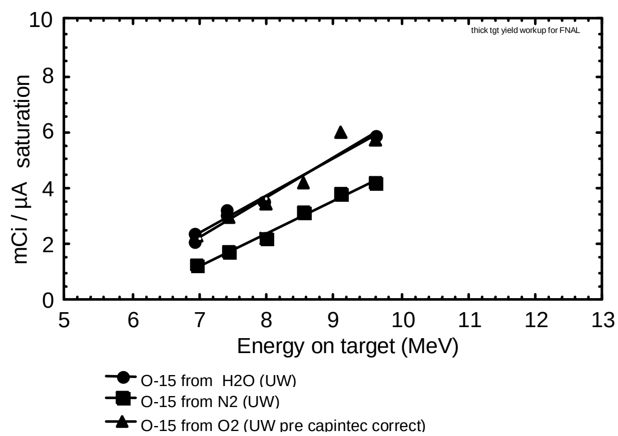

Fig. 8.1-2. ^{15}O yields from different nuclear reactions.

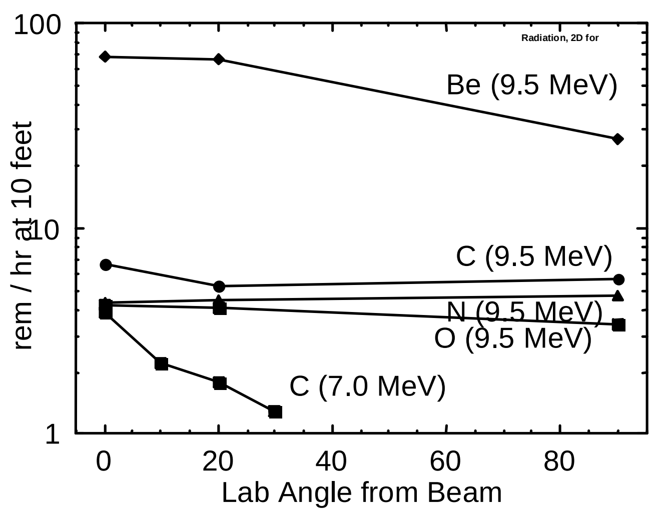

Fig. 8.1-3. Angular dependence of neutrons from ^{3}He irradiation of target materials.

8.2 Proton induced solar cell degradation

D.L. Oberg[*] and D.A. Russell[*]

The University of Washington Nuclear Physics Laboratory tandem Van de Graaff was used to produce a uniform proton beam over a 6-inch diameter for the purpose of irradiating solar cells and determining the proton induced degradation. This information is used in calculating the lifetime of solar cells in earth orbit. Using ~5 and 10† MeV protons and tantalum scattering foils, we were able to verify multiple scattering calculations.

Tantalum scattering foils were placed in the beam line 10 feet upstream from a 6 inch diameter exposure chamber. The final proton energies at the sample plane were 3 and 8 MeV with a beam flux of 3×10^9 cm^2-s. A small Faraday cup was scanned across the scattered beam to measure beam uniformity. The beam uniformity and intensity were as predicted with uniformity better than 10% over the 6 inch diameter.

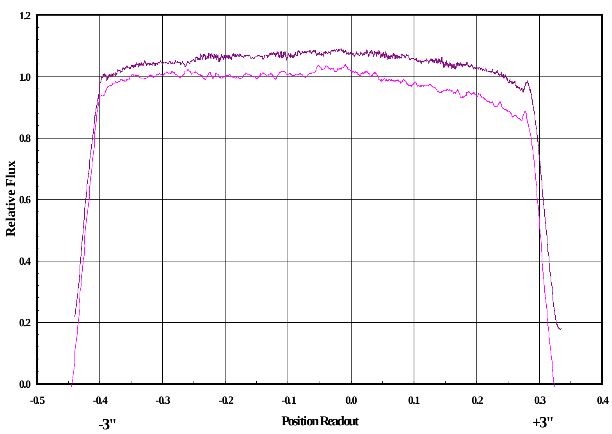

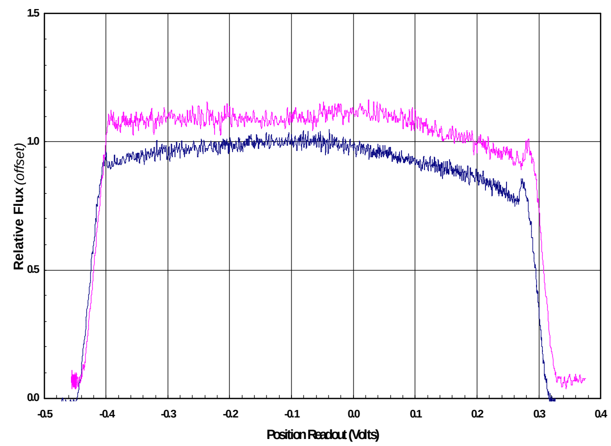

Fig. 8.2-1 and Fig. 8.2-2. Beam profiles used in the solar cell tests are shown for 8 MeV protons (left) and 3 MeV protons (right). In both cases higher energy protons (9.8 and 4.5 MeV) were incident on 1 and 2 mil tantalum scattering foils.

---

[*] Boeing Company, Seattle, WA.

8.3 Tests of radiation hardness of charge-coupled devices under exposure to protons

J. Hubbs,* G. Soli* and M. Weeks*

A test program was performed to characterize the radiation hardness of the Scientific Imaging Technologies, Inc. (SITe) SI003A Charge-Coupled Device (CCD) for possible use in the Advanced X-ray Astrophysics Facility - Imaging (AXAF-I) Aspect Camera (AC). Intended to be a replacement for the SITe TK1024 CCD, the SI003A incorporates a 3 micron mini-channel in the parallel and serial registers and a Multi-Phase Pinned (MPP) implant in the transfer gate, improvements which should enhance the radiation hardness of the CCD.

The objectives of the test program were: 1) to obtain a data set that will be used to compare the radiation hardness of the SI003A and TK1024 imagers; 2) to expose the SI003A to a radiation environment which simulates as closely as possible the expected on-orbit environment; and 3) to characterize the pre- and post-radiation performance of the SI003A CCDs under flight-like operating conditions.

Radiation Test Program Methodogy

Two of the SI003A CCDs were exposed to the same shaped proton energy spectrum that the TK1024 CCDs were exposed to during a previous AXAF-I ACA radiation program. The objective of this method is to allow for a direct comparison of the radiation tolerance of the SI003A CCD to the TK1024 CCD radiation tolerance.

Radiation Sources

The cyclotron at the University of California Davis and the Tandem Van de Graaff generator at the University of Washington were used to cover the spectrum of proton energies needed.

At the UW a broad distribution of protons was produced by scattering through gold foils located a few meters upstream of the 60" scattering chamber. The proton flux was checked using a silicon detector with a pinhole aperture, and was found to be uniform within a few percent over the area defined by the shadow of the collimator holder. This was sufficiently larger than the CCD's. Exposures were made to protons in the range of about 1 to 5 MeV.

This work was performed for Ball Aerospace by Spectrum Industries, Inc. of Santa Clara, California.

* Spectrum Industries, Santa Clara, CA.

9. NUCLEAR PHYSICS LABORATORY PERSONNEL

Faculty

Eric G. Adelberger, Professor
John G. Cramer, Professor
Hans Bichsel, Affiliate Professor
Ludwig De Braeckeleer, Research Assistant Professor[1]
Peter J. Doe, Research Professor
Steven R. Elliott, Research Assistant Professor
George W. Farwell, Professor Emeritus
Jens H. Gundlach, Research Assistant Professor
Isaac Halpern, Professor Emeritus
Blayne R. Heckel, Professor
John P. Lestone, Research Assistant Professor
R.G. Hamish Robertson, Professor
Kurt A. Snover, Research Professor
Derek W. Storm, Research Professor; Director, Nuclear Physics Laboratory
Thomas A. Trainor, Research Associate Professor
Robert Vandenbosch, Professor
William G. Weitkamp, Professor Emeritus
John F. Wilkerson, Professor

Research Staff

Marcus Beck, Research Associate
Ann Caraley, Research Associate
Jean-Marc Casandjian, Research Associate
Joseph V. Germani, Research Associate[2]
Jun Jien (Felix) Liang, Research Associate[3]
Reena Meijer Drees, Research Associate
Steven D. Penn, Research Associate
Gregory Smith, Research Associate
Thomas D. Steiger, Research Associate
Josephus P. van Schagen, Research Associate
Dhammika Weerasundara, Research Associate
Zhiping Zhao, Research Associate[4]

Predoctoral Research Associates

Qazi Rushdy Ahmad
Stephen Bailey[5]
James C. Beck
Michael Browne
Gopal Brugalette
Lincoln Carr
Christopher Cooper[7]
Charles Duba
Christian D'Urso
Melanie Felton[7]
Michael Harris
Karsten Heeger
Bruce Henry
Rebecca Hoffenberg[6]
Charles D. Hoyle
Michael Kelly
Diane Markoff
Hans Pieter Mumm
Alan W.P. Poon
Jeffrey Reid
Miles Smith
Alejandro Sonzogni
Kenneth Swartz[8]

---

[1] Now at Duke University, Durham, NC.
[2] Now at WRQ Company, Seattle, WA.
[3] Now at Oak Ridge National Laboratory, Oak Ridge, TN.
[4] Now at McKinsey & Co., Atlanta, GA.
[5] Now at Harvard University, Cambridge, MA.
[6] Physics Department, University of Washington.
[7] Now at Sante Fe, NM.
[8] Now at Yale University University, New Haven, CT.

Professional Staff
John F. Amsbaugh, Research Engineer
Thomas Burritt, Research Engineer
James Franklin, Research Engineer
Gregory C. Harper, Research Engineer
Mark A. Howe, Research Engineer
Carl E. Linder, Research Engineer
Duncan Prindle, Research Scientist
Richard J. Seymour, Computer Systems Manager
H. Erik Swanson, Research Physicist
Timothy D. Van Wechel, Electronics Engineer
Douglas I. Will, Research Engineer

Technical Staff
Dean T. Corcoran, Engineering Technician[9]
James Elms, Instrument Maker
Allan Myers, Electronics Technician
Hendrik Simons, Instrument Maker, Shop Supervisor
John A. Wootress, Accelerator Technician[10]
Steve Zsitvay, Instrument Maker

Administrative Staff
Barbara J. Fulton, Administrative Assistant
Karin M. Hendrickson, Office Assistant

Part Time Staff
Ryan Allen[11]
Brandon Allgood[11]
Michael Beard
Vassilious Bezzerides[11]
Matthew Blakley
John Catton
Ralph Chestine[11]
Jaime Freeman[11]
Lisa Goodenough
Jennifer Harvilla
Karsten Isaacson[11]
Tim Kalka[11]
Hadley Lawler
Ludwig Reid
Steve Martin
Kim Mauldin[11]
John McGrath[11]
Keven McKenney
Erik Power[11]
Curtis Reynolds
Christina Scovel
Andrew Sharp
Michael Strombach[11]
Amy Supple[11]
Matthew Wilson
Phil Williams[11]

[9] Now at InControl, 6675 185th NE, Redmond, WA.
[10] Retired.
[11] No longer associated with the Nuclear Physics Laboratory.

10. DEGREES GRANTED, ACADEMIC YEAR, 1996-1997:

"A short range test of the universality of free fall," Gregory Smith, University of Washington (1996).

"Transfer and surface vibration couplings in the fusion of $^{40}Ca+^{46,48,50}Ti$ at near-barrier energies," Alejandro Sonzogni, University of Washington (1997).

11. LIST OF PUBLICATIONS FROM 1996-97

Published papers:

"New developments in high precision, high particle density tracking with time projection chambers," A. Kuehmichel and NA49 Collaboration (including J.G. Cramer, D. Prindle, T.A. Trainor and D. Weerasundara), Nucl Instrum. Methods A 360, 52 (1995).

"Terminal ion source for an FN tandem," G.C. Harper, Nucl. Instrum. Methods Phys. Res. A. 382, 97 (1996).

"A beat frequency buncher," D.W. Storm, D.T. Corcoran and G.C. Harper, Nucl. Instrum. Methods Phys. Res. A 382, 182 (1996).

"NA49 TPC electronics," P. Jacobs and NA49 Collaboration (including J.G. Cramer, D. Prindle, T.A. Trainor and D. Weerasundara), Nucl. Instrum. Methods A 385, 535 (1997).

"Fragment emission from modestly excited nuclear systems," D. Prindle, A.A. Sonzogni, R. Vandenbsoch and others, Nucl. Phys. A 604, 219 (1996)..

"Anti-baryon production in sulphur nucleus collisions at 200-GeV per nucleon," T.Albers and NA49 Collaboration (including J.G. Cramer D. Prindle, T.A. Trainor and D. Weerasundara) Phys. Lett. B. 366, 56 (1996).

"Search for 1s2s $^3S_1$ - 1s2p $^3P_2$ decay in U^{90+}," P. Beiersdorfer *et al*., (including S.R. Elliott) Phys. Rev. A **53**, 4000 (1996).

"Near- and sub-barrier ^{12}C + ^{232}Th fission fragment anisotropies," J.P. Lestone, A.A. Sonzogni, M.P. Kelly and D. Prindle, Phys. Rev. C **55**, R16 (1997).

"Nonstatistical g emission in ^{3}He and $\alpha -$ induced reactions," J.A. Behr, K.A. Snover, C.A. Gossett, G. Feldman, J.H. Gundlach and M. Kicinska-Habior, Phys. Rev. C **53**, 1759 (1996).

"Standard neutrino spectrum from ^{8}B decay," J.N. Bahcall, D.E. Alburger, L. De Braeckleer, S.J. Freedman and J. Napolitano, Phys. Rev. C **54**, 411 (1996).

"Disappearance of entrance channel dependence of fission fragment anisotropies at well-above barrier energies," R. Vandenbosch, J.D. Bierman, J.P. Lestone, J.F. Liang, D.J. Prindle, A.A Sonzogni, S. Kailas, D.M. Nadkarni and S.S. Kapoor, Phys. Rev. C **54**, R977 (1996).

"Structure of ^{18}Ne and the breakout from the hot CNO cycle," K.I. Hahn, A. Garcia, E.G. Adelberger, P.V. Magnus, A.D. Bacher, N. Bateman, G.P.A. Berg, J.C. Blackmon, A.E. Champagne, A.J. Howard, J. Liu, B. Lund, Z.Q. Mao, P.D. Parker, M.S. Smith, E.J. Stephenson, K.B. Swartz, S. Utku and R.B. Vogelaar, Phys. Rev. C **54**, 1999 (1996).

"Fusion barrier distributions for heavy ion systems involving prolate and oblate target nuclei," J.D. Bierman, P. Chan, J.F. Liang, M.P. Kelly, A.A. Sonzogni and R. Vandenbosch, Phys. Rev. C **54**, 3068 (1996).

"Isospin mixing in ^{37}K and spin decomposition of Gamow-Teller strength in ^{37}Ca β decay," N.I. Kaloskamis, A. Garcia, S.E. Darden, E. Miller, W. Haeberli, P.A. Quin, B.P. Schwartz, E. Yacoub and E.G. Adelberger, Phys. Rev C **55**, 630 (1997).

Kaloskamis, A. Garcia, S.E. Darden, E. Miller, W. Haeberli, P.A. Quin, B.P. Schwartz, E. Yacoub and E.G. Adelberger, Phys. Rev C **55**, 630 (1997).

"New technique for measuring Newton�s Constant *G*," J.H. Gundlach, E.G. Adelberger, B.R. Heckel and H.E. Swanson, Phys. Rev. D **54**, R1256 (1996).

"Experimental fusion barrier distributions reflecting projectile octupole state coupling. to prolate and oblate target nuclei," R. Vandenbosch, J.D. Bierman, P. Chan, J.F. Liang, M.P. Kelly and A.A. Sonzogni, Phys. Rev. Lett. **76**, 1587 (1996).

"Probability of a solution to the solar neutrino problem within the minimal standard model," K.M. Heeger and R.G.H. Robertson, Phys. Rev. Lett. **77**, 3720 (1996).

"Trapped-ion technique for measuring the nuclear charge radii of highly charged radioactive isotopes," S.R. Elliott, P. Beiersdorfer and M.H. Chen, Phys. Rev. Lett. **77**, 4278 (1996).

"The Russian-American Gallium experiment (SAGE) Cr-neutrino source measurement," J.N. Abdurashitov, (36 authors including J.F. Wilkerson and S.R. Elliott), Phys. Rev. Lett. **77**, 4708 (1996).

"Energies of neon-like n=4 to n=2 resonance lines," J. Nilsen, P. Beiersdorfer, K.Widmann, V. Decaux and S.R. Elliott, Phys. Scripta **54**, 183 (1996).

"Development of a compact 20 MeV gamma-ray source for energy calibration at the Sudbury Neutrino Observatory," A.W.P. Poon, M.C. Browne, R.G.H. Robertson, C.E. Waltham and N. Kherani, in Particles and Cosmology (World Scientific, 1996), editors, E.N.Alexeev, V.A. Matveev, Kh.S. Nirov and V.A. Rubakov, p. 248.

"Neutrino," J.F. Wilkerson, McGraw-Hill Encyclopedia of Science and Technology, Eighth Edition, (1997).

"Giant Resonances," K.A. Snover, McGraw-Hill Encyclopedia of Science and Technology, Eighth Edition, (1997).

Papers submitted or to be published:

"Study of the β-decay of ^{37}Ca and ^{36}Ca," W. Trinder, E.G. Adelberger, B.A. Brown, Z. Janas, H. Keller, K. Krumbholz, V. Kunze, P. Magnus, F. Meissner, A. Piechaczek, M. Pfützner, E. Roeckl, K. Rykaczewski, W.-D. Schmidt-Ott and M. Weber, submitted to Nucl. Phys.

"Measurement of electron-impact ionization cross sections for hydrogenlike high-Z ions," R.E. Marrs, S.R. Elliott and J.H. Scofield, submitted to Phys. Rev. A.

"Measurement of L-shell electron-impact ionization cross sections for highly charged uranium ions," Th. Stohlker, A. Kramer, S.R. Elliott, R.E. Marrs and J.H. Scofield, submitted to Phys. Rev. A.

"Analysis of a -particle emission from ^{19}F + ^{181}Ta reactions leading to evaporation residues," J.P. Lestone, Phys. Rev. C, to be published.

"Translation of multipoles for a 1/*r* potential," C. D�Urso and E.G. Adelberger, Phys. Rev. D, in press.

"Short-range test of Equivalence Principle," J.H. Gundlach, G.L. Smith, E.G. Adelberger, B.R. Heckel and H.E. Swanson, Phys. Rev. Lett.

"Entrance channel dependent light-charged particle emission of the ^{156}Er compound nucleus," J.F. Liang, J.D. Bierman, M.P. Kelly, A.A. Sonzogni, R. Vandenbosch and J.P.S. van Schagen, accepted by Phys. Rev.

"Entrance channel dependent light-charged particle emission of the ^{156}Er compound nucleus," J.F. Liang, J.D. Bierman, M.P. Kelly, A.A. Sonzogni, R. Vandenbosch and J.P.S. van Schagen, accepted by Phys. Rev. Lett.

Invited talks, Abstracts and other conference presentations by NPL personnel:

"The Principle of Equivalence and the search for new fundmental physics," E.G. Adelberger, Invited talk, *Western Regional Conference of the Canadian Association of Physics*, Lake Louise, Canada, Feb., 1996.

"Solar neutrinos: remarkable measurements, surprising implications," R.G.H. Robertson, Invited talk, *Pacific Northwest Association of College Physics Meeting*, Auburn, WA, March, 1996.

"Sub-barrier fusion-fission reactions," R. Vandenbosch, Presented at *Conference on Nuclear Dynamics at Long and Short Distances*, Angra do Reis, Brazil, April, 1996.

"Using beta decay to search for time reversal invariance violation," J.F. Wilkerson, Contributed talk, Joint Meeting of The APS and the AAPT, Indianapolis, IN, May, 1996.

"Neutrino mass from the Tritium spectrum," R.G. H. Robertson, Invited Review, *ITAMP Workshop on the Tritium Beta Decay Spectrum: the Negative Mass-Squared Issue*, Harvard-Smithsonian Center for Astrophysics, Cambridge, MA, May, 1996.

The Solar Neutrino Deficit," R.G.H. Robertson, Invited talk, Inventors Recognition Dinner, Allied Signal Corp., June, 1996.

"Neutrino Mass at Los Alamos" R.G.H. Robertson, Invited talk, *Reines Symposium*, Los Alamos National Laboratory, Los Alamos, NM, Aug., 1996.

"Parity mixing in light nuclei," E.G. Adelberger, Invited talk, *Osaka International Symposium on Weak Interactions Detected in Nucleus*, Osaka, Japan, Aug., 1996.

"Fundamental symmetries and nuclear astrophysics: recent progress and new challenges," E.G. Adelberger, Invited talk, Fall meeting of the American Physical Society, Bull. Am. Phys. Soc. **41**, 1214 (1996).

"Influences of the spatial and temperature dependence of the effective nucleon mass on the density of nuclear levels," J. Lestone, F. Liang, D. Prindle, A. Sonzogni, J. van Schagen, and R. Vandenbosch, Fall meeting of the American Physical Society, Bull. Am. Phys. Soc. **41**, 1264 (1996) presented by J. Lestone.

Talk on "The Principle of Equivalence and the search for new fundmental physics," E.G. Adelberger, Invited talk, AAPT meeting, Greensboro, NC, Nov., 1996,

"Trapped-ion based technique for measuring the nuclear radii of highly-charged radioactive isotopes," S.R. Elliott, P. Beiersdorfer and M.H. Chen, *Proceeding of the International Conference on the Application of Accelerators in Research and Industry*, Denton, Texas, Nov., 1996, to be published, presented by S.R. Elliott.

"Scaled correlation analysis and symmetry reduction in nuclear collisions," T.A. Trainor, Event-by-Event Forum, CERN PPE Division, CERN, Switzerland, Nov., 1996.

"Scaled correlation analysis of NA49 transverse mass spectra," D.D. Weerasundara, Event-by-Event Forum, CERN PPE Division, CERN, Switzerland, Nov., 1996.

"Scaled correlation analysis of NA49 transverse mass spectra," D.D. Weerasundara, Event-by-Event Forum, CERN PPE Division, CERN, Switzerland, Nov., 1996.

"Event-by-event physics at the CERN SPS," T.A. Trainor, *Thirteenth Winter Workshop on Nuclear Dynamics*, Marathon Key, FL, Feb., 1997.

"Event-wise physics: measures and interpretation," T.A. Trainor, *1997 RHIC/INT Winter Workshop on "Hadronic Signals of New Physics at RHIC*," Lawence Berkeley National Laboratory, Berkeley, CA, Feb., 1997.

"CNO Reactions in the Sun," R.G.H. Robertson, Summary talk, *INT Workshop on Fusion Reactions in the Sun*, Seattle, WA, Feb., 1997.

"Plans for a $^{7}\mathbf{Be}(\mathbf{p},\gamma)$ experiment at Seattle," K.A. Snover, *INT Workshop on Fusion Reactions in the Sun*, Seattle, WA, Feb., 1997.

"Nuclear reaction rates in the CNO cycle," C. Duba and K. Heeger, *INT Workshop on Fusion Reactions in the Sun*, Seattle, WA, Feb., 1997.

"The $^{7}\mathbf{Be}(\mathbf{p},\gamma)$ cross section," E.G. Adelberger, *INT Workshop on Fusion Reactions in the Sun*, Seattle, WA, Feb., 1997.

"Detection of the RF pulse associated with cosmic ray air showers," J.L. Rosner and J.F. Wilkerson, Appendix to Auger Technical Proposal, EFI-97-10, 7 pp, e-Print Archive:hep-ex/9702008 (1997).

"Effects of shape and transfer degrees of freedom on sub-barrier fusion," R. Vandenbosch, *Fusion 97 Internat.Workshop on Heavy Ion Collisions at Near Barrier Energies*, South Duras, Australia, March, 1997.

"Event-by-event physics," T.A. Trainor, Invited plenary talk, *3rd International Conference on Physics and Astrophysics of Quark-Gluon Plasma*, Jaipur, India, March, 1997.

"Near- and sub-barrier fission fragment anisotropies and the failure of the statistical theory of fission decay rates," J.P. Lestone, *Fusion 97 Internat.Workshop on Heavy Ion Collisions at Near Barrier Energies*, South Duras, Australia, March, 1997.

"Carbon chains: from graphite sputtering to Buckyball unzipping," R. Vandenbosch, talk given at "*Joint Japan - U.S. Clustering Phenomena in Nuclear and Mesoscopic Systems*, Honolulu, HI, Dec., 1995.

Conference presentations by collaborators of NPL personnel:

"Recent results from Sage," V.M. Vermul (36 authors including J.F. Wilkerson and S.R. Elliott), *Proceedings of the International Conference on Neutrino Telescopes*, Venice, Italy, Feb., 1996, to be published, presented by V.M. Vermul..

"The Russian-American Gallium experiment Cr-neutrino source measurement," V.N. Gavrin (36 authors including J.F. Wilkerson and S.R.Elliott), *Proceedings of the International Conference on Neutrino Telescopes*, Venice, Italy, Feb., 1996, to be published, presented by V.N. Gavrin.

"Strange and nonstrange (anti-) baryon production at 200-GeV per nucleon," D. Rohrich and the NA49 collaboration (including J.G. Cramer, D. Prindle, T.A. Trainor and D. Weerasundara) ,talk given at *Workshop on Strangeness in Hadronic Matter* (Strangeness 96), Budapest, Hungary, May, 1996.

collaboration (including J.G. Cramer, D. Prindle, T.A. Trainor and D. Weerasundara) ,talk given at *Workshop on Strangeness in Hadronic Matter* (Strangeness 96), Budapest, Hungary, May, 1996.

"Strangeness enhancement in sulphur - nucleus collisions at 200-GeV/N," J. Eschke and the NA49 collaboration (including J.G. Cramer, D. Prindle, T.A. Trainor and D. Weerasundara), talk given at *Workshop on Strangeness in Hadronic Matter* (Strangeness 96), Budapest, Hungary, May, 1996, also submitted to Heavy Ion Phys.

"Particle correlations in Pb+Pb collisions at the CERN-SPS - results from the NA49 experiment," K. Kadija and the NA49 collaboration (including J.G. Cramer, D. Prindle, T.A. Trainor and D. Weerasundara), *Quark Matter 96, Twelfth International Conference on Ultra-Relativistic Nucleus-Nucleus Collisions*, Heidelberg, Germany, May, 1996.

"Hadron yields and hadron spectra from the NA49 experiment," P.G. Jones and the NA49 collaboration (including J.G. Cramer, D. Prindle, T.A. Trainor and D. Weerasundara), *Quark Matter 96, Twelfth International Conference on Ultra-Relativistic Nucleus-Nucleus Collisions*, Heidelberg, Germany, May, 1996.

"The calibration of solar neutrino results from SAGE," V.N. Gavrin (36 authors including J.F. Wilkerson and S.R.Elliott), *Proceedings of the 17th International Conference on Neutrino Physics and Astrophysics*, Helsinki, Finland, June, 1996, to be published, presented by V.N. Gavrin.

"Recent results from hadronic observables at the CERN SPS," P. Jacobs and the NA49 collaboration (including J.G. Cramer, D. Prindle, T.A. Trainor and D. Weerasundara), Proceedings of HIPGAS 96, Wayne State University Detroit, MI, Aug., 1996.

"Progress in particle correlation studies at NA49," B. Lasiuk and the NA49 collaboration (including J.G. Cramer, D. Prindle, T.A. Trainor and D. Weerasundara), presented at CERN, Switzerland and Fall meeting of the American Physical Society, Bull. Am. Phys. Soc. **41**, 1234 (1996) Summary from a lecture given at the Triangle Meeting, *School and Workshop on Heavy Ion Collisions*, Bratislava, Slovakia, Sept., 1996.

"Recent results from the N49 lead beam experiment," P. Seyboth and the NA49 collaboration (including J.G. Cramer, D. Prindle, T.A. Trainor and D. Weerasundara), contribution to the *XXVI Symposium on Multiparticle Dynamics*, Faro, Portugal, Sept., 1996.

"First results of the NA49 event-by-event analysis of Pb+Pb collisions at the SPS," G. Roland and the NA49 collaboration (including J.G. Cramer, D. Prindle, T.A. Trainor and D. Weerasundara), *International Workshop XXV on Gross Properties of Nuclei and Nuclear Excitations*, Hirschegg, Austria, Jan., 1997.

"Correlations in 158 GeV PB+PB collisions measured by NA49," P. Seyboth and the NA49 collaboration (including J.G. Cramer, D. Prindle, T.A. Trainor and D. Weerasundara), contribution to the *Workshop on Correlations*, Nijmegen, Netherlands, Oct.,1996.

"Measurements of nuclear parameters of high-Z isotopes performed on an high-energy electron beam ion trap," P. Beiersdorfer, S.R. Elliott, J. Crespo Lopez-Urrutia and K. Widmann, Proceedings of STORI-96, Nucl. Phys. A (in press), presented by P. Beiersdorfer.